Doctoral Program in Biochemistry and Molecular Biology Bibim 2.0 – Cycle XXXVI

Development and Validation of Accurate HPLC-MS-MS Based Methods to Investigate the Vitamin D Status Involved in COVID-19

Candidate

Beatrice Campi

Supervisor

Prof. Alessandro Saba

Academic year 2022/2023

SSD BIO/10

Content

Abbreviation Index

1,25-(OH)2D: 1α,25-dihydroxy-vitamin D3

24,25-(OH)$_2$D: 24,25-dihydroxy-vitamin D3

25-OHD: 25-mono-hydroxy-vitamin D3

ACE2: angiotensin converting enzyme 2

ALB: albumin

ARDS: acute respiratory distress syndrome

BAVD: bioavailable vitamin D

CID: collision-induced dissociation

COVID-19: coronaVirus Disease 2019

DBP: vitamin D binding protein

ESI: electrospray ionisation

FGF23: growth factor of fibroblasts 23

Glicoprotein S: spike (S) glycoprotein

LC-MS/MS: Liquid chromatography tandem mass spectrometry

LIT: linear ion trap

m/z: mass to charge ratio

MeNH$_2$: methylamine

MRM: multiple reaction monitoring

PTAD: 4-phenyl-1,2,4-triazoline-3,5dione

PTH: parathyroid hormone

RAAS: renin-angiotensin-aldosterone system

RDB: receptor binding domain

RF: radio frequency

SARS-CoV: severe acute respiratory syndrome

VDD: vitamin D deficiency

VDR: vitamin D receptor

VMR: vitamin D metabolite ratio

Abstract

Background: Vitamin D status has been suggested to play a possible role in human skeletal and non-skeletal health problems. Recent literature has focused on the role of vitamin D3 in the immune system, asserting its involvement in regulation, modulation of innate and adaptive responses, and the production of antibacterial and antiviral proteins. Recent studies have also shown an inverse correlation between Vitamin D status and increased susceptibility to respiratory infections, such as acute respiratory distress syndrome (ARDS), one of the most severe complications of coronavirus disease 2019 (COVID-19). In March 2020, COVID-19 spread as a pandemic emergence, with uncertain outcomes in the absence of definite effective therapies and vaccines. Other than specific treatments, public health measures were required to characterize risk factors and prevent the infection or the progression of the disease to reach its most aggressive form. Among multiple factors that could eventually contribute to COVID-19, the vitamin D status was proposed as a credible candidate. This research project focused on the role of vitamin D3 in COVID-19. Commonly, to define Vitamin D status, most routine analytical methods quantify 25-hydroxyvitamin D3 (25OHD3), the most abundant circulating metabolite. However, vitamin D3 is characterized by complex metabolic and catabolic pathways, and simultaneous measurement of vitamin D3 in its biologically active and inactive forms may provide a more accurate interpretation of vitamin D status in the pathophysiological context of COVID-19.

Methods: This study firstly aimed to investigate the blood levels of Vitamin D metabolites and catabolites in COVID-19 positive patients and in healthy subjects to evaluate any differences in the vitamin D3 status and obtain some information about vitamin D3 metabolism and catabolism during SARS-CoV2 infection. In this retrospective study, we analyzed 30 plasma samples from healthy subjects, used as controls, and 69 samples from COVID-19 patients hospitalized at the University Hospital in Pisa between March and May 2020. Secondly, the study focused on the relationship between vitamin D status, considered as 25-OHD3, and a biochemical panel of inflammatory markers in a cohort of patients (n=93) with COVID-19-related pneumonia. For the first aim of the study, a selective analytical method based on liquid chromatography coupled to tandem mass

spectrometry (LC-MS-MS) to quantify vitamin D3 and three of its metabolites, such as 25-OHD3, 24,25-(OH)2D3, 1,25-$(OH)_2$D3, in plasma samples, was developed and validated. All analyses were performed with an Agilent Infinity UHPLC system, coupled to Sciex QTrap 6500+ mass spectrometer, equipped with an IonDrive Turbo-V electrospray (ESI) ion source. Chromatographic separation was achieved by a phenyl column, under gradient conditions. The MS method to assay 25-OHD3, 24,25-(OH)2D3, vitamin D3, and their ISs was based on positive ion mode multiple reaction monitoring (MRM), while the MS the quantification of both 1,25-$(OH)_2$D3 and its IS was based on positive ion mode MS3 (MS/MS/MS). Regarding the relationship between 25-OHD3 levels and inflammatory markers, the analysis of cytokines (IL-6, and IL-10; tumor necrosis factor-a, TNF-α) was performed by a fully automated ELISA processing system, using commercial ELISA assays. Hemogasanalysis was performed by GEM Premier 4000 Blood Gas Analyzer, and gas exchange impairment was evaluated using arterial partial pressure of oxygen (PaO2) to fraction of inspired oxygen (FiO2) (P/F).

Results: The LC-MS-MS method provided satisfactory results in terms of selectivity, reproducibility, sensitivity as well as in recovery, accuracy and stability. The high linearity allows an accurate quantification of the analytes. The method was used for the simultaneous quantification of vitamin D3 and three of its metabolites in plasma samples. Our data indicated a statistically significance decrease in the concentration levels of the four analytes of interest in COVID-19 positive patients compared to the controls. As regards the relationship between 25OHD3 and inflammatory markers, sixty-five percent of patients presented hypovitaminosis D3 (25OHD3 $\leq$ 20 ng/ml) and showed significantly higher levels of IL-6, CRP, TNF-a, D-dimer, and IL-10. A considerable inverse correlation was found between 25OHD and all these markers, even adjusted for age and sex. Hypovitaminosis D3 was prevalent in patients with severe ARDS, compared with the other groups, and 25OHD3 levels were lower in non-survivor patients.

Conclusions: The LC-MS-MS method developed in our laboratory revealed to be very useful instrument to understand the role of vitamin D metabolites in COVID-19 disease. Nevertheless, this powerful analytical tool could be exploited

to examine in depth on routine or research basis the complex interaction between vitamin D3, bone homeostasis and immune system. However, this thesis work is a preliminary study, carried out on a small sample population; the extension of the study to a larger number of samples could allow the identification of a reliable biomarker, among the metabolites of vitamin D3, that may be related to the degree of severity of COVID-19 disease. The relationship between 25OHD3 levels and inflammatory markers suggests that vitamin D status needs to be considered in the management of these patients. If vitamin D is a marker of poor prognosis or a possible risk factor with beneficial effects from supplementation, this still needs to be elucidated.

I. Introduction

1.1. The vitamin D

Vitamin D has a crucial role in several physiological processes, affecting not only the metabolism of calcium and phosphorus (skeletal effects), but being also responsible for extra-skeletal effects [1],[2]. It has been shown that *vitamin D deficiency* (VDD) status, which is the most common nutritional deficiency, can be associated with an increased incidence and progression of a wide range of diseases, including calcium metabolism disorders, autoimmune diseases, cardiovascular diseases, infectious diseases, certain types of neoplasm, and type 2 diabetes mellitus [3]–[7]. According to the major health agencies, up until recently the main cause of this deficiency was due to wrong intake. 200 international units (IU, unit used for measuring the activity of many vitamins, hormones, enzymes and drugs; 1 IU corresponds to the amount of a substance needed to induce a certain biological effect [8]), which is twice as much than what is needed to prevent skeletal abnormalities associated with rickets [1], was considered as a sufficient amount for a good state of health. These quantities are now considered largely insufficient, and the American National Institutes of Health (NIH) suggests that the daily intake average amounts should be much higher, i.e. 400 IU (10 μg) for infants up to 12 months, 600 IU (15 μg) for children and adults in the age range 1-70, and 800 IU (20 μg) for adults >71 years old (Table 1) [9].

Age	Male	Female	Pregnancy	Lactation
0-12 months*	10 mcg (400 IU)	10 mcg (400 IU)		
1–13 years	15 mcg (600 IU)	15 mcg (600 IU)		
14–18 years	15 mcg (600 IU)	15 mcg (600 IU)	15 mcg (600 IU)	15 mcg (600 IU)
19–50 years	15 mcg (600 IU)	15 mcg (600 IU)	15 mcg (600 IU)	15 mcg (600 IU)
51–70 years	15 mcg (600 IU)	15 mcg (600 IU)		
>70 years	20 mcg (800 IU)	20 mcg (800 IU)		

*Adequate Intake (AI)

Table 1-Recommended Dietary Allowances (RDAs) for Vitamin D [11].

Current guidelines consider 25-monohydroxy-vitamin D (25-OHD), which is the most abundant metabolite of vitamin D in blood, as the best marker of vitamin D status. In the scientific literature plenty clinical studies highlight a significant association between 25-OHD levels and biochemical, functional, and clinical markers [1], [3], [5], [10]. The literature data regarding optimal 25-OHD blood levels are, however, rather controversial. The less recent literature states that levels of 25-OHD must be greater than 30 ng/ml in order to satisfy the organism's request of the active metabolite, namely 1α,25-dihydroxy-vitamin D (1,25-$(OH)_2$D), which interacts with the VDR receptor (vitamin D receptor) for the implementation of the physiological actions of vitamin D [1], [3], [4], [2]. Most recent literature and NIH state, however, that 20 ng/ml (50 nmol/L) are adequate to ensure good bone health, and the concentrations <12 ng/ml (30 nmol/L) are too low and may cause health problems, as well as concentrations

>50 ng/ml (125 nmol/L) (Table 2) [3], [11].

nmol/L*	ng/mL*	Health status
<30	<12	Associated with vitamin D deficiency, which can lead to rickets in infants and children
30 to <50	12 to <20	Generally considered inadequate for bone and overall health in healthy individuals
≥50	≥20	Generally considered adequate for bone and overall health in healthy individuals
>125	>50	Linked to potential adverse effects, particularly at >150 nmol/L (>60 ng/mL)

Table 2-Serum 25-Hydroxyvitamin D (25OHD) Concentrations and Health. *Serum concentration of 25(OH)D are reported in both nanomoles per liter(nmol/L) and nanograms per milliliter(ng/mL). One nmol/L=0.4 ng/mL, and 1ng/mL= 2.5 nmol/L [11].

1.2. The Biosynthesis and Catabolism of Vitamin D

The term vitamin D identifies a group of secosteroids, which differ from traditional steroid hormones by the B-ring of the nucleus cyclopentanoperidrophenantrenic, which is open. The main form of vitamin D are D3 (cholecalciferol), which is the animal form, and D2 (ergocalciferol), which is the vegetable form; the two forms differ from each other for the structure of the side chains, and in particular, vitamin D2 differs from D3 due to the exclusive presence of a double bond between the carbon 22 and 23 and a methyl group on carbon 24 (Fig. 1) [1], [3],[2].

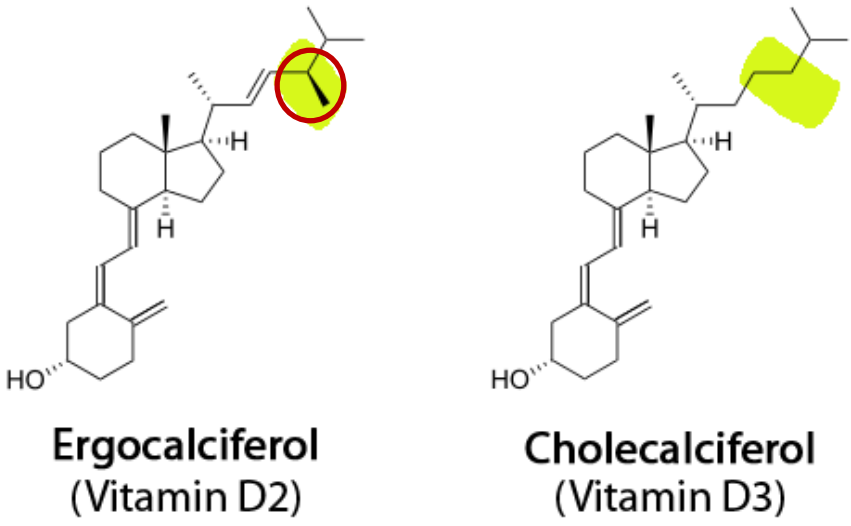

Fig. 1 - Structures of vitamin D2 and D3.

In humans the source of vitamin D2 is represented by diet and supplements while the source of vitamin D3 is represented by endogenous synthesis induced by sunlight, as well as by diet and supplements [1]–[3], [12]. As for the intake from dietary sources, vitamins D3 and D2 are incorporated into the chylomicrons and transported by the lymphatic system into the venous circulation. Endogenous synthesis is, instead, a little more complex and takes place at the skin level, and in particular in the plasma

membrane of the cells of the epidermis and dermis, where 7-dehydrocholesterol (pro-vitamin D) is localized, with higher concentration levels in the cells of the basal and spinous layer of the epidermis itself; 7-dehydrocholesterol is not only a precursor of vitamin D, but is also an intermediate of the biosynthetic cholesterol pathway, from which steroid hormones (androgens, estrogens, glucocorticoids, mineralocorticoids, and progestins) originate; this is reason why vitamin D and its derivatives are usually considered the sixth class of steroid compounds [2].The conversion of pro-vitamin D to vitamin D occurs due to the absorption of UVB radiation with a wavelength between 290-315 nm [1]–[3], which results in the breakdown of the bond between carbon 9 and 10, with the formation of the pre-vitamin D3. Pre-vitamin D3 converts into the most thermodynamically stable isomer (vitamin D3) by spontaneous rotation around the bond located between carbons 5 and 6. (Fig. 2)

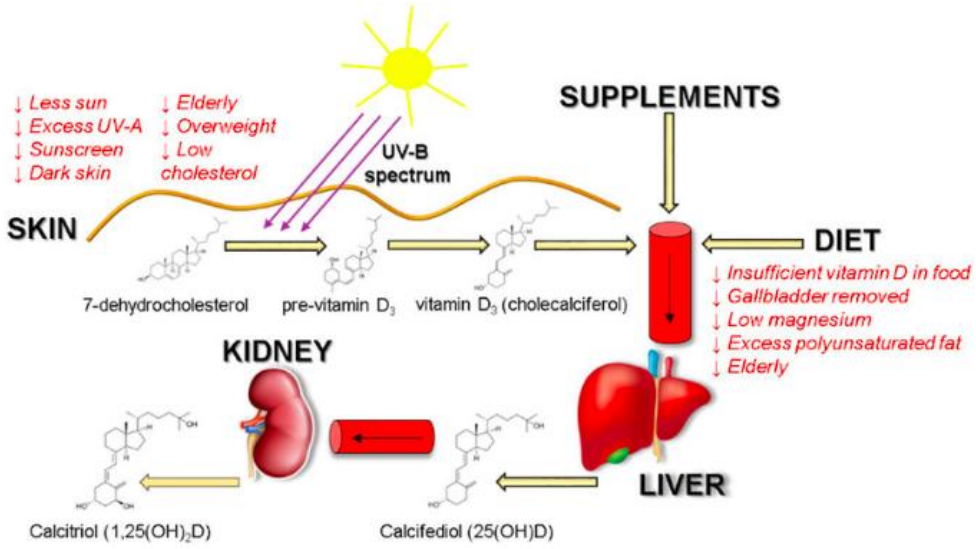

Fig. 2 - Vitamin D3 sources, biosynthesis and possible factors affecting absorption. Downward arrows show factors that are associated with decreased vitamin D absorption and synthesis in the organism.

The process of isomerization interrupts hydrophobic and hydrophilic interactions, which maintain pre-vitamin D3 at the level of the plasma membrane, thus allowing

the release of vitamin D3 into the interstitial fluid and from there into the circulation, where it largely binds to Vitamin D binding protein (DBP), a protein structurally linked to albumin (ALB) that is present in the capillaries of dermis [2], [13]–[15]. Regardless of whether it has been synthesized in the skin or comes from dietary/supplemental intake, Vitamin D is transported to the adipose tissue, where it is stored, or in the liver. In this latter tissue the first stage of biologically active conversion (hydroxylation reaction) takes place [2] at the expense of carbon 25, promoted primarily by the cytochrome enzyme P450 CYP2R1 and secondly also by enzymes P450 CYP27A1, CYP34A4 o CYP2D5, with the formation of 25-OHD. The second stage of the production process of the active form (1,25-$(OH)_2$D) takes place, instead, mainly at the level of the proximal tubules of the kidney and consists in the hydroxylation of 25-OHD on the carbon in position 1, by the enzyme P450 CYP27B1. This enzyme is also localized in many extra-renal tissues; therefore, it is able to give rise to the bioactive molecule in autocrine and paracrine mode [1], [2], [14], [16]. Only 0.03% of 25-OHD and 0.4% of 1,25-$(OH)_2$D circulate in plasma in free form while the remaining fraction of both analytes is associated with DBP, 85%, and with ALB, 15%. DBP is present in molar excess compared to the vitamin D metabolites, considering that it is found at concentrations about 20 times higher and therefore only 5% of this is actually the carrier of Vitamin D metabolites and serves as a large reservoir of vitamin D that prevents its deficiency in case of low availability. According to the hypothesis of the free hormone, only the unbound fraction is able to enter into the cells and exert biological effects; an exception to this is represented by the kidney, in which the entry of vitamin D is allowed by megalin, exposed on the apical side of the proximal tubule cells of the kidney, which serves as a receptor of vitamin D-DBP complex [13]–[15]. Also, the catabolism of vitamin D

occurs mainly through hydroxylation reactions at the level of the kidney; in humans the primary catabolic pathway begins with the hydroxylation of carbon 24, and ends, with the production of calcitroic acid, which is excreted in bile. The first step, and probably also other subsequent steps, is catalyzed by the mitochondrial enzyme P450 CYP24A1, which has extreme affinity for the substrate 1,25-$(OH)_2D$, and converts it into 1,24,25-trihydroxy-vitamin(1,24,25-$(OH)_3D$). P450 CYP24A1 has affinity also for 25-OHD, which is thus converted into 24,25-dihydroxy-vitamin D (24,25-$(OH)_2D$). Although 24,25-$(OH)_2D$ is a product of the catabolism of vitamin D, it maintains a certain biological activity, such as in the chondrocyte's physiology of the growth plates modulation and the function of the parathyroid gland [2], [17]. There is also another metabolic pathway, which is called C3-epimerization, by which the main metabolites of vitamin D are first converted (isomerized) in their respective epimeric forms and subsequently metabolised through the C-24 oxidation pathway (Fig. 3) [18].

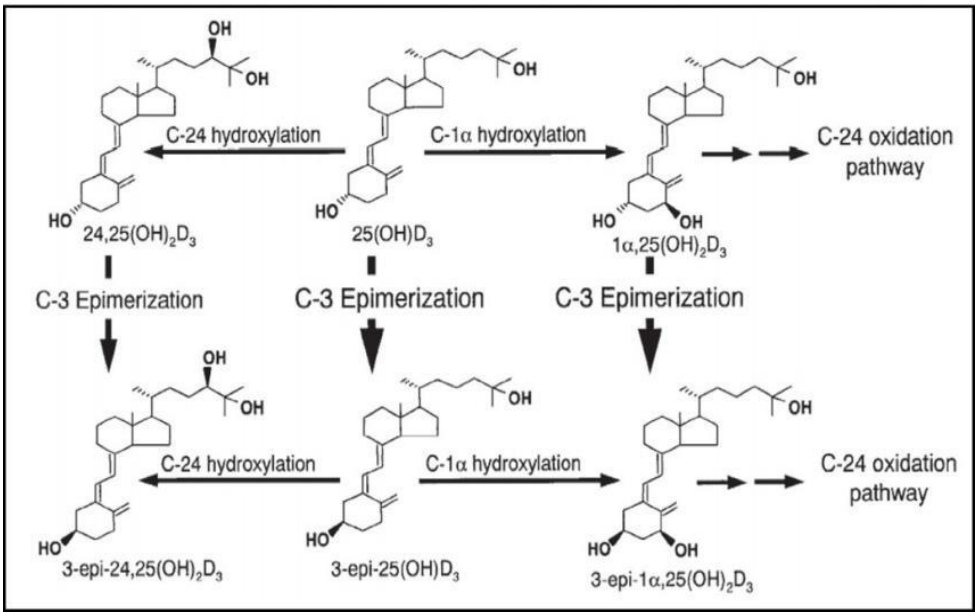

Fig. 3 - C3-epimerization of the main metabolites of vitamin D3

1.3. The maintenance of vitamin D homeostasis

The maintenance of vitamin D homeostasis is ensured mainly by the renal production of the bioactive molecule 1,25-$(OH)_2$D, promoted by the enzyme cytochrome P450 CYP27B1. Different molecules act as indirect or direct regulators of the relative biosynthetic pathway (Fig. 4).

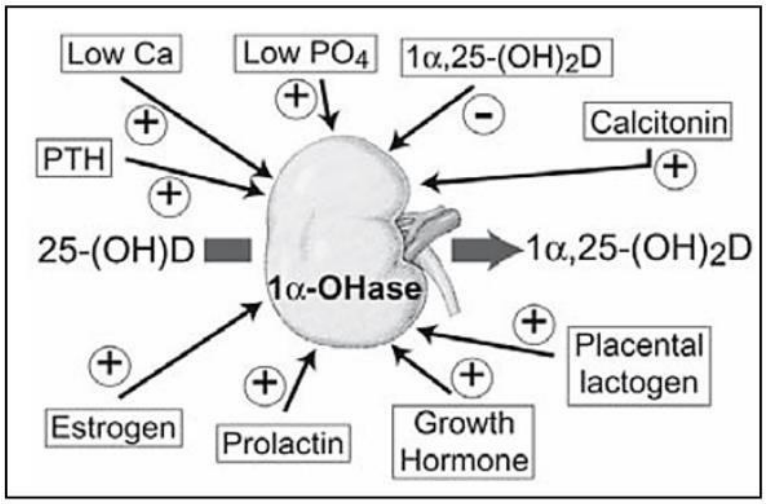

Fig. 4 - Regulating the production of 1,25-$(OH)_2$

Low blood levels of Ca^{2+} (hypocalcemia) stimulates the conversion of 25-OHD to the active 1,25-$(OH)_2$D in the proximal renal tubule of the kidney, while normal or high blood levels of Ca^{2+} (normal/hypercalcemia) promote the catabolic enzyme P450 CYP24A1, which converts 25-OHD to the 24,25-$(OH)_2$D. Hypophosphatemia (low blood levels of Pi) stimulates the renal activity of CYP27B1 and the production of 1,25-$(OH)_2$D; while hyperphosphatemia (high blood levels of Pi) inhibits the conversion of 25-OHD to the active 1,25-$(OH)_2$D [1], [2], [19]. In vitro experiments have shown that the insulin-like growth factor 1 (IGF-1) increases the hypophosphatemia, which in turn promotes the activity of the CYP27B1 enzyme [20]. Parathyroid hormone (PTH), secreted by the

parathyroid glands, induces the expression of CYP27B1 resulting in a rise of 1,25-$(OH)_2$D and it suppresses the expression of CYP24A1. Moreover, the PTH secretion is stimulated by the hypocalcemia and inhibited by the growth factor of fibroblasts 23 (FGF23), which exerts its inhibitory effect on the biosynthetic pathway of the 1,25-$(OH)_2$D. FGF23 inhibits CYP27B1 activity and 1,25-$(OH)_2$D synthesis and induces the expression of CYP24A1. 1,25-$(OH)_2$D itself, by negative feedback, acts on the metabolic vitamin D pathway; it inhibits the secretion of PTH and it determines an over-expression of FGF23. Moreover the 1,25-$(OH)_2$D is a very strong inducer of 24-hydroxylase expression (CYP24A1), and thus induces its own catabolism [1], [2], [16], [20].

1.4. Assessment of vitamin D status

25-OHD is currently considered as the most indicative marker of vitamin D status. In fact, it is the most abundant metabolite in the blood, has a relatively long half-life (2-3 weeks) and its concentration represents the sum of the endogenous synthesis of vitamin D and its intake [2], [13], [15], [21]. It is also considered a good marker of the ability of extra-renal tissues to produce the bioactive molecule 1,25-$(OH)_2$D, since it is assumed that the concentration of the circulating 25-OHD is positively correlated to the synthesis of the bioactive molecule. Although 25-OHD reflects vitamin D status rather well, its immunometric assay, which are widely used in clinical diagnostics, presents some limitation. Immunoassay is not able to discriminate 25-monohydroxy-vitamin D2 (25-OHD2) from 25-monohydroxy-vitamin D3 (25-OHD3). In addition, its accurate quantification requires its preliminary separation from the proteins that ensure its transport (DBP and ALB). For these and other reasons there is the hypothesis that other surrogate markers of vitamin D metabolism can

better reflect pathophysiology and predict its clinical outcome with greater accuracy. 1,25-$(OH)_2D$ may be available candidate because it is the bioactive molecule, but its blood concentration, which is regulated by PTH, Ca^{2+}, FGF23 and Pi, is about three orders of magnitude lower than that of the 25-OHD and this makes dosing extremely difficult. In addition, some pathological conditions can lead to an alteration in the metabolism of 1,25- $(OH)_2D$ and therefore to incorrect clinical interpretations. This is the case of subjects with VDD who undergo secondary hyperparathyroidism, a complication that stimulates the renal expression of the enzyme CYP27B1 and consequently determines normal or even high serum concentrations of 1,25-$(OH)_2D$. Finally, its half-life is very short (4-8 hours) and this results in extreme intra-individual variability [1], [2], [16]. Nevertheless, the quantification of this metabolite is useful for the evaluation of hypercalcemia conditions, associated with granulometric disorders or congenital disorders of the action of vitamin D, for the monitoring of vitamin D status in chronic kidney disease patients and for the monitoring of therapy with active vitamin D metabolite [22].We can therefore conclude that the information derived from the 25-OHD and 1,25-$(OH)_2D$ levels is complementary and both useful for diagnostic purposes.

1.4.1. BAVD and the ratio of 25-OHD to 24,25-$(OH)_2D$

Another possible marker of vitamin D status is bioavailable vitamin D (BAVD), which is the fraction of vitamin D not bound to DBP, and thus able to cross the cell membrane thus becoming a substrate available for enzymatic conversion to 1,25-$(OH)_2D$[23], [24]. However, even the use of BAVD has limitations mainly related to the absence of a reliable direct quantification method; therefore, the concentration is currently estimated on the basis of that of 25-OHD, DBP and

ALB, although the analysis of the latter two is still rather critical due to the lack of accurate dosing methods [24]. A metabolite that has recently aroused considerable interest is the 24,25-$(OH)_2$D which is the product of the direct conversion of 25-OHD, catalyzed by the enzyme CYP24A1. There is therefore a direct correlation between the concentrations of the two substrates (black population: r=0,86, p<0,001; Caucasian population r=0,90, p<0,001) [25] and their ratio ([24,25-$(OH)_2$D]/[25-OHD]), called Vitamin D metabolite ratio (VMR), which is an indicator of bone health and is, inter alia, useful for the prevention of mutation-induced hypercalcemia of the CYP24A1 enzyme, or as part of the diagnostic workup, in patients with hypercalcemia of unknown etiology [26]. In addition, VMR is indicative of the response to vitamin D3 supplementation: higher levels of 24,25-$(OH)_2$D, and therefore higher VMR, are associated with a lower risk of hip fracture, although 25-OHD is not directly associated with hip fracture risk [1], [2], [27]. Accurate measurement of 24,25-$(OH)_2$D is now possible thanks to methods based on LC-MS (liquid chromatography coupled to mass spectrometry), and even can be dosed simultaneously with 25-OHD [28]. This analytical technique offers, in fact, two significant advantages: a) proteins are eliminated during the preparation of the sample and therefore the quantification of the analyte is not affected by DBP or other proteins present in the matrix; b) the high specificity of the analytical method makes possible to minimize the effects of the presence in the matrix of interfering metabolites of 24,25-$(OH)_2$D. Serum concentrations of 24,25-$(OH)_2$D are still very low, in the nanomolar order (1.1-13.5 nmol/L), and instrumental sensitivity may not be sufficient for accurate dosing, even when very sensitive spectrometers are used. In this case, derivatization of the sample may be

necessary to modify the structure of the analyte to increase its response in MS [29]–[31].

1.5. The autocrine and paracrine physiology of 1,25-$(OH)_2D$

Vitamin D is classically mentioned for its primary involvement in the regulation of calcium and phosphorus metabolism (the endocrine action of the active metabolite, 1,25-dihydroxyvitamin D, has been well-characterized to contribute to maintaining plasma calcium and phosphate homeostasis through regulation of intestinal absorption); however recent studies have shown that the VDR receptor, which binds the bioactive molecule 1,25-$(OH)_2D$, is also expressed in several cell types unrelated to the metabolism of such elements, including immune cells, enterocytes, myocytes, neurons and glial cells. These evidence suggest that vitamin D3 has an autocrine action (that is, the activity of vitamin D3 arises from 1,25-$(OH)_2D$ synthesised within those cells), and/or a paracrine action (that is 1,25-$(OH)_2D$ is synthesised in one cell type and acts within adjacent cells). Such activities of vitamin D have been best characterised in skin tissues and the immune system where it regulates cell differentiation and maturation as well as the innate immune system. Recent data are now available to implicate autocrine/paracrine activities in each of the major bone cell types where it also regulates cell proliferation and differentiation. Thus 1,25-$(OH)_2D$ is involved not only in skeletal metabolism, but also in many other physiological processes which determine extra-skeletal effects [1], [3], [16].

1.5.1. The skeletal effects of vitamin D

As regards the involvement of vitamin D in the metabolism of calcium and phosphorus, this contributes to ensuring adequate levels of these elements for

metabolic functions and bone mineralization [1], [10], [16], [27]. The target cells of the 1,25-(OH)2D express on their surface the VDR receptor, and these cells are found in the intestine, kidney, and bone (osteoblasts). At the renal and intestinal level, mainly at the level of the small intestine, it determines the increase in the reabsorption of Ca^{2+} and Pi. As far as the Ca^{2+} resorption is concerned, it is known that the ligand-receptor binding effect is the activation of a signal transduction pathway that stimulates the expression of the epithelial Ca^{2+} channel (ECaC, TRPV5), Ca^{2+} transport protein subtype 1 (CaT1,TRPV6) and calbindins D9K and D28K, which are a vitamin D-dependent calcium binding protein. Ca^{2+} spreads from the intestinal lumen into the cytosol of the cell, is bound to calbindins D9K or D28K and pumped into the blood through the plasma membrane calcium ATPase (PMCA1b) and NCX1 (sodium/calcium exchanger) (Fig. 5). CaT1 and ECaC are remarkably calcium-selective channels which serve as apical calcium entry mechanism in absorptive and secretory tissues. A major difference between the properties of TRPV5 and TRPV6 lies in their tissue distribution: TRPV5 is predominantly expressed in the distal convoluted tubules (DCT) and connecting tubules (CNT) of the kidney, with limited expression in extrarenal tissues. In contrast, TRPV6 exhibits a broader expression pattern, showing prominent expression in the intestine with additional expression in the kidney, placenta, epididymis, exocrine tissues (i.e., pancreas, prostate, salivary gland, sweat gland), and a few other tissues. Thus, while TRPV5 plays a key role in determining the level of urinary Ca^{2+} excretion, the physiological roles of TRPV6 are not limited to intestinal Ca^{2+} absorption [20] CaT1 in the intestine is highly responsive to 1,25-dihydroxyvitamin D3 and shows both fast and slow calcium-dependent feedback inhibition to prevent calcium overload. In contrast,

ECaC only shows slow inactivation kinetics and appears to be mostly regulated by the calcium load in the kidney. Outside the calcium-transporting epithelia, CaT1 is highly expressed in exocrine tissues such as pancreas, prostate, and salivary gland. In these tissues it probably mediates re-uptake of calcium following its release by secretory vesicles [13], [32].

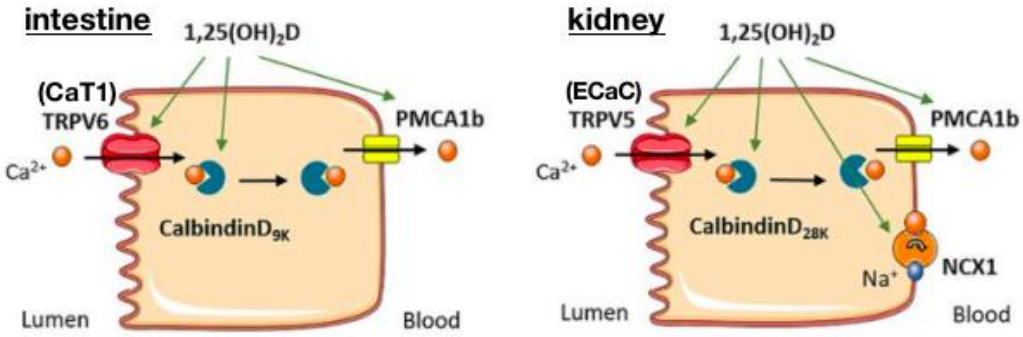

Fig. 5 - Resorption of Ca^{2+}.

In addition, vitamin D acts on the metabolism of calcium and phosphorus also indirectly, through the reduction of PTH levels. In fact, the parathyroid glands, site of synthesis of PTH, also have expression of the enzyme CYP27B1 [19], [33]; 25-OHD is then internalised by parathyroid cells and converted, by activity of the enzyme CYP27B1, into 1,25-$(OH)_2$D, which acts in intracrine mode going to reduce the production and secretion of PTH [17]. It is therefore obvious that the VDD state is associated with lower levels of Ca^{2+}, which leads to an increase in PTH levels. The variation in PTH levels has a direct impact on bone metabolism, since parathyroid hormone has the following effects:

- stimulates the production of the metabolite 1,25-$(OH)_2$D;
- stimulates the activity of osteoclasts through osteoclastogenesis, and then bone resorption. Both PTH and 1,25-$(OH)_2$D determine, at the level of osteoblasts, the over-expression of the RANK ligand (RANKL), whose

receptor (RANK) is expressed on the surface of the preosteoclast, hematopoietic precursors of osteoclasts. As a result of the RANK-RANKL bond, preosteoclasts become mature osteoclasts and provide for the removal of calcium and phosphorus from bone for the maintenance of the right blood levels [3, 18].

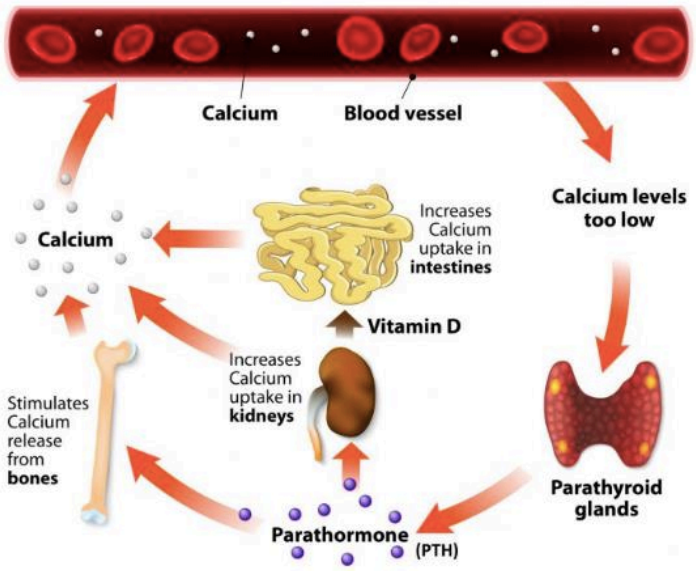

Fig. 6 - Traditional Ca2+, parathyroid hormone (PTH), and vitamin D axis for regulation of Ca2+ homeostasis

In 2018, Shieh *et al.* subjected 25 subjects aged ≥18 to aggressive repletion of vitamin D for a duration of 16 weeks, to evaluate the possible physiological role of BAVD at the level of renal cells and parathyroid cells. In fact, it is known that in the serum of healthy individuals more than 99.9% of the total 25-OHD is linked to DBP or ALB, while only a quantity less than 0.1% is in its free form. From this survey it emerged that the early increase (from the basal level to 4 weeks) in BAVD is strongly associated with increasing levels of 24,25-$(OH)_2$D, chosen as a downstream biomarker of 25-OHD in renal cells, and decreasing levels of PTH, chosen as a biomarker downstream of the entry of 25-OHD into parathyroid cells.

This result was unexpected because both renal and parathyroid cells express megalin, which acts as a receptor of the vitamin D-DBP complex; it could be hypothesized that at the renal level, the production of 24,25-$(OH)_2$D is more efficient in those districts that do not express megalin, or that BAVD is physiologically relevant even at the level of those tissues that express megalin. Between 4 and 16 weeks, with reference to the increase in levels of 24.25-$(OH)_2$D, direct proportionality with the increase in levels of 25-OHD total, and with reference to the decline in levels of PTH, no correlation was found. This suggests that once 25-OHD levels begin to stabilize, that is after the fourth week, the metabolite's entry into the renal cells is guided by megalin; therefore, only DBP-bound 25-OHD will pass into the cytosolic environment, while at the parathyroid cell level, the entry of the metabolite is no longer physiologically significant and the expression of PTH is mainly regulated by the calcium-sensitive receptor, which inhibits its secretion [17]. In addition, in reference to the skeletal effects of vitamin D, several preclinical studies have shown that the metabolite 24,25-$(OH)_2$D can also play a role in the development and maintenance of the skeleton. In fact, it would seem that it may have a beneficial effect on bone mass. In particular, from a study conducted on a group of patients aged 1-18 years with osteogenesis imperfecta (OI), the most frequent primary bone fragility disorder in children and adolescents, it emerged that serum 24,25$(OH)_2$D levels were significantly higher in OI type III than in OI type I or IV (differences between the different types of OI will be described in the next paragraph). Moreover, when type III OI was present, serum 24,25$(OH)_2$D concentrations were positively correlated with serum 25OHD levels and negatively correlated with serum PTH levels and were not correlated with serum

1,25$(OH)_2$D; this is consistent with the results obtained from in vitro studies, which showed that PTH negatively regulates the renal activity of the enzyme CYP24A1. However, there was no correlation between these concentrations and lumbar bone mineral density (LS-aBMD) or biochemical bone markers, confirming that there is no difference in bone mass or bone metabolism between patients with different forms of OI. The increase in serum levels of 24,25-$(OH)_2$D, in patients with type III OI, seems induced by an increase in the activity of the enzyme CYP24A1, which affects the amount of vitamin D that must be fed to reach the optimal serum level of 25OHD. The reasons for an increase in activity are unclear, but experiments conducted on experimental animal models (mice) showed that during the repair of fractures, which in OI type III patients are extremely frequent, circulating levels of 24,25-$(OH)_2$D increase. In addition, if mice are knock-out for CYP24A1, there is a chronic delay in healing fractures, which is resolved by administering suitable amounts of 24,25-$(OH)_2$D [34].

1.5.2. Osteogenesis imperfecta

Osteogenesis imperfecta (OI) represents a heterogeneous group of pathologies characterized by susceptibility to bone fractures, with varying severity, and in most cases presumed or proven defects of type I collagen biosynthesis. Other clinical manifestations include short stature, blue sclera, imperfect dentinogenesis and hearing loss. According to the 1979 classification of Sillence et al., which is still in force, there are four types of OI [34]–[37]:

- OI Type I: patients who do not have major bone deformities and whose height falls or is close to the reference range;
- OI type II: usually lethal in the perinatal period;
- OI type III: more severe form in children surviving the neonatal

period; patients are very small in stature and have deformities in the limbs and spine that are secondary to multiple fractures;

- OI Type IV: Patients of variable short stature with mild to moderate bone deformities [34].

1.5.3. The extra-skeletal effects of vitamin D

As regards the extra-skeletal effects of vitamin D, it is generally known that the VDR receptor, which has as a ligand the active metabolite 1,25-$(OH)_2$D, is expressed in a wide range of cell types and this supports the hypothesis that vitamin D can have a wide variety of functions [1], [3][38].In reference to this, several years ago a role of vitamin D in the regulation of the immune system was also proposed [4], [6], [10], [39]. It has been shown that vitamin D has pleiotropic immunomodulatory properties [10], and the active metabolite of vitamin D, 1,25-$(OH)_2$D, is also produced by macrophages; in addition, the VDR receptor has also been isolated from activated human inflammatory cells [40]. The expression of the cytochrome P450 enzyme CYP27B1, which catalyzes the conversion of the metabolite 25-OHD into 1,25-$(OH)_2$D, is also expressed in other immune cells (e.g dendritic cells, epithelial cells, B cells, activated T lymphocyte and in APCs-antigen presenting cells), which are able to respond to vitamin D not only in endocrine and paracrine mode but also intracrine mode [41]. Experimental studies have shown that 1,25-$(OH)_2$D generates immunologic activities on the innate and adaptive immune system and endothelial membrane stability. 1,25-$(OH)_2$D promotes the innate immune response and inhibits the adaptive immune response [4], these immunologic activities are mediated by the VDR receptor. After the ligand binding, the VDR receptor, located in the nucleus, forms a heterodimer with the retinoid X receptor (RXR) which corresponds to the active form of the transcription factor. The latter is able to bind vitamin D-response

elements (VDREs), which are localized at the level of the promoter region of the genes regulated by vitamin D, and in this way the expression of genes involved in immunity is modulated [42].

The most important effects of metabolite 1,25-$(OH)_2$D on the immune system are listed below:

- Its presence is necessary for the maintenance of the tight joints of the epithelial cells of the epidermis and mucous membranes. 1,25-$(OH)_2$D induces the expression of occludin (Zonula occludens proteins, ZO-1 and ZO-2), connexin 43 (Cx43), and E-cadherin [43], [44]. These proteins are important for the maintenance of the epithelial physical barriers of innate immunity.

- It stimulates the synthesis of anti-microbial peptides, such as cathelicidins (LL-37 and hCAP18) and β2-defensins (DEFB) by macrophages and epithelial cells; these peptides disrupt the membrane of pathogens and neutralize endotoxins, thus helping to reduce virulence and microbial load [45], [46]. In general, it is known that in the innate immune response the Toll-like receptors (TLRs), belonging to the family of pattern recognition receptors (PRRs), play a key role. TLRs respond to exogenous infectious ligands (pathogens-associated molecular pattern, PAMPs), and they can recognize the possible presence of pathogens. The exposure of TLRs to PAMPs results in activation of the NF-kB (nuclear factor kappa-light-chain-enhancer of activated B cells) transcription factor that becomes free to migrate into the nucleus thus promoting the expression of target genes. The various effects observed include the expression of anti-microbial peptides, over-expression of the VDR receptor and the CYP27B1

enzyme, which in turn enhances the expression of anti-microbial peptides (positive feedback circuit) [42], [45], [47]. However, it has emerged that, 1,25-$(OH)_2$D inhibits the expression of TLR2 and TLR4 while promoting the expression of their CD14 co-receptor; based on this study it has been hypothesized that inhibition of PRR expression in the APCs may be a mechanism to prevent hyper-inflammation mediated by helper-1 T cells (Th1) and a possible autoimmune reaction [39], [48]

- It induces autophagy in several cell types including monocytes and tumor lines, by increasing the concentration of Ca^{2+} ions in the cytoplasm; as a result of the bond 1,25-$(OH)_2$D-VDR there is the activation of a signal transduction pathway that affects the expression levels of calcium regulatory proteins, this phenomenon leads to stress of the endoplasmic reticulum (RE) and causes over-expression of the antimicrobial cathelicidin protein (hCAP18/LL-37) resulting in activation of surface receptors that mobilize Ca^{2+} ions. The increase of the cytosolic levels of Ca^{2+} leads to the activation of the protein Ca^{2+}/calmodulin-dependent kinase kinase-β (CaMKK-β), a powerful inductor of the autophagic process through the activation of AMP-kinase (AMPk) that determines the inactivation of the target rapamycin complex-1 (mTORC1). Moreover, in monocytes it was found that hCAP18 (human cationic antimicrobial protein) over-expression increases the levels of the LL-37 peptide and this leads on the one hand to over-expression of beclin-1 and ATG5 (Autophagy related 5) and, on the other hand, promotes the maturation of autophagosomes in autolysosomes [49].

- It induces apoptosis, in fact it has emerged that through a mechanism

dependent on caspase 3 it determines over-expression of the pro-apoptotic protein Bim [42].

- It stimulates the cytotoxic activity of natural killer cells (NK) involving PKC (protein kinase C) and extra-cellular Ca^{2+} ions, which have been shown to be factors mediating the exocytosis process of the pre-formed granules containing hydrolytic molecules (e.g. serine esterase, perforine) [50].
- Improves the expression of membrane glycoprotein ACE2 *(angiotensin converting enzyme 2)* [51].
- It induces the polarization of the macrophage towards the M2 phenotype. The M2 macrophage inhibit the inflammatory response through secretion of interleukin-10 (IL-10) and transforming growth factor-β (TGF-β), through TIM-3 (T-cell immunoglobulin and mucin domain-containing-3) over-expression [52].
- It affects the maturation of naive $CD4^+$ T cells in T helper-2 (Th2) and regulatory T cells (Treg) (Fig. 7). It suppresses the production of interleukin-12 (IL-12), interleukin-6 (IL-6) and interleukin-23 (IL-23) [39], [45], [53]. In contrast to its inhibitory effects on inflammatory cytokines, 1,25-(OH)2D3 stimulated expression of high levels of transcription factor forkhead box P3 (FoxP3) and cytotoxic T-lymphocyte antigen 4 (CTLA-4). These results suggest that $1,25\text{-}(OH)_2D3$ acts as a potent anti-inflammatory agent and physiologic inducer of adaptive Tregs [53], [54].
- It suppresses the proliferation of resting $CD4^+$ T cells with a synergic anti-

inflammatory action of IL-2 [54].

- It affects the interaction between APC cells and naive T cells. In reference to dendritic cells (DC), it inhibits their differentiation from monocytes, in addition it has an inhibitory effect on the maturation of these cells through the suppression of the MHC-II (expression of the greater complex of histocompatibility of class II) and co-stimulator ligands [55]; in reference to macrophages it may regulate the interaction of monocytes with T cells, promoting the differentiation of naive T lymphocytes into Th1 lymphocytes; it reduces the production of the expression of cytokines pro-inflammatory, mainly interferon-γ (IFN-γ), inteleukin (IL)-1β, tumor necrosis factor (TNF)-α and the expression of surface co-stimulating molecules (CD80, CD86) [56].
- It promotes programmed cell death (apoptosis) of activated B cells and inhibits their differentiation into plasma cells and memory cells [40], [57].

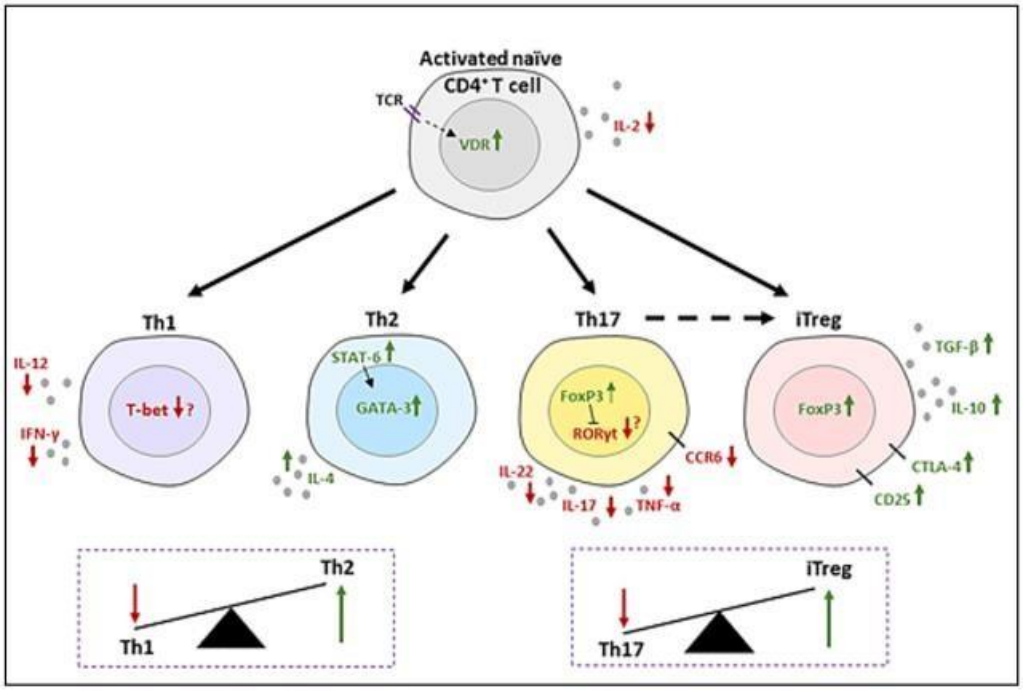

Fig. 7 - Vitamin D and $CD4^+$ T lymphocytes maturation

1.5.4. Vitamin D and respiratory infections

Pulmonary epithelium is the first line of defense against airborne infectious viruses and microorganisms; it has emerged that lung epithelial cells are also able to convert the circulating 25-OHD into the active metabolite 1,25-$(OH)_2$D. Hence the hypothesis that the immune response to pulmonary infections, from which derives the risk of occurrence and severity of lung disease, may depend on adequate 25-OHD concentration levels [38], [46], [58]. A meta-analysis showed that vitamin D supplementation reduces the risk of acute respiratory infections. So that, a daily/weekly vitamin D supplementation provides protection against infections, with greater protective effects in those subjects with very low basal levels of vitamin D, while supplementation with a massive dose not fractionated in time, does not lead to the same effect. On the basis of these results, Vieth *et al.* proposed that the supplementation with a massive dose of vitamin D determined the dysregulation of the enzymes involved in the synthesis and catabolism of its active form, 1,25-(OH)2D3, resulting in a decrease in its concentration in extra-renal tissues [11]. Thus, the state of VDD could increase the risk of infection and the incidence of autoimmune diseases [4], as suggested by several studies showing an inverse correlation between VDD and increased susceptibility to respiratory infections, such as acute severe pneumonia, community acquired pneumonia (PAC), sepsis, acute respiratory distress syndrome (ARDS), heart failure and secondary mortality from lung infections [38], [45], [46], [58], [59]. In fact, the direct consequence of the VDD state is the reduction of the expression levels of the VDR receptor, which causes denaturation, cornification, and proliferation of the respiratory epithelial mucosa, with drastic impairment of clearance function and accumulation of pro-inflammatory molecules, which

trigger uncontrolled inflammatory reactions [58]. In general, antimicrobial effects mediated by vitamin D appear to be transient, ranging from differential regulation of immune response to regulation of pathogenesis in a direct or indirect way [39].

1.6. The new coronavirus SARS-CoV2

There are three coronaviruses capable of causing, by overcoming the species-specific barrier, fatal pneumonia in humans: they are *coronavirus of severe acute respiratory syndrome* 1 (SARS-CoV), *coronavirus of severe acute respiratory syndrome* 2 (SARS-CoV2), and the *coronavirus of Middle Eastern respiratory syndrome* (MERS-CoV) [60]. SARS-CoV2 is a single-stranded positive-sense RNA (ssRNA) virus of about 30.000 bases (30 kb), which belongs to the Order Nidovirales, Family Coronaviridae, Subfamily Orthocoronavirinae, Genus β-coronavirus, Subgenus Sarbecovirus, Species Severe acute respiratory syndrome-related coronavirus and individuum SARS-CoV-2 with the addition of the strain/sequence, e.g., SARS-CoV-2 Wuhan-Hu-1 as the reference strain. This virus could rather easily transmit from person to person and rapidly spread worldwide, causing the respiratory illness known as Coronavirus disease 2019 (COVID-19). For clarity, SARS-CoV-2 is the name of the virus, and coronavirus disease 2019 (COVID-19) is the name of the disease it causes. SARS-CoV-2 was declared a pandemic by the World Health Organization on March 11, 2020. As of July 6, 2020, there have been 11 565 541 SARS-CoV-2 infections in the world, with 536658 deaths. The virions are approximately spherical or moderately pleomorphic, therefore with heterogeneity of aspect, with a diameter of approximately 60-140 nm. The coronavirus virion is made up of the

Nucleocapsid (N) protein, membrane (M) protein, envelope (E) protein and Spike (S) protein, each of these structural proteins being essential to compose the viral particles. S protein is assembled as a homotrimer and is inserted in multiple copies into the membrane of the virion giving it, if observed under the electron microscope, its crown-like appearance, while membrane glycoprotein (M) and envelope protein (E) give the ring structure (Fig. 8) [61], [62]. Several similarities have emerged between SARS-CoV and SARS-CoV2, including origin (in bats). Indeed, there is an increasing number of data suggesting that SARS-CoV2 is a chimeric virus, with a high degree of affinity with the genome of a bat coronavirus [61]. Unlike SARS-CoV, for which the intermediate host for zoonotic transmission is known, several hypotheses have been put forward for SARS-CoV2, but no certainty exists [60]. In general, the viral genome (Fig. 8) contains 14 open reading frames (ORFs) that encode for 27 proteins in the SARS-CoV-2 genome. The genes ORF1ab and ORF1a are located at the 5′-end of the SARS-CoV-2 genome. ORF1ab is the largest gene. It encodes the polypeptide (pp) 1ab protein and 15 non-structural proteins (nsps) (nsp1–10 and nsp12–16), while the ORF1a gene encodes pp1a protein, which contains 11 nsps (nsp1–11).

The ORFs, at the 3'UTR end, codes for the four structural proteins (Spike, envelope, membrane, and nucleocapsid proteins) [63]–[67], and a 8 of accessory proteins (3a, 3b, p6, 7a, 7b, 8b, 9b and ORF14), some of which share less than 80% nucleotide sequence identity with SARS-CoV.

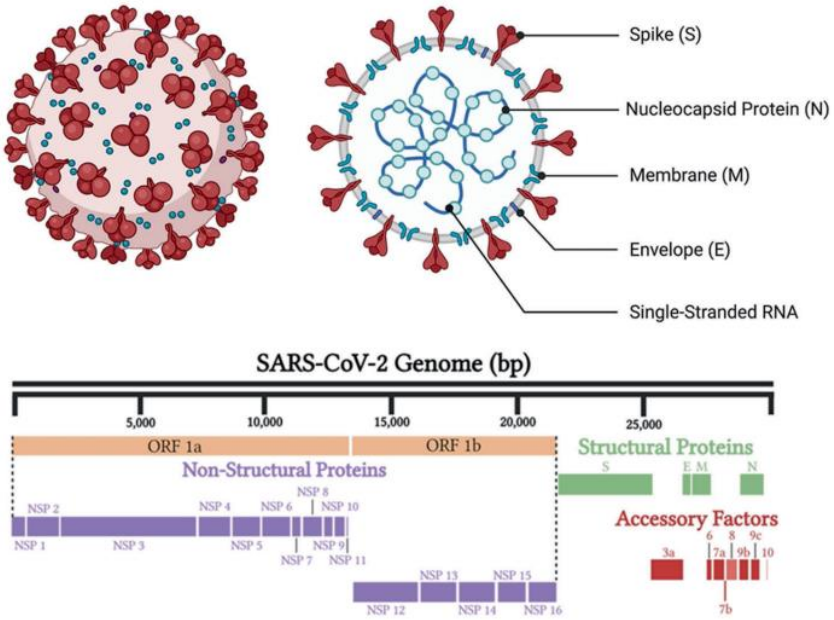

Fig. 8 - Human SARS-CoV-2 structure. Structural elements of the virus, including the spike protein, envelope, membrane, and internal components such as the viral single-stranded RNA and nucleocapsid proteins (above). SARS-CoV-2 genome components (below).

The analysis of the amino acid sequence of the seven domains of the replication system, encoded by ORF1ab and used for the classification of CoV species, showed that these shares 94.4% of identity with SARS. This suggests that these viruses belong to the same species. Simplot analysis has shown that the coronavirus genome BatCoVRaTH13 presents a total genomic sequence identity of 96.2% with SARS-CoV2; moreover, by phylogenetic analysis of the genome and genetic sequence of RdRp (RNA polymerase-dependent RNA) and of S glycoprotein has been shown that, for all sequences, RaTH13 is the closest relative of SARS-CoV2 [66].

1.7. SARS-CoV2 interaction with target cells

Viruses are obligate intra-cellular parasites that must enter target cells and usurp the host cellular machinery to produce a progeny virus for their own replication and diffusion. The entry of the coronavirus into the target cells is mediated by glycoprotein S that is organized into homotrimers, which protrude on the viral surface membrane. Each monomer of glycoprotein consists of two subunits:

- Subunit S1: it is composed of 672 amino acids and organized into four domains, a N-terminal domain (NTD), a C-terminal domain (CTD), which is also known as the *receptor binding domain* (RBD), and two subdomains (SD1-SD2). RBD is responsible for ligand-receptor binding, thereby mediating virus binding to the surface of the target cell; in addition, it contributes to stabilization of the perfusion state of the S2 subunit.
- S2 subunit: it is a transmembrane subunit composed of 588 amino acids. It forms the stalk, promotes structural rearrangements and is responsible for the fusion of the viral membrane with the cell membrane [68]. It comprises various α-helical secondary structural motifs, including the FP (fusion peptide) domain, a short segment (15-20 aa) composed mainly of hydrophobic residues, which mediates the anchorage to the cell membrane, the HR1 domain, which is located at the C-terminal end of the FP domain, the HR2 domain, located at the N-terminal end of the TM (trans-membrane domain) domain which, downstream, mediates the anchorage of glycoprotein S to the viral membrane, central helices (CH), connector domain (CD), SH, and cytoplasmatic tail (CT), which form a fusion-competent state after cleavage at the S2' sites [68]. SARS-CoV and several SARS-related coronaviruses (SARSr- CoV) interact with the host receptor directly through their (SB)

domain. The receptor binding SA or SB (depending on which CoV species) determinants are transiently exposed (up-conformation) or hidden (down-conformation) through a hinge-like movement. SARS-CoV-2, just as SARS-CoV, uses ACE2 as its receptor for entry into cells. ACE2 was discovered 20 years ago and received its name because of its homology with ACE. ACE2 is a type I transmembrane glycoprotein with a single zinc metalloprotease active site that acts as a monocarboxypeptidase cleaving a single amino acid, always phenylalanine. In fact, ACE2 cleaves the phenylalanine amino acid from Ang II to form Ang 1–7 and from Ang I to form Ang 1–9. To determine whether SARS-CoV2 also uses ACE2 as a cellular entry receptor, Zhou P. *et al.* conducted virus infectivity studies using HeLa cells that expressed or did not express ACE2 proteins from humans, Chinese horseshoe bats, civets, pigs and mice. (Fig. 9) [64].

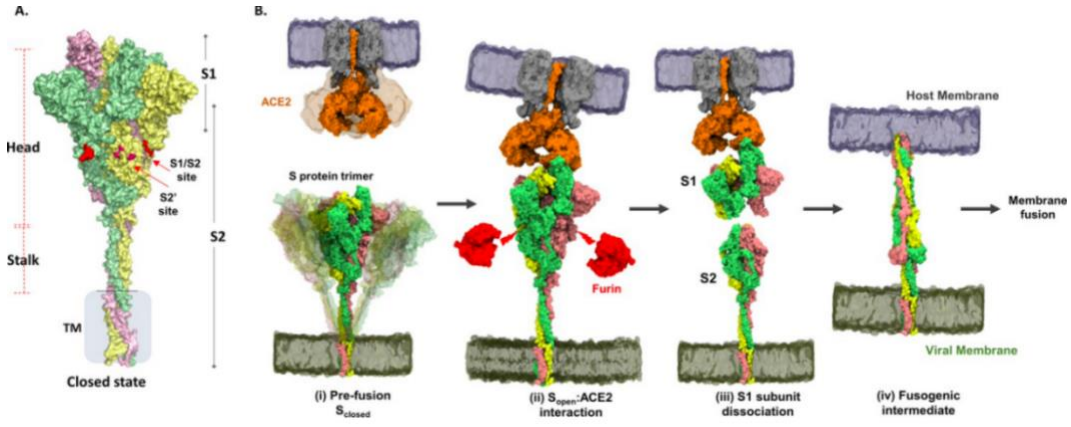

Fig. 9 - Structure and domain organization of trimeric spike (S) protein showing steps in the virus–host entry initiated by S recognition and binding to angiotensin-converting enzyme 2 (ACE2) receptor.

Several studies have been shown that the sequence similarity of the RBD region of SARS-CoV and SARS-CoV-2 S protein is between 73 and 76%. Fourteen residues of the SARS-CoV S protein RBD have been reported to interact with

human ACE2 (Fig. 10). These are Tyr436, Tyr440, Tyr442, Leu443, Leu472, Asn473, Tyr475, Asn479, Gly482, Tyr484, Thr486, Thr487, Gly488 and Tyr491. Only eight of these residues are conserved in SARS-CoV-2. The equivalent conserved residues in SARS-CoV-2 are Tyr449, Tyr453, Asn487, Tyr489, Gly496, Thr500, Gly502, and Tyr505, while Leu455, Phe456, Phe486, Gln493, Gln498 and Asn501 are substituted. Recent studies have highlighted that SARS-CoV-2 S RBD binds to ACE2 with a higher binding affinity compared to SARS-CoV S RBD, since the latter was linked to five substituted residues. Importantly, SARS-CoV-2 residues Gln493 and Asn501 (Asn479 and Thr487 in SARS- CoV) are located near viral binding hotspot residues Lys31 and Lys353 on human ACE2. It has been reported that SARS-CoV-2 residues Gln493 and Asn501 target these hotspot residues more efficiently than SARS-CoV. Additionally, Leu455, Phe486 and Gln498 of SARS-CoV-2 have also been suggested to interact with these hotspot residues more favourably than equivalent residues of SARS-CoV, thereby enhancing the ability of SARS-CoV-2 to bind to ACE2. Evaluation of the binding of SARS-CoV-2 and SARS-CoV RBDs with ACE2 have revealed more hydrogen bonds and electrostatic interactions in SARS-CoV-2.

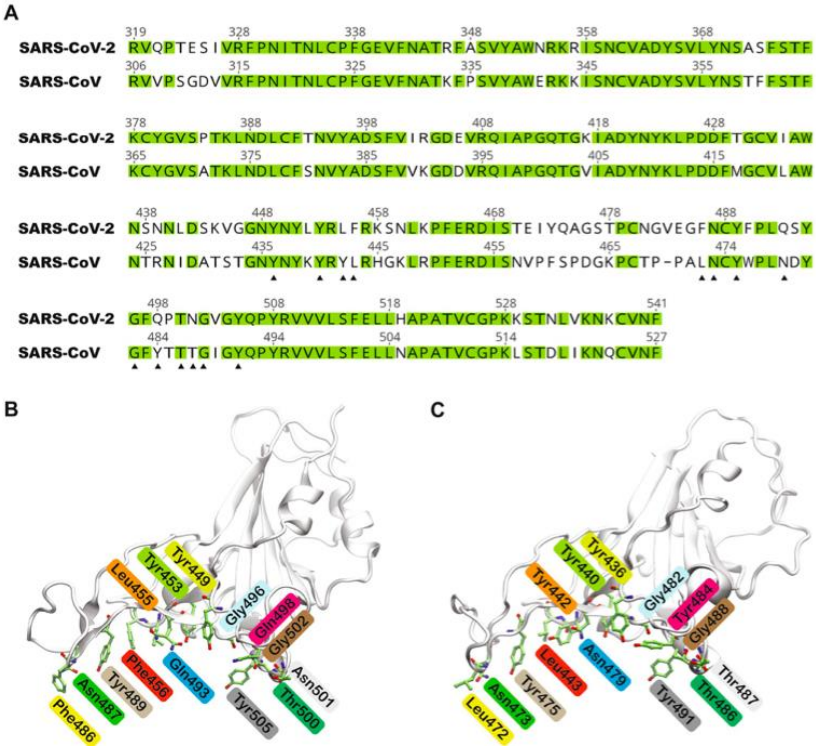

Fig. 10 - (A) Sequence alignment of the SARS-CoV-2 and SARS-CoV S protein RBD.(B) Structure of the SARS-CoV-2 S protein RBD with the fourteen residues shown in green stick representation. (C) Structure of the SARS-CoV S protein RBD with the fourteen residues shown in green stick representation.

Recent studies confirm that the RBD portion of SARS-CoV2 binds to ACE2 with greater affinity than the RBD portion of SARS-CoV [69]. After the ligand-receptor bind there is the intervention of host cell proteases, including TMPRSS2 serine 2-protease, which catalyse the cleavage of glycoprotein S into subunits S1 and S2 by binding to one of the furin cleavage sites located at the interface between the S1 subunit and the S2 subunit. In this way there is the transition from the prefusional conformation to the hairpin one (conformation that mediates the coupling). In the hairpin conformation there is the exposure of the FP domain that, therefore, is free to go and insert itself in the membrane of the target cell. Following the anchoring, HR1 located near the cell membrane, folds to HR2, located near the viral membrane, going to form a 6 helix structure and, in this

way, there is the fusion of the two membranes resulting in the release in the cellular cytoplasm of the viral genome [62], [68].

1.8. Coronavirus disease 2019 (COVID-19)

With reference to SARS-CoV2, on 11 March 2019 the World Health Organization (WHO) declared COVID-19 a global pandemic disease [62]. The main mode of transmission, from person to person, is represented by saliva or respiratory secretions (respiratory droplets), which are excreted when a person coughs, sneezes, or speaks. Although most cases are symptom-free or mild, including cough, pharyngitis, hyposmia (total or partial inability to smell), nasal congestion, and rhinorrhea, some cases present as acute respiratory distress syndrome (ARDS), with rapid progression towards septic shock, severe manifestation of sepsis (syndrome characterized by malfunctioning of several organs simultaneously) to which are added increased lactic acid in the blood, indicative of cellular suffering, and low blood pressure [64], [70]–[73]. A study carried out on a sample of patients infected with SARS-CoV2 to establish their clinical and laboratory characteristics showed that people over 50 years of age are more likely to develop more severe symptoms. This may be due to the fact that with age increases the risk to develop comorbidity; this is consistent with the fact that in the sample of subjects analyzed hypertension, cardiovascular disease and diabetes mellitus were the most common "underlying" diseases [74]. In these pathologies, the administration of inhibitors of the renin-angiotensin-aldosterone system (RAAS) represents the key point of the therapeutic approach, and in particular ACE-I (*angiotensin-converting enzyme inhibitors)* and ARBs (*angiotensin II receptor blockers*) are administered. ACE-I increase the

expression and activity of ACE2, while ARBs promote the activity of ACE2. The daily use of these drugs may lead to increased susceptibility to infection but, on the other hand, it has been shown that, as a result of infection pathways is a reduction in and levels of ACE2 expression resulting in excessive production and Ang-II, and then progression towards pneumonia, so the Administration of ACE-I/ARBs could prevent the occurrence of severe lung injury [61], [69], [75].

1.9. Diagnostic methods for the identification of SARS-CoV2

It has been shown that asymptomatic and pre-symptomatic subjects are still capable of transmitting the infection; hence the importance of having accurate and efficient diagnostic tests available to identify infected subjects and therefore, counteract the spread of the virus [76]. On 22 May 2019, the database held by the foundation for Innovative New Diagnostics, which is the WHO Collaborating Centre for Laboratory Strengthening and Diagnostic Technology Evaluation, contained 560 lSARS-CoV2 laboratory tests for the diagnosis of COVID-19. These comprised 273 molecular assays and 287 immunological assays [77]. Current diagnostic tests to identify SARS-CoV2 infection are based on the detection of nucleic acid, antibodies, and proteins [78].

1.9.1. Diagnostic tests based on nucleic acid detection.

Case identification and monitoring of SARS-CoV2 diffusion is mainly carried out by the molecular diagnostic method *reverse transcription-polymerase chain reaction* (RT-PCR). PCR is a quantitative method to amplify or increase, the amount of a specific DNA sequences, in this case for SARS-CoV2 (Fig. 11) [62].

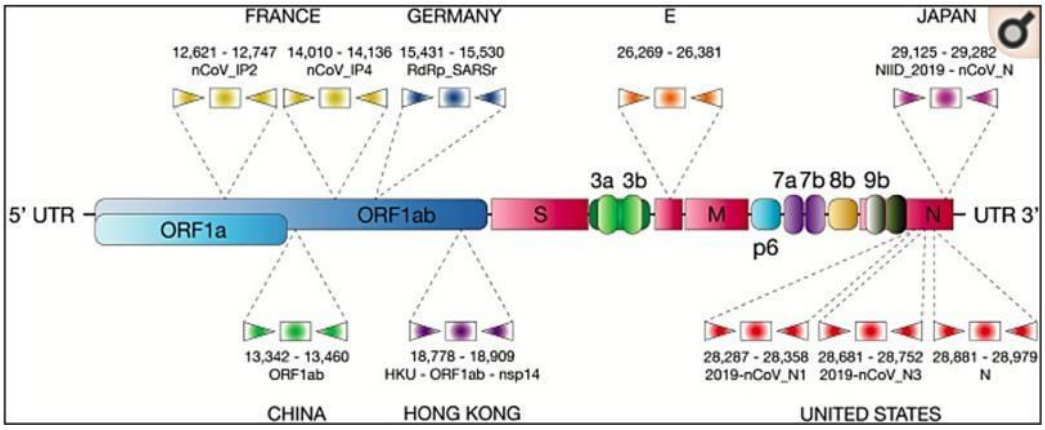

Fig. 11 - Relative positions of Primers pairs on the SARS- CoV2 genome.

Viral RNA is extracted from the clinical sample obtained by nasopharyngeal or oropharyngeal swabs and via reverse transcription it is converted into cDNA; if the cDNA, which represent the template filament, contains the specific target sequence, it will undergo amplification. The amplification process leads to in the generation of double stranded DNA molecules (dsDNA). The amplification process is monitored in *real time* through the use of a fluorescent molecule (SYBRGreen method), or a combination of a quencher, cDNA complementary DNA probe, and reporter (TaqMan method).It has been shown that RT-PCR SARS-CoV2 tests have a detection limit of less than 10 copies/reaction and this limit, in the incubation or in the final stages of infection where there is a low viral load, can lead to false negatives; as well as mutations in the target sequence may cause false positives, despite the high specificity of the test. Although the RT-PCR method is the gold standard for the diagnosis of SARS-CoV2 due to its high sensitivity, specificity, and ability to process a large number of samples, its widespread use is hampered because it requires expensive laboratory instruments and qualified laboratory personnel; about this, some companies have developed

high-productivity equipment with automatic extraction, assembly and detection. The automatic equipment reduces some problems such as unavailability of reagents, consumables, and qualified personnel, and it accelerates the time of analysis [62], [76], [77]. As an alternative to the RT-PCR diagnostic method, the *isothermal amplification mediated by reverse transcription loops* (RT-LAMP) test has been developed, which is highly sensitive, infact it can detect SARS-CoV2 specifically even if it is present at low copies [79]. Loop-Mediated Isothermal Amplification (LAMP) is an amplification reaction, which takes place under isothermal conditions (62-65 ºC) and in a single step, based on the synthesis of "strand-scaling" DNA with automatic cycle in which four to six Primer, and a DNA polymerase is used, with high exonuclease activity. In general, when four Primers are used, two internal Primers, one forward and one reverse, respectively called FIP (*forward inner primer*) and BIP (*backward inner primer*), and two external Primers will be used (Fig. 12). In the case of RNA samples, LAMP is preceded by a retrotranscription and synthesis of the cDNA, which is complementary to the template RNA filament. Recently, a point-of-care test for the detection of SARS-CoV2 based on this technology and able to provide positive results in just 5 minutes and negative results in 13 minutes, it has received permission EUA (emergency use authorization) to use in an emergency by the Food and Drug Administration (FDA) of the States [62]. The latest technological approach for molecular diagnosis of SARS-CoV2 was presented by Ackerman *et al.* and is represented by the detection platform "Combinatorial Arrayed Reactions for Multiplexed Evaluation of Nucleic acid (CARMEN)", which is able to identify the possible presence of a whole range of infections in a given sample, including SARS-CoV2 infection [80]. In detail, a single chip is

able to identify a specific viral strain in over a thousand samples or, different types of viral strains in a few samples. This technology uses a CRISPR RNA (crRNA) sequence, which includes a complementary trait to the target sequence, complexed with Cas13, which is different from other Cas proteins. Cas13 digests only RNA and not DNA and exerts its action on any RNA molecules it encounters. The presence of the target sequence, and therefore pairing with the trait of crRNA complementary activates Cas13 (CARMEN principles). The enzyme, in its active form, will catalyze the cleavage of both on-target RNA (in a cis manner), and a Single-stranded RNA (ssRNA) reporter sequence (in trans mode). ssRNA consists of a quencher and a fluorophore joined by a short RNA oligomer; the separation of the fluorophore from the quencher causes subsequent emission of the fluorescent signal. The process starts with isothermal amplification of the target RNA sequence, by *recombinase reverse transcription polymerase amplification* (RT-RPA) in which a forward primer is used. The forward primer adds a T7 promoter to the amplified RNA and allows its transcription. In detail (Fig. 12), for each amplified RNA sample a unique color code is assigned through the addition of a dye, then the sample is emulsified with oil in order to generate droplets (droplets) of 1 nanoliter. At the same time are also produced the detection mixtures, containing the reporter probe and the crRNA sequence complexed with Cas13, and they are also assigned a unique color code, based on the target sequence to which the crRNA sequence stroke is complementary, and create droplets. The droplets are placed in a single tube, pipetted, and loaded into a micro-well array polydimethylsiloxane (PDMS) chip. Each micro-well of the chip is capable to accommodate two droplets and, in this way, from a probabilistic point of view, all possible combinations are generated

and therefore, each amplified RNA sample is exposed to each detection mixture, in multiple replicates and in different positions. Following the application of an electric field each pair of droplets, contained in each micro-well, melts and if there is pairing of the target sequence with the crRNA sequence, for complementarity of the bases, then Cas13 is activated and catalyzes the splitting of the reporter probe resulting in the generation of a fluorescent signal, indicative of a particular viral infection in the person from whom the sample comes [79]–[85].

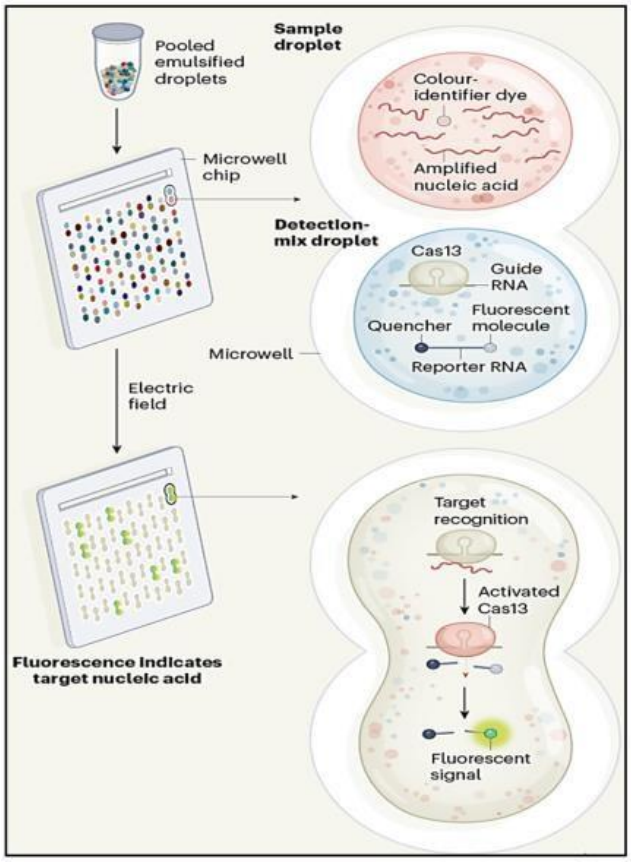

Fig. 12 - Schematic representation of the CARMEN-Cas13 platfor

1.9.2. Diagnostic tests based on antibody detection.

The synthesis of antibodies directed against SARS-CoV2 is a part of the primary immune response to the infection; in particular, neutralizing antibodies are found, by the seventh day, in 50% of infected individuals and, by the fourteenth day, in all infected individuals [78]. Immunoglobulin G (IgG), M (IgM) e A (IgA) are taken into consideration as potential markers for COVID-19, these imunnoglobulin can be detected through traditional methods, such as colloidal gold-based immunochromatographic assay (GICA), magnetic chemiluminescence enzyme immunoassay (CLIA) and enzyme-linked immunosorbent assay (ELISA) [86]. Rapid immunological tests (POC) have also been developed for the rapid detection of IgM and IgG directed against SARS-CoV2. These tests are generally based on lateral flow immunoassay (LFIA). The primary advantage of these tests is to obtain a diagnosis without sending samples to centralized laboratories. The identification of subjects exposed to SARS-CoV2 can be carried out by analyzing a drop of blood obtained with the "finger pricks". A further advantage is the low cost of production, storage, and distribution [77]. However, they cannot be used for diagnosis acute phase of the disease but represent an indication of infection that should be used to confirm late cases of COVID-19 or to assess the immunity of healthcare professionals [79]. Such tests could also be used, to understand how many individuals have been affected from COVID-19 and how many have developed immunity [77].

1.9.3. Protein detection diagnostic tests (viral antigens)

Enormous efforts have been made to develop rapid tests to detect SARS-CoV2 antigen, tests designed for direct detection of viral particles in biological samples from the respiratory tract such as nasopharyngeal secretions. The possible antigen, in these tests, is only detected if the virus is actively replicating. When the SARS-COV2 antigen is present it is bound to the antibodies affixed to a strip of paper that is enclosed in a plastic casing. As a result, the generation of a visually detectable signal (within half an hour) indicates an acute or early infection. These diagnostic tests, as well as those based on the detection of antibodies, have the advantage of rapid diagnosis, ease of interpretation and limited technical skills and infrastructure required, while the main limitations are represented by sensitivity and specificity [77], [78]

1.9.4. SARS-CoV-2 LC-MS Kit (RUO)

The SARS-CoV-2 LC-MS Kit (RUO) enables the direct detection and quantification of SARS-CoV-2 Nucleocapsid (NCAP) peptides, without the need to amplify the target analytes as required for PCR. The application of LC-MS to detect tryptic digest peptides of SARS-CoV-2 proteins has been successfully demonstrated. However, these studies also highlight that the technique suffers from matrix effects due to interferences arising from the constituent components of the sample matrix, such as viral transport medium (VTM), limiting the analytical sensitivity of the methods. Therefore, to improve detection levels, there is a need for sample clean-up and enrichment. The Kit allows for the quantification of viral proteins to be used alongside infection biomarkers to identify potential prognostic biomarkers or investigate the impacts of the virus in

research studies. The workflow includes denaturation, digestion, enrichment, and UHPLC-MS/MS analysis of three peptides; AYNVTQAFGR (AYN), NPANNAAIVLQLPQGTTLPK (NPA), and ADETQALPQR (ADE) derived from the SARS-CoV-2 NCAP protein. The samples are denatured with a Waters proprietary denaturant (RapiGest) at 56 °C for 15 minutes and digested with Trypsin solution at 37 °C to generate tryptic peptides. The three SARS-CoV-2 NCAP peptides are selectively captured along with their associated stable labelled internal standard using anti-peptide antibodies immobilized onto magnetic beads to facilitate the enrichment process. The peptides are washed to remove unbound matrix/sample interferences and eluted as a clean and concentrated sample, ready for UHPLC-MS/MS. The calibration range was shown to be linear from 3–50000 amol/μL across the three peptides, thus SARS-CoV-2 LC-MS Kit (RUO) is able to reveal SARS-CoV-2 at very low concentration [87].

1.10. Host defense against SARS-CoV2 infection.

With regard to the response against viral SARS-CoV2 infection, a synergistic participation of both innate and adaptive immunity has been demonstrated, with significant relationship between the severity of pathology, levels of cytokines pro-inflammatory and immune cell subsets. In fact, COVID-19 disease, in its most aggressive form, consists of a hyperinflammatory syndrome due to the excessive production of pro-inflammatory cytokines (cytokine storm) and dysfunction of the immune response, leading to chronic inflammation resulting in tissue damage. It is generally known that the innate immune response counteracts viral infections mainly through the production of the interferon-type cytokine I (IFN-α e IFN-β) by the infected cell and the plasma cytoid cells, and through killing infected cells by NK cells. In fact, very often in virus infected cells there is a reduced expression of MHC that leads to disparity between activating and inhibiting receptors of NK cell activity. The production of IFN type I is mediated by several biochemical signals including the binding of viral nucleic acid to endosomial TLR, cytoplasmic RIG-like receptors (viral RNA) or viral STING (viral DNA); these allow the activation of a signal transduction pathway, which converges on the interferon factor (IRF) regulation, which promotes the expression of IFN-α e IFN-β. The IFN type I are bound to the receptor for IFN type I, expressed ubiquitously. The activation of a transduction of the signal that stimulates the expression of genes involved in different antiviral mechanisms, and in particular resulting as:

- expression of genes whose products inhibit viral replication by binding to the type I IFN receptor, expressed on the surface of cells not yet infected;
- a segregation of lymphocytes in lymph nodes, increased cytotoxicity of

NK cells and cytoxic T cells, and differentiation of naive T cells into Th1 lymphocytes;

- expression of class I MHC proteins, binding to the type I IFN receptor, expressed on the surface of infected cells, increasing the susceptibility of the cell to killing by cytotoxic T cells.

Adaptive immunity is mediated by antibodies, effective against viruses at the early stage (before the virus enters the target cell) and when the virus, as the consequence of the lysis of the infected cell, is released into the extra-environment cell. In viral infections the antibodies mainly play a neutralizing action, prevent the viral entry into the target cells and promote the activity of phagocytic cells. With regard to cytotoxic T cells, antiviral effects are mainly due to their ability to kill infected cells; but there are also other mechanisms that can contribute to their antiviral activity, including the secretion of antiviral cytokines, as IFN-γ, that activates the phagocytes [70], [71], [88]–[90].

1.10.1. The cytokinic storm

Cytokinic storm is a common feature of patients with severe symptoms of COVID-19, and is a major cause of ARDS and multiple organ failure.It consists of a complex network of severe molecular events, unified by a clinical phenotype of systemic inflammation and multiorgan failure. It can be a consequence of lung, gastrointestinal, urinary, central nervous system (CNS) and other body districts infections. In general, the intensity of the inflammatory response reflects a balance between pro-inflammatory cytokines and a number of factors that modulate their activity including, the presence of similar soluble receptors/ inhibitors that, going to bind to them, modulate the availability, the production of

anti-inflammatory cytokines and the regulation of the activity of specific cell types. If one or more of these mechanisms fails, the result can contribute to a cytokine storm, in which there is excessive or uncontrolled release of pro-inflammatory cytokines. In the serum, of the patients with severe COVID-19 symptomatology, among the numerous molecules whose level is found to be increased they are INF-γ, IL-1β, IL-6, IL-12, IL-17, and the tumor necrosis factor α (TNF-α) [90], [91].

1.11. Immunophenotype of COVID-19 patients

Several studies have been conducted to try to identify "an immune signature" associated with the pathology, despite the heterogeneity of the characteristics of the host (for example, ethnicity, age, sex, presence of comorbidity). With this in mind, a study was published on a highly heterogeneous cohort of 63 patients with COVID-19 to identify common immunological traits in peripheral blood. From this emerged a number of shared immunophenotypic characteristics, including:

- presence of high levels of specific SARS-CoV2 antibodies; presence of plasmablasts, immature forms of plasma cells; presence of IL-6, which is a pro-inflammatory cytokine produced mainly by activated macrophages and dendritic cells; presence of IL-8, which is a chemokine stimulating chemotaxis, mainly neutrophils and monocytes, and their phagocytic activity; presence of IL-10, a anti-inflammatory cytokine, which is produced mainly by macrophages (negative feedback mechanism). IL-10 stimulates the proliferation of B lymphocytes, and therefore their differentiation into plasma cells and memory cells; presence of chemokine *interferon γ-inducedprotein 10* (IP-10), whose receptor is highly expressed on the surface of cytotoxic Th1, T, natural killer (TNK) and NK cells. IP-10 stimulates chemotaxis. In particular, it was demontrated that increased levels of plasmablasts, IL-6, IL-10 and IP-10 is related to the severity of COVID-19 pathology;
- altered composition of B cells population with significant reduction of B1 lymphocyte subpopulation ($CD5^+$).
- drastic depletion of plasmacytoid dendritic cells (pDC) that, unlike classical DC, are poorly phagocytic but, following a viral infection, differentiate into

cells similar to DC and present viral antigens to T cells in addition to secreting high levels of IFN-α;

- increase of not completely mature forms of monocytes and neutrophils;
- reduction of NK cell levels
- drastic reduction in T ϒδ lymphocyte levels, therefore of those T cells which, unlike the cells T αβ (classical T cells), express TCR receptors (T cell receptor) formed, not by the polypeptide chain α e β, but by the polypeptide chain ϒ e δ. While, in reference to αβ T cells, there is selective depletion of T cells helper-17 (Th17) e Th1;
- increased frequency of effector T cells (TEM), both T helper and cytotoxic lymphocytes, therefore lymphocytes CD25CD4 e CD25CD8 (CD25 is α chain of IL-2 receptor and is the T cell activation marker). However, in severe cases, a marked reduction in naive T cells, cytotoxic T_{EM} and cytotoxic central memory T lymphocytes was observed (T_{CM}), cells that if stimulated by APC cells proliferate and differentiate into T_{EM} [92].

1.12. Age, a factor involved in the degree of severity.

A number of studies have shown that age is one of the factors involved in the degree of severity of the disease, there after it is found the presence of SARS-CoV2 there is an increased risk of developing a symptomatic infection and progression towards criticality [93], and in old age the sequence of events that occurs in response to infection, is altered and the anti-inflammatory signaling pathways are not activated efficiently. One of the consequences of aging is a decrease in the synthesis of the enzyme ACE2, which is a pro- inflammatory condition. In a study in rats of both sexes with three distinct ages (young adults: 3

months, middle-aged: 12 months, elderly: 24 months), able to determine the expression of ACE2 in the lung and the effect of aging and gender on it emerged that with aging itself the expression is drastically reduced in both sexes, with males undergoing a more drastic decrease [94]. In particular, another study showed that subjects over 60 years of age have a higher risk of developing symptoms and that females have a 52.7% lower probability of developing chronic diseases [93].

1.13. Angiotensin converting enzyme 2

Angiotensin converting enzyme 2 (ACE2), glycoprotein belonging to the family of dipeptidil-carboxypeptidases of angiotensin conversion [95], is expressed on the surface of different cell types, including alveolar epithelial cells of type I and type II of the lung, cells of the nasal, oral, and nasopharyngeal mucous [96]. It has remarkable homology with the enzyme ACE, a monomeric transmembrane glycoprotein type I expressed in the lungs, intestines, kidneys, brain, aorta, and adrenal medulla; and as a whole have key functions in the RAAS system. While ACE catalyzes the conversion of angiotensin to AngII, through the cleavage of two amino acids, ACE2 catalyzes the conversion of Ang II into Ang (1-7) [61], [97]. The RAAS system controls plasma sodium concentration, blood pressure and extra-cellular volume, playing a fundamental role in the regulation of homeostasis of the organism [98]. ACE2, via ACE2/Ang (1-7)/Mas, acts as a negative regulator of this system. In detail, ACE2 regulates AngII levels through catalysing the AngII conversion reaction to Ang (1-7), which binds to Mas receptors resulting in activation of a signal transduction pathway that has vasodilator, antiproliferative, anti-inflammatory and antifibrotics effects. Specifically, the ACE2/Ang (1-7)/Mas pathway counteracts the

ACE/AngII/AT1R pathway, in which the ACE enzyme catalyzes the conversion of angiotensin into AngII, which can bind to two distinct receptors: the type 1 angiotensin receptor (AT1R) and the type 2 angiotensin receptor (AT2R). AT1R binding leads to activation of a signaling cascade responsible for mediating the "classical" effects of AngII, including vasoconstriction, stimulation of aldosterone release, increased renal tubular sodium resorption, fibrosis, and inflammation; while the one with the AT2R receptor leads to the activation of a signaling cascade that counterbalances the effects induced by the ACE/AngII/AT1R signal transduction pathway [61], [99]. In COVID-19 syndrome, the RAAS system can represent a double-edged weapon in fact, it has been shown that, the over-expression of ACE2 has a positive impact, suggesting its protective role against lung damage in patients infected with SARS-CoV2; however, at the same time, with increased enzyme expression there is a risk of increasing susceptibility [61].

1.14. Respiratory distress syndrome.

As a result of infection with SARS-CoV2 few subjects have been developed acute respiratory distress syndrome (ARDS). Sepsis, pneumonia, and shock are the most common conditions predisposing to ARDS. Other typical predisposing conditions include gastro-pulmonary aspiration, trauma, and massive blood product transfusion. Atypical respiratory infections, including viral (influenza) and fungal (Pneumocystis jiroveci, Histoplasma spp., Blastomyces spp.) infections, are unusual but important causes of ARDS, especially in patients with compromised immune systems. Several pathogens, such as severe acute respiratory syndrome (SARS-CoV and SARS-CoV2), Middle East respiratory syndrome-coronavirus, and epidemic H1N1 influenza, increased risk for ARDS. Additional patient risk factors include gastroesophageal reflux disease, chronic silent aspiration, and drug exposures [100]. ARSD is the most serious form of acute lung injury; it is a clinical syndrome characterized by a high mortality rate (30-60%) caused by alveolar, capillary, and epithelial damage, which often rapidly proceeds in the onset of renal failure, cyanosis, and severe potentially progressive arterial hypoxia towards multiple organ failure [71], [97], [101]. In general, it is known that the alveolar-capillary membrane consists of two separate portions, which are respectively the microvascular endothelium and the alveolar endothelium; in ARDS one, or more commonly, both of these portions are compromised; in the latter case this syndrome leads to increased vascular permeability, loss of surfactant and makes the alveolar unit unable to expand. Although the molecular and cellular mechanisms of ARDS are not yet well defined in detail, it has been suggested that the diffuse lung damage results from an imbalance between pro- and anti-inflammatory mechanism. In detail, when

pulmonary macrophages are exposed to inflammatory stimuli, they increase the production of pro-inflammatory cytokines such as TNF, IL-1, IL-6, IL, and IL-8, which is a powerful chemotactic factor, and it activates neutrophils. This causes the activation of the endothelium and a consequent migration of neutrophils. In fact, neutrophils migrate from pulmonary microvascular circle to the alveolar interstitium, where they secrete factors that cause the damage (Fig. 13) [101].

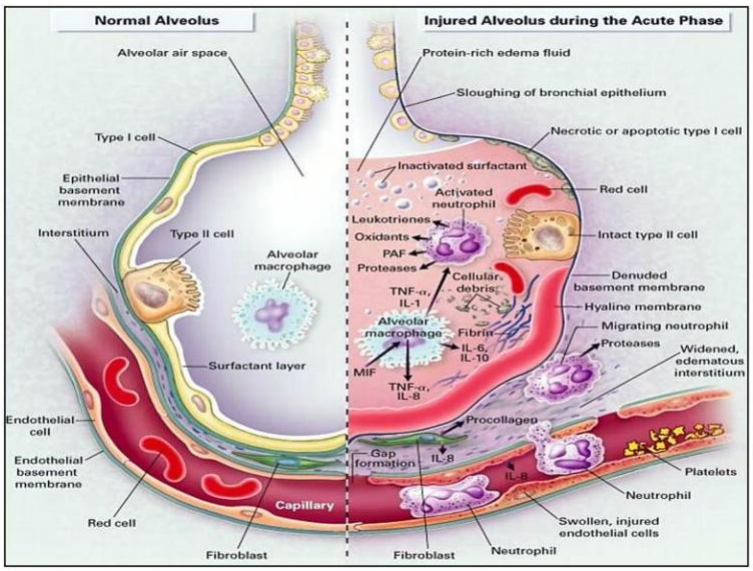

Fig. 13 - Schematic representation of alveolar-capillary barrier in a normal alveolus and a injured alveolus during the acute phase of ARDS.

In a study aimed to understanding the pathogenesis of ARDS and carried out on mouse models, it was found that both the enzyme ACE2, via the ACE2/Ang (1-7)/Mas pathway, and the AT2R receptor have a protective role against acute lung injury, while the ACE enzyme, via the ACE/AngII/AT1R pathway, promotes the pathogenesis of ARSD [97].

1.15. Cardiovascular implications of the COVID-19

Although it was initially reported as a cluster of pneumonia cases, it quickly became apparent that COVID-19 is not merely a respiratory tract infection. Cardiovascular complications are also possible and contribute significantly to mortality associated with COVID-19. It has been shown that subjects infected with SARS-CoV2, with pre-existing cardiovascular diseases, have a higher risk of developing severe symptoms, but cardiovascular complications can also be a direct consequence of infection. A recent study conducted on 41 patients with COVID-19, in Wuhan, demonstrated that a first cardiovascular complications is myocarditis, which is an inflammation of the heart muscle with myocardial lesions associated with SARS-CoV2 infection. 5 of these patients (12%) had troponin I at high levels to above the threshold of 28 pg/ml; subsequently it has been shown that myocardial lesions with a high level of troponin can occur in 7-17% of hospitalized patients infected with SARS-CoV2 and in the 22-31% of hospitalized patients admitted to the intensive care unit (ICU)[102]. In United States and other developed countries, the most common cause of myocarditis is viral infection. In the case of COVID-19, myocarditis could be due to the high expression of ACE2 in the cardiovascular system and in the cardiac pericytes, alternatively, it could be caused by systemic infection due to cytokines generated by an unbalanced response from Th1 and Th2 lymphocytes. A third possible mechanism, which can lead to cardiovascular damage, is hypoxemia due to acute respiratory dysfunction caused by COVID-19. In fact, pneumonia, due to infection, causes a significant alteration of the gas exchange that leads to hypoxemia which, in turn, causes a significant decrease in energy intake by cellular metabolism, with increased anaerobic fermentation, a subsequent intra-

cellular acidosis and generation of oxygen free radicals (ROS). ROS damage the phospholipids of the cell membrane; at the same time the inflow of calcium ions, induced by hypoxia, leads to heart disease lesions and therefore apoptosis [103], [104].

1.16. The COVID-19 vaccines

The SARS-CoV2 gene sequence was published on 11 January 2020. Since then, scientists, industries and other organizations around the world have worked together to develop safe and effective vaccines. The vaccines approved to date are based on two different vaccine platforms: the anti-COVID-19 vaccine ChAdOx1-S produced by Oxford University and AstraZeneca, and Ad26.COV2.S produced by the pharmaceutical company Janssen (Johnson & Johnson), are viral vector vaccines, while the COVID-19 vaccine mRNA BNT162b2 (Comirnaty) produced by Pfizer e BioNTech, and mRNA-1273 produced by Moderna, are messenger RNA (mRNA) vaccines. Although there are substantial differences between the two types of vaccines, they all carry the gene information of the SARS-CoV2 virus protein S, so that, following the transient expression of this, there is the trigger of the immune response. Vaccines based on nucleic acids and viral vectors must undergo the translation of nucleic acid into immunogenic protein within the host cell. Therefore, if a vaccinated person comes into contact with SARS-CoV2, his immune system will recognize protein S and be ready to intervene [105].

1.17. Vitamin D and COVID-19 disease

A number of studies have been carried out to assess a possible association of vitamin D levels and outcomes of SARS-CoV2 infection, in particular COVID-19 related severity and mortality, a negative correlation has emerged from these studies [6], [106], [107]. Radujkovic et al. analyzed vitamin D levels in outpatients and hospitalized patients (inpatients =patients admitted). This study showed that patients admitted had significantly lower average vitamin D levels than outpatients, and they presented a greater risk of requiring invasive mechanical ventilation (IMV). However, the lack of high quality randomized controlled trials (RCTs) to investigate the impact of vitamin D on SARS-CoV2 infection, makes difficult to determine with certainty the relationship between vitamin D status and severity of COVID-19 [100]. The lack of information mainly due to the lack of standardization and robustness of the methods by which vitamin D deficiency levels and the optimal supplementation dose are determined.

1.17.1. Factors influencing vitamin D status

There are several factors that adversely affect vitamin D levels and at the same time increase COVID-19 susceptibility and mortality:

- Age: Ageing adversely affects vitamin D levels mainly due to lower sun exposure, endogenous synthesis [2], [38] and it is known that age is a factor involved in the severity of COVID-19 disease;
- Seasonality: limited exposure to the sun during the winter when living above and below approximately 33° latitude, leads to a reduced endogenous synthesis of vitamin D3; it is known that the outbreak of COVID-19 developed

in winter, with fewer cases (hospitalization and death) in the southern hemisphere and high mortality in northern hemisphere [78];

- Increased skin pigmentation: skin pigmentation decreases vitamin D synthesis; it is known that in the African-American population of the United States there is an increased COVID-19 morbidity and mortality [46], [108].
- The Diet: in addition to endogenous synthesis, fish and dairy products represent an important source of vitamin D and these foods are consumed in high quantities in the Scandinavian countries (Norway and Denmark); it is known that Scandinavian population have vitamin D deficiency rates of 15-30% and COVID-19 much less severe than other countries such as Italy, Greece and Spain (Europe), which have vitamin D deficiency rates of around 70-90% and COVID-19 has been more severe [109].
-

1.17.2. The anti-inflammatory effects of vitamin D

Vitamin D exerts pronounced impacts on the ACE2/Ang (1-7)/Mas axis, inducing an increase in the expression of ACE2 receptor that is exploited by SARS-CoV2 to enter in the target cells. Therefore, vitamin D could increase the risk of infection [39], [48]. However, it is known that one of the most severe complications of COVID-19 disease is ARDS [62], where ACE2 has been shown to play a protective role [97]. In addition, it has been shown that the complement system is an important instrument in pathogen clearance via recruitment and activation of immune cells. The conversion of Th1 effector cells into cells which produce IL-10 is promoted by the complement system, thus vitamin D/paracrine cycle is self-regulated. Complement factor 3 (C3) is cleaved to generate activation fragments, of which C3b binds CD46 receptors on T cells. We have

shown that CD4+ T lymphocytes in the lungs of patients with COVID-19 have a CD46-activated signature. CD46, engaged by T cell-generated C3b in an autocrine fashion, works co-operatively with T cell receptor stimulation to drive both Th1 differentiation and subsequent T cell shutdown. In reference to the phase of arrest of Th1 cells, it was found that, as a result of ligand-receptor binding, there is the expression of a whole series of target genes including VDR. Thus, the silencing of the expression of IFN-γ and interleukin-17 (IL-17) and the expression of IL-6 and IL-10 are indicative of the conversion of the metabolite 25-OHD into the active metabolite 1,25-$(OH)_2$D. 1,25-$(OH)_2$D, binding to VDR, induces a cascade of events leading to the activation of the expression of STAT3 and IL-6. IL-6, acting in autocrin/paracrin mode, and it promotes the expression of IL-10 through the phosphorylation of STAT3 [48].

1.18. Mass spectrometry

Mass spectrometry (MS) is an analytical technique that is used to identify the structure of organic molecules (untargeted analysis) and to determine unknown concentrations of substances or elements (targeted analysis). It is commonly combined with separative techniques such as gas chromatography (GC) or liquid chromatography (LC) and it is used for both characterization of unknown molecules and quantitative analysis of molecules with known structure. The basic principle of mass spectrometry is to generate ions from either organic and inorganic compound (ionization) by suitable methods, then separate them by their mass/charge ratio (m/z) and detect them qualitatively and quantitatively according to respective values of m/z and abundance. The ratio m/z, a dimensionless quantity by definition, is the ratio between the atomic mass (m), and the number of elementary charges of the ion (z) (regardless of sign) that is usually equal to 1 for the small molecules. The analytes of interest are introduced into the spectrometer source, where they are thermally ionized, by electric fields or by interaction with electrons, ions or photons thus acquiring positive or negative charges. Separation of ions is achieved by their interaction with static or dynamic electric and/or magnetic fields within the analyzer. After their separation, the ions arrive at the detector ordered according to their m/z ratio, were electric signals proportional to their ion abundance are generated. An analog to digital converter turns electric signals into digital ones, which are then processed by a data system that produces a mass spectrum, which is a diagram showing the relative abundance of ions as a function of their mass/charge ratio. [110] As mentioned above, to enhance selectivity and accuracy in the analytical determination, MS are commonly coupled to chromatographic techniques such

as GC or LC. These techniques separate the components of a complex mixture according to their different interaction with both the chromatographic column and the eluent mixture. Chromatography allows the introduction of each component of the mixture into the mass spectrometer at different times. The final result is a total ion current chromatogram, where signal intensity is related to the ion abundance of all compounds eluted by the column as a function of their retention time. In practice, the chromatogram is the result of the sequence of mass spectra from the eluate. In the last decade, tandem mass spectrometry with ionization by Electrospray Ionization Mass Spectrometry (ESI-MS/MS) coupled to high performance liquid chromatography (HPLC) has become an important investigation technique in clinical laboratories as it provides sensitive, robust and reliable results for the study of trace molecules in samples with a volume in the order of µl. ESI is a ionization technique suitable for the study of non-volatile and thermally labile molecules that cannot be analysed by other commonly used techniques. Moreover, mass spectrometry coupled to liquid chromatography (LC-MS/MS) has become a technique of choice in the laboratories because it allows the analysis of both large and small molecules with various polarities in complex biological samples [111].

1.18.1. ESI (Electrospray ionization)

ESI is considered as a "soft" ionization technique that uses high voltage to promote the ion transfer from the solution to the gas phase, at atmospheric pressure, without ion fragmentation. The ions formed are then directed towards the high vacuum zone of the analyser [110], [112]. ESI is widely used for the analysis of ionic analytes in solution or neutral analytes able to be easily

converted to ionic form in solution or in gaseous phase by a process of protonation, deprotonation or adduct formation. Adduct ions are formed by the interaction of the analytes with other species already endowed with positive or negative charge (cations or anions). ESI-MS is a technique suitable for the analysis of compounds with medium polarity or ionic compound with a molecular weight between 10 and 106 uma. The amount of sample that is required for the analysis depends on the concentration of the analyte, the structure of the compound and the flow of the mobile phase used for chromatography (Flow Rate) [111], [112]. The transfer of ionic species from solution into the gas phase by ESI involves three steps:

- Droplet Formation: Dispersal of a fine spray of electrically charged droplets
- Desolvatation: Solvent evaporation and reduction of the charged droplets size
- Gas Phase Ion Formation: Emission of ions in the gaseous phase

The LC flow passes through a capillary (~75 μm diameter) and a mist of highly charged droplets with the same polarity as the capillary voltage is generated. The nebulization capillary is maintained at a potential of 2.5-6 kV and the capillary tip is placed about 0.5-1 cm from the inlet of the mass spectrometer (vacuum zone). At the outlet of the capillary the liquid is exposed to a high voltage electric field that induces the separation of charge in the electrolytic solution until the formation of a cone, called the Taylor cone [113]. When a certain threshold voltage has been reached the slightly rounded cone tip inverts and emits a jet of liquid. The jet coming out of the cone apex cannot remain stable for a long time

but collapses into small droplets, which due to their charge move away from each other by Coloumb repulsion. This process results in the generation of a finely divided fog (plume) of charged droplets which gives rise to the term electrospray (Fig. 14) [114][115].

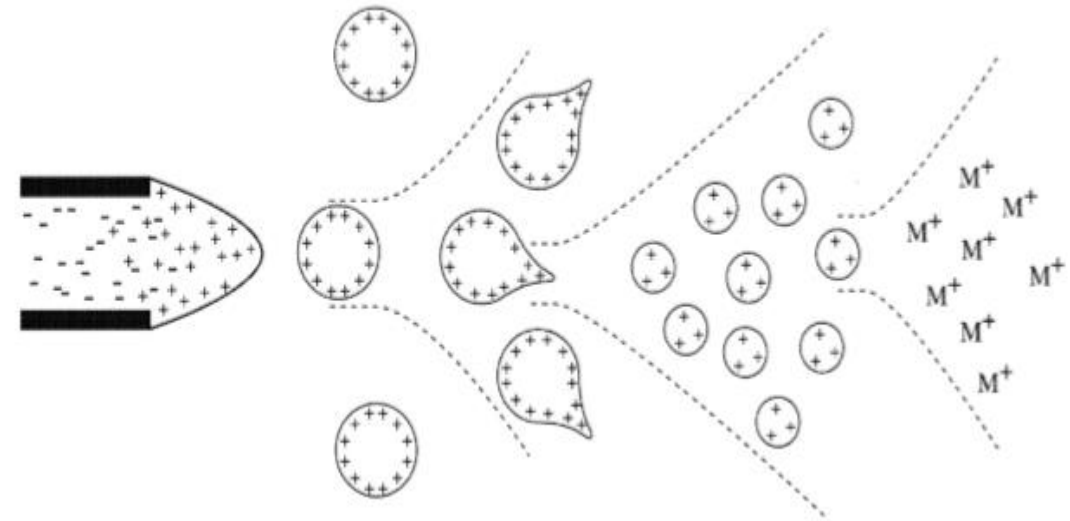

Fig.14 - Electrospray ionization.

When the solvent evaporates from a small droplet, this results in an increase in the charge density. As soon as the electrostatic repulsion force exceeds the conservative force of the surface tension, the droplet is divided into smaller particles. The point at which this phenomenon occurs is known as the Rayleigh limit and is a phenomenon that subsequently reproduces on the smaller droplets that form to generate micro-droplets of ever smaller dimensions [111].

The final stage of ion formation in ESI can be explained by two models (Fig.15):

Charged Residue model (CRM)

This model assumes that the complete desolvation of ions occurs by the subsequent loss of all solvent molecules by droplets that are small enough to contain only one analytical ion. At the end of a cascade process, the charges are part of the last droplet and transfer to the molecule and the ion is released when the solvent evaporates[116]. Important characteristics of this model are that the ionization rate is strongly independent of the ion. The generation of very small droplets and the efficiency of solvent evaporation determine the ion current and not primarily the physicochemical properties of the ion. The ionization process is not limited by the mass of the analyte. Noncovalent complexes can be expected to survive the process because they are cooled by solvent evaporation and do not have to overcome an energy barrier with subsequent acceleration in an electric field. The available charge to the molecule depends on the Rayleigh stability limit because the final droplet comes from a spraying process caused by a Taylor Cone.

Ion evaporation model (IEM)

This model explains the formation of ions by direct evaporation from the surface of heavily charged droplets, the energy required for this process is provided by the electric field. It has been observed that for ion evaporation an electric field of 109 V/m corresponding to that of a droplet with a diameter of 10 nm is required [117]–[119]. Droplets shrink by evaporation until the field strength at their surface is sufficiently large that solvated ions can be expelled from the droplet. There are three important characteristics of this process. The first is a geometric parameter: ion evaporation is expected to play a role when the droplet reaches a

very small size of about 20 nm in diameter. Second, the reaction rate kinetic is heavily influenced by chemical properties of the ion. The ion evaporation rate constant depends exponentially on the difference in reaction free enthalpy that needs to be overcome when the ion is expelled from the droplet. Even though the ion is solvated by a small shell, this is a function of the physicochemical properties of the ion itself. Finally, at the onset of ion evaporation, the surface charge density of the droplet is below the maximal possible surface charge density at the Rayleigh limit. In their early work, Fenn and coworkers favored the evaporation model over the charge residue model as an explanation for the generation of large ions from electrosprayed droplets.

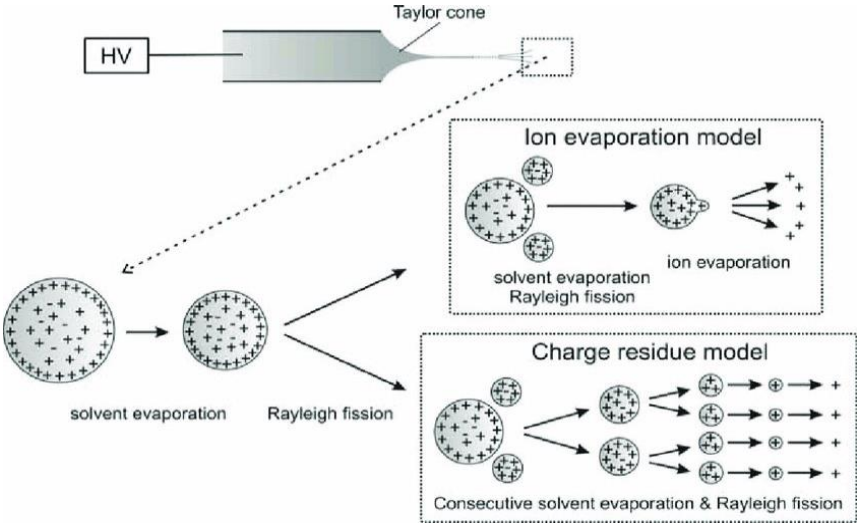

Fig.15 - ESI final stage of ion formation.

The factors that have the greatest effect on the appearance of the ESI spectrum are the pH of the spray solution, the flow of the sample solution, the flow of the spray gas, the flow and temperature of the desolvatation gas or the temperature of the desolvatation capillary. In general, the number of charges deposited on a molecule in ESI depends on its molecular weight and the number of potential charge sites available, namely sites of protonation, deprotonation or cationisation

[120], [121].

1.18.2. Triple Quadruple(QqQ)

A widely used tool for chemical and clinical investigations is the triple-quadrupole mass spectrometer, which consists of three quandrupole mass analyzers in series. A quadrupole mass analyzer consists of four linear metal rods that ideally the rods are hyperbolic, although cylindrical rods with a specific ratio of rod diameter-to-spacing provide an easier-to-manufacture adequate approximation to hyperbolas (Fig.16). Each opposing rod pair is electrically connected in order to maintain the rods of each pair at the same electrical potential, which is composed of a direct current (DC) and an alternating current (AC) component. The potential on the two diagonal pairs is instantly of opposite value. When an ion enters into the quadrupolar system along the z-direction, it undergoes an attractive force from one of the bars whose charge at that time is opposite to that of the ion. If the applied voltage consists of a DC voltage (U) and a Radio Frequency (rf) voltage (V) with w frequency, the total potential φ0 is given by:

$$\varphi 0 = U + V \cos wt$$

For a given combination of U, V e w the total motion of the ion may result in a stable trajectory whereby ions of a given value of m/z or of an interval of m/z will cross the quadrupole, in general the path stability of a given ion is defined by the amplitude of the rf V voltage and the U/V ratio. So only ions of a certain mass-to-charge ratio will reach the detector for a given ratio of voltages: other ions have unstable trajectories and will collide with the rods. This permits selection of an ion with a particular m/z or allows the operator to scan for a range

of m/z-values by continuously varying the applied voltage. Mathematically this can be modeled with the help of the Mathieu differential equation.

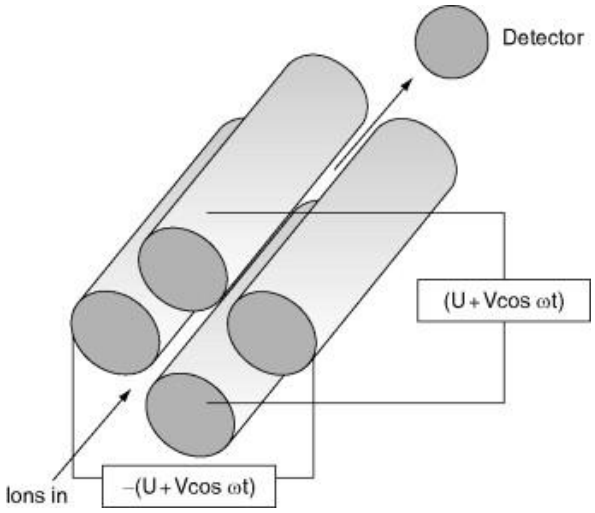

Fig.16 - Diagram of a quadrupolar analyzer.

In general, the quadrupole works as a mass filter instead of a momentum or energy separator, so the term quadrupolar mass filter has spread. Quadruple mass analyzers generally operate at so-called unit resolution which limits their use for low resolution (LR) applications [122]. If the DC voltage is set to 0 the quadrupole is transformed into a broadband filter for ions and these systems are commonly known as quadrupole radio frequency only (rf). This property leads to the use of quadruples and derivatives as ionic guides and collision cells. RF-only ion guides are used in many ways to transfer low kinetic energy ions from one functional unit to another without losses or are used to couple ESI, APCI and ambient MS ion sources to mass analyzers [60]. The traditional triple quadrupole usually has a quadrupole placed after the ion source that operates as an ion guide (Q0), two quadrupoles working as mass filters (Q1 and Q3) and a quadrupole, placed between Q1 and Q3, which is used as a collision cell (Q2) [122], [123].

1.18.3. Tandem Mass Spectrometry (MS/MS)

Tandem mass spectrometry combines various techniques in which selected ions are subjected to a second mass spectrometry analysis. It includes the acquisition and study of the spectra of product ions and precursor ions of species with a given m/z ratio, or precursor ions of a defined neutral loss. Two spatially separated analyzers are used in tandem mass spectrometry to perform the two consecutive analyses. Separation of ions with specific m/z ratios is carried out in a first analyser, then the ions undergo to dissociation in an intermediate area of the instrument (Q2) that in a triple quadrupole mass spectrometer is placed between Q1 and Q3, and finally the fragment ions produced are transmitted to a second analyzer for mass analysis. Triple quadrupole QqQ mass spectrometers (Fig.17) are becoming the gold standard for LC-MS/MS applications, especially when accurate quantitative analysis is required. As mentioned above, the first quadrupole Q1 is used to select ions, the second (Q2) is used for ion fragmentation in rf-only mode and for this is also named collision cell, and finally Q3 analyzes the fragment ions generated in Q2. Ion fragmentation is carried out by the Collisionally Induced Dissociation (CID) technique, which consists in the interaction between the ion beam containing the analytes and a suitable collision gas such as helium, nitrogen or argon, inside the collision cell. Collisionally induced dissociation of an ion (AB+) by a neutral species (N) can be considered a two-stage process in which first we have the collision between the two species and then we have the activation of the ion (AB+*). Total internal energy of the ion corresponds to the sum of the ion's internal energy and the energy transferred during the collision, in the second phase there is the random redistribution of internal energy, which cause the ion fragmentation [124].

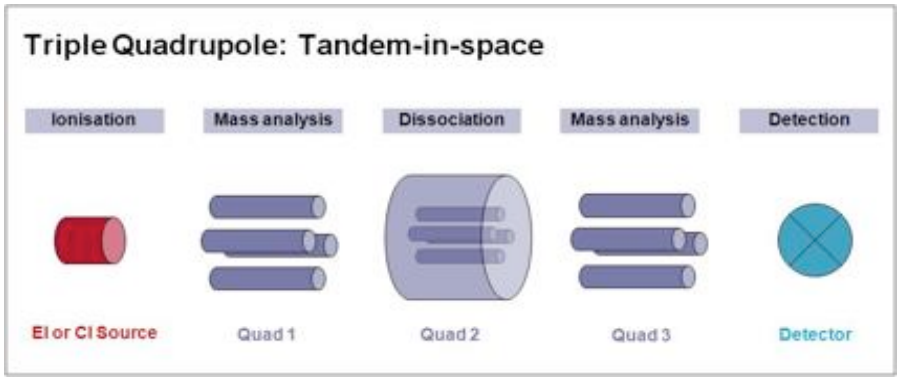

Fig.17 - Triple-quadrupole mass spectrometer.

Varying the operating modes of the first (Q1) and the third (Q3) quadrupole, different types of experiment can be carried out (Fig. 18).

Full Scan: Q1 or Q3 work in scanning mode and all the ions are monitored. Q1 and Q3 allow the passage of ions with m/z in a wide mass range established by the operator. Full Scan is mainly used for qualitative applications.

Product Ion Scan (MS2): All product ions of the selected precursor ion are recorded. Q1 allows the passage of a selected precursor ion, which is fragmented into Q2, and Q3 scans the product ions in a defined mass range. MS2 is mainly used for quantitative target analysis.

Precursor Ion Scan (Prec): All precursors of the product ion of interest are identified. Q3 is set to allow only a specific product ion of one m/z ratio to pass and Q1 scans in a defined mass range; in this mode the presence of a precursor ion is confirmed, or more commonly, different molecular ions that share a product ion are identified. Only compounds which give that specific product ion are detected. Prec. is used for screening experiments where a group of compounds all give the same fragment ion.

Neutral Loss Scan (NL): The loss of a neutral fragment by several precursors is identified. Both Q1 and Q3 scan in a synchronized manner, so as to identify the loss of the same neutral fragment by several precursors. Only those compounds which give a fragment having that specific loss are detected. NL is used for screening experiments where a group of compounds give the same loss.

For the monitoring of ions (SIM) or reactions (SRM) selected we have the modes:

SIM (Selected Ion Monitoring) one (or more) ion to monitor is selected. In the case of multiple ions, the term MIM is sometimes used (Multiple Ion Monitoring).

SRM (Selected Reaction Monitoring) one (or more) precursor ion/product ion pairs are selected. In the case of several transitions, the term MRM is sometimes used (Multiple Reaction Monitoring) [125].

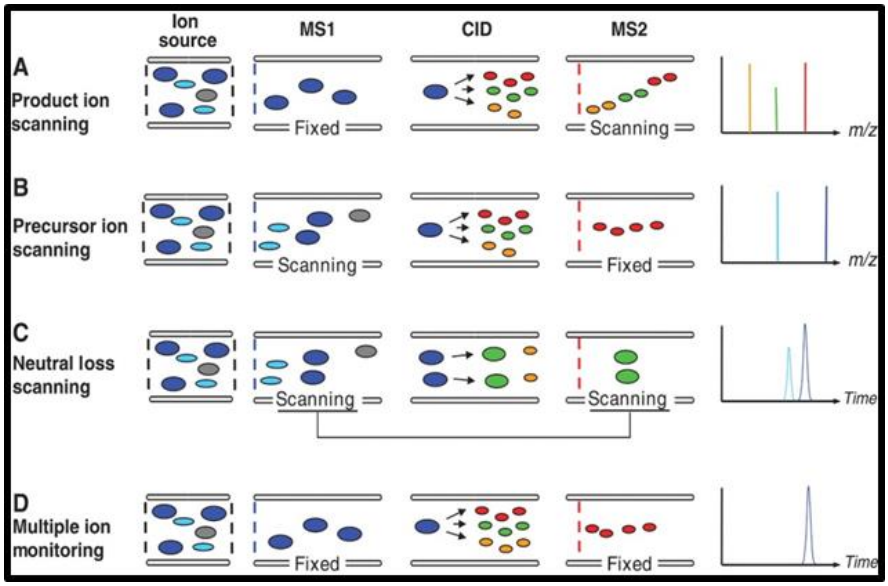

Fig.18 - Scanning mode of triple quadrupole.

1.18.4. RF Linear multipolar ion traps (LIT) with axial ejection

The linear ion trap (LIT) is a type of ion trap mass analyzer for mass spectrometry. In a LIT, ions are confined radially by a two-dimensional radio frequency (RF) field, and axially by stopping potentials applied to end electrodes. LITs have high injection efficiencies and high ion storage capabilities.[1] Collisional cooling, is an important aspect of the behaviour of ions in a quadrupole field. The collision of the ions with the nitrogen collision gas, can almost cancel the translational movement of ions along the axis of an RF-only multipole, by transforming the multipolar ion guide in a device for the accumulation of ions. By placing two electrodes, with appropriate potential, near the front and rear openings of the multipole it is possible to create a potential hole that traps the ions. The Sciex 6500 Mass Spectrometer, which has been used for this thesis, can operate both as a conventional triple quadrupole mode, than in LIT mode. In particular, by setting the electrode located near the front opening of Q3 at low potential and the electrode near the rear opening of Q3 at high potential, it is possible to trap the ions in Q3. The time that allows the accumulation of ions is limited by the reflection of fast ions due to the potential wall, placed at the level of the rear opening of Q3. Therefore, to prevent the lighter ions, which must be trapped, from exiting the LIT through the front opening, there must be appropriate regulation of the potential of the Q3 input electrode. By gradually decreasing the potential of the Q3 output electrode, the ions exit in a control manner from the LIT and then scan them (Fig. 19)[111], [126].

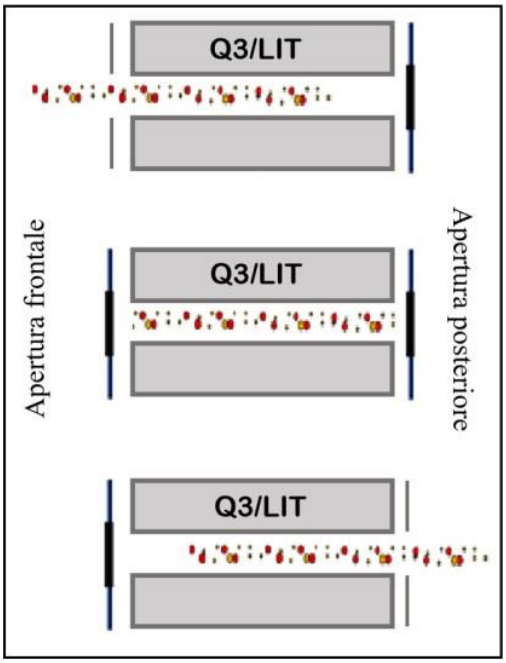

Fig. 19 - LIT with axial ejection

The types of scanning in LIT mode are mainly used for qualitative purposes, but with appropriate precautions can provide good results even for quantitative determinations. The scanning mode evaluated for the development of the methods used in this thesis are:

Enhanced Product Ion (EPI): scanning mode used to obtain a high-quality mass spectrum (MS/MS) for a specific ion. In this mode, the precursor ion is selected in Q1 using a large window from 1 to 4 and then subjected to CID in Q2, with generation of fragment ions that are captured in the linear ion trap and scanned with one of the three available scanning speeds based on the required resolution power (Fig.20)

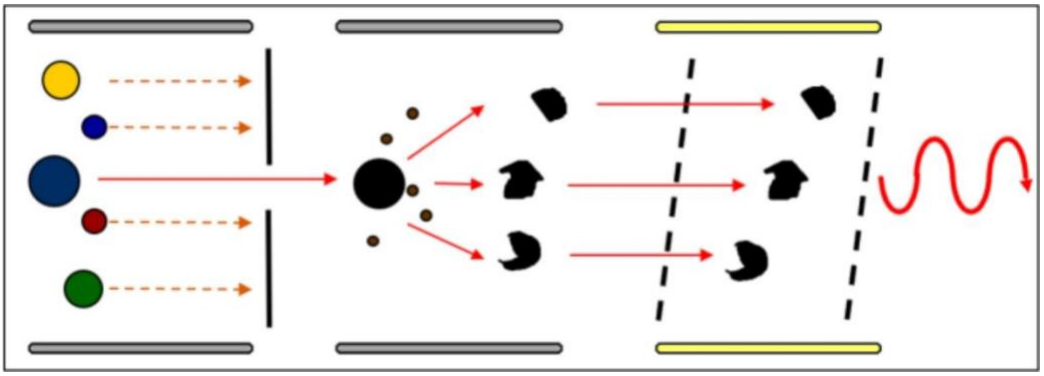

Fig. 20 - Principle of EPI.

MS/MS/MS (MS3): the precursor ion is selected in Q1 and fragmented in Q2, with the generation of product ions that are transmitted to the LIT, in which only produced ion is isolated and then it is fragmented, always in the LIT; the resulting ions are scanned, out of the trap, with one of the three above mentioned scanning speeds [126].

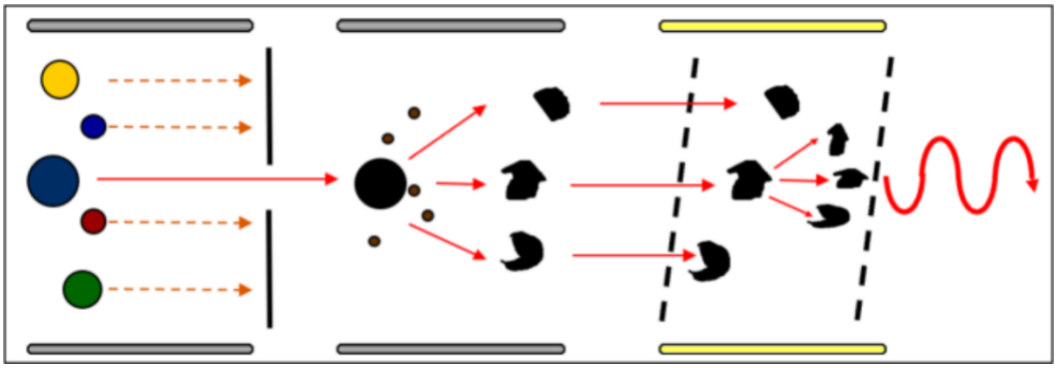

Fig. 21 - Principle of MS3

1.18.5. 6500+ Qtrap-Theory of Operation

The mass spectrometer has a series of quadrupole filters that transmit ions according to their mass-to-charge (m/z) ratio. The first quadrupole in this series is the IonDriveTM QJet ion guide located between the orifice plate and the Q0 region. The IonDriveTM QJet ion guide does not filter ions but focuses them before they enter the Q0 region. By prefocusing the larger ion flux created by the wider orifice, the IonDriveTM QJet ion guide increases system sensitivity and improves the signal-to-noise ratio. In the Q0 region, the ions are again focused before passing into the Q1 quadrupole.

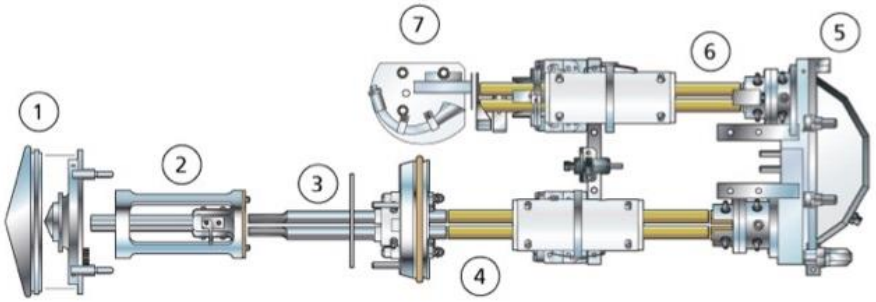

Item	Description
1	Orifice plate
2	QJet ion guide
3	Q0 region
4	Q1 quadrupole
5	Q2 collision cell
6	Q3 quadrupole
7	Detector

Fig. 22 - Ion Path.

The Q1 quadrupole is a filtering quadrupole that sorts the ions before they enter the Q2 collision cell. The Q2 collision cell is where the internal energy of an ion is increased through collisions with gas molecules to the point that molecular bonds break creating product ions. This technique allows users to design experiments that measure the m/z of product ions to determine the composition

of the precursor (or parent) ions. After passing through the Q2 collision cell, the ions enter the Q3 quadrupole for additional filtering, and then arrive at the detector. In the detector, the ions create a current that is converted into a voltage pulse, which are directly proportional to the quantity of ions entering into the detector. The system monitors these voltage pulses and converts the information into a signal, which represents the ion intensity for a particular m/z value and the system shows this information as a mass spectrum. The QTRAP® system linear ion trap (LIT) functionality provides a number of enhanced modes of operation. A common factor of the enhanced modes is that ions are trapped in the Q3 quadrupole region and then scanned out to produce full spectrum data. Many spectra are rapidly collected in a short period of time and are significantly more intense than spectra from a comparable standard quadrupole mode of operation. During the collection phase, ions pass through the Q2 collision cell where the CAD gas focuses the ions into the Q3 that operates with the main RF voltage applied only. Ions are prevented from passing through the Q3 quadrupole rod set and are reflected back by an exit lens to which a DC barrier voltage is applied. After the fill time elapses (a time defined by the user, or determined by the Dynamic Fill Time feature), a DC barrier voltage is applied to a Q3 entrance lens (IQ3). This confines the collected ions inside Q3 and stops additional ions from entering. Both the entrance and exit lens DC voltage barriers, as well as the RF voltage applied to the quadrupole rods confine the ions within Q3. During the scan out phase, the voltage on the exit lens and the auxiliary RF voltage are ramped simultaneously. An auxiliary AC frequency is applied to the Q3 quadrupole. The main RF voltage amplitude is ramped from low to high values, which sequentially brings masses into resonance with the auxiliary AC

frequency. When ions are brought into resonance with the AC frequency, they acquire enough axial velocity to overcome the exit lens barrier and are axially ejected towards the mass spectrometer ion detector. Full spectra data can be acquired from the ions collected in Q3 by rapidly scanning the main RF voltage[126].

1.18.6. Ion Source Overview

The IonDrive Turbo V ion source can be used for either electrospray ionization (ESI) or atmospheric pressure chemical ionization (APCI). It was designed to provide more heat and better desolvation and ionization in ESI mode, especially at high-flow rates. It features increased heater diameter for improved ionization, a larger sweet spot, and less performance variability.

ESI Mode: ESI produces gas phase ions of analytes in a sample by applying a high voltage to the sample effluent flowing through a needle. With the aid of heated gas flow, ESI produces singly and multiply charged ions in a relatively mild condition so that it is suitable for a wide range of compounds including small molecules, such as drugs or pesticides, and larger molecules, such as peptides, proteins, and other biopolymers. The sensitivity depends on chemical properties of the analyte, gas flow rate, temperature, voltage, and mobile phase composition. ESI technique is mild enough to be used with labile compounds, such as peptides, proteins, and thermally labile pharmaceuticals. It provides satisfactory performances with flow rates from 5 μL/min to 3,000 μL/min and it vaporizes 100% aqueous to 100% organic solvents.

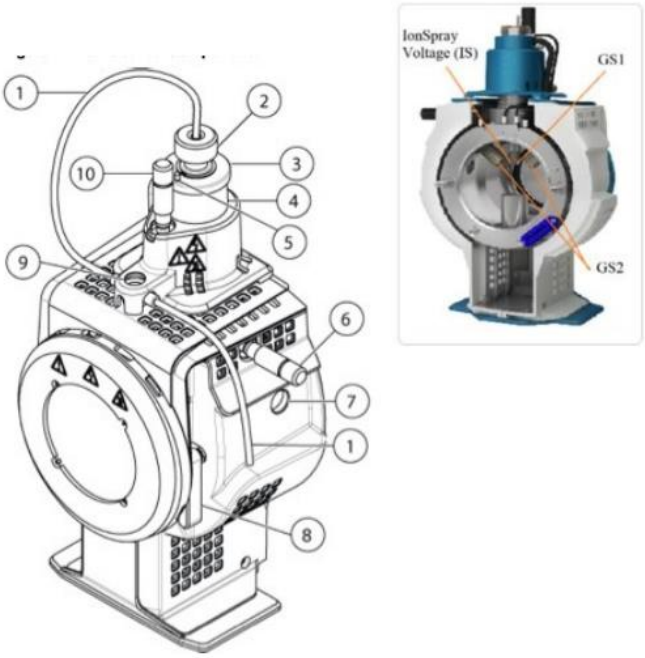

Fig.23- Ion Source Component-Item n. 1 Sample tubing, n.2 Electrode adjustment nut, n.3 Retaining ring, n.4 Probe tower,n.5 Corona discharge needle ajustment screw, n.6 Micrometer used to position the probe in the horizontal axis for ion source sensitivity adjustments, n.7 Window port, n.8 One of two source latches that secure the ion source to the mass spectrometer, n. 9 Grounding union.It is not visible below the ion source cover, n.10 Micrometer used to position the probe on the vertical axis for ion source sensitivity adjustments

The TurboIonSpray probe consists of 300 µm outer diameter (o.d.) (0.012 inch) stainless steel electrode. It is located centrally with respect to two turbo heaters, placed at a 45 degree angle to each side. Samples introduced through the TurboIonSpray probe are ionized within the tubing, by the application of high voltage (IonSpray Voltage in the Analyst software), then they are nebulized and ions in the gas phase are produce according to the mechanisms described above[127].

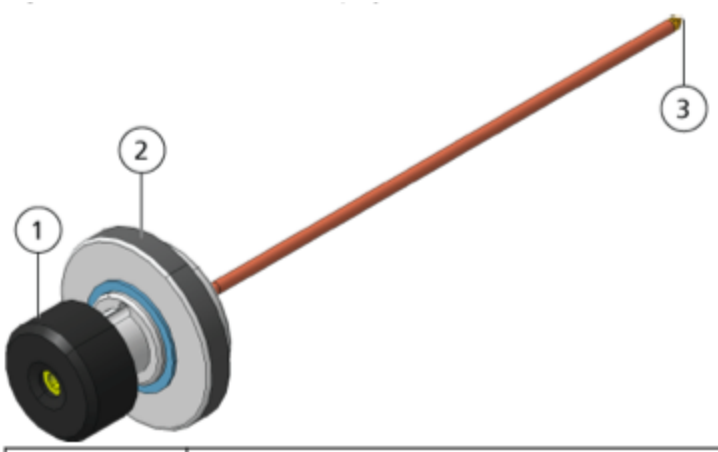

Item	Description
1	Electrode adjustment nut (black collar) that adjusts the extension of the electrode tip
2	Retaining ring that fastens the probe to the probe tower on the ion source housing
3	Electrode tip through which samples are sprayed in the sample inlet area of the ion source

Fig.24 - TurboIonSpray Probe

1.18.7. Instrumental parameters

The working parameters constitute the set of instrument parameters optimized to provide each analytical method with the maximum sensitivity.

- ESI-Source and gas parameters: include spray solvent composition, auxiliary gas flow rate, sample infusion rate or HPLC flow rate, and spray voltage
- Compound parameters: consist mostly of voltages in the ion path. Optimal values for compound-dependent parameters vary depending on the structure of the compound being analyzed.
- Resolution parameters: affect the resolution and calibration.
- Detector parameters: affect the detector sensitivity.

The instrumentation parameters to be optimized for maximum sensitivity during the development of the method are as follows:

1.18.7.1. Curtain Gas (CUR) and Declustering Potential (DP)

The CUR parameter controls the gas flow of the Curtain GasTM interface. The Curtain GasTM interface is located between the curtain plate and the orifice. It prevents the contamination of the ion optics. The declustering potential (DP) is the potential difference between orifice and curtain plate. DP basically controls the orifice voltage, whose optimization helps to minimize the formation of ion clusters, originated by the association of solvent and analyte between the orifice and the IonDriveTM QJet ion guide. f the DP parameter is too high, unwanted fragmentation might occur. The typical values of DP range from 20 to 150 V; a DP value too low, will lead to less ionic intensity and potential interference of ion clusters, while a too high DP value can cause the in-source fragmentation of the

analyte. During optimization, the DP is set to the value that determines the maximum intensity.

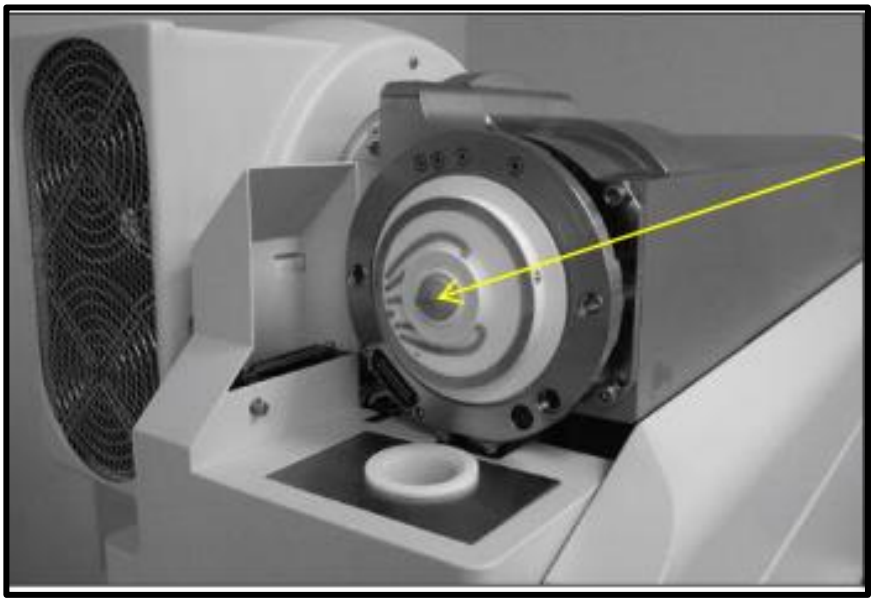

Fig.25 - The image represents the Orifice which is the opening into which ions enter the mass.

1.18.7.2. Entrance Potential (EP)

The EP parameter controls the potential difference between the voltage on Q0 and ground. The entrance potential guides and focuses the ions through the high-pressure on the Q0 region. As already stated, Q0 do not act as mass filters (rf-only) but serve to guide and focus ions in the mass spectrometer. It is usually set to 10 V for positive ions or -10 V for negative ions, it is not always necessary an optimization for this parameter because having a limited impact on compound optimization, it can be left at predefined values.

1.18.7.3 Collision Energy (CE)

Collision energy (CE) refers to the amount of energy needing to accelerate the precursor ions entering the Q2 collision cell, where they collide with gas molecules and fragment. CE parameter controls the potential difference between Q0 region

and Q2 collision cell. The CE is optimized for efficient molecule fragmentation, inappropriate CE values can drastically reduce the sensitivity of analyses.

1.18.7.4. Collision Cell Exit Potential (CXP)

Collision Cell Exit Potential (CXP) focuses and accelerates ions from Q2 to Q3. It is optimized for each fragment ion formed from the precursor ion. The CXP parameter is only used in Q3 and MS/MS scan types.

1.18.7.5. Collision Gas (CAD)

CAD is the inert gas (N2) present within Q2, which allows the fragmentation of precursor ions, but it is also used to focus and cool ions. The CAD parameter controls the pressure of the CAD gas in the collision cell during Q3 scan, MS/MS, and LIT scans. For Q3 scans, the collision gas helps to focus the ions as they pass through the Q2 collision cell. The preset value for the CAD parameter is in fixed mode. For MS/MS scan types, the CAD gas helps to fragment the precursor ions. When the precursor ions collide with the collision gas, they dissociate to form product ions. For LIT scan types, the collision gas helps to focus and trap ions in the linear ion trap.

1.18.7.6. Ion Spray voltage, GS1, and GS2

Gas Source 1 (GS1) is the parameter that controls the nebulizer gas. It helps to generate small drops of the spray that are quickly desolvated in the source. Gas Source 2 (GS2) is the parameter that controls the gas of ceramic Heaters and helps evaporate the solvent from the drops. The ionspray voltage (IS) is the voltage applied to the electrode in the TurboIonSpray® probe that ionizes the sample in the ESI source. The optimal value depends on the polarity of the molecule and affects

its ionization efficiency; it also has an influence on the stability of the spray and the sensitivity of the analysis. Thus, the parameter can be compound-dependent and should be optimized for each compound.

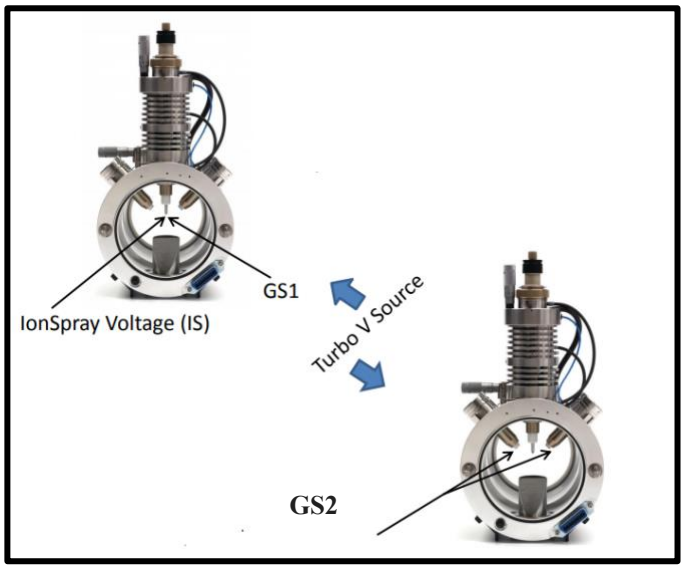

Fig.26 -Turbo-V spray Source.

1.18.7.7. Temperature (TEM)

TEM is the parameter that controls the additional temperature of the ceramic heaters from which GS2 flows, helps to quickly evaporate the droplets from the spray. Not all compounds require additional heat to ionize and in the case of thermolabile molecules the additional heat may cause thermos-degradation and adversely affect the sensitivity of the method. [126], [127] The maximum temperature for heaters is 750 ºC [127], and the optimum value may depend on the flow of eluate from HPLC.

1.18.7.8 Q0 Trapping

The Q0 trapping parameter controls the storage of ions in the Q0 region. It is used to increase sensitivity and duty cycle by trapping ions in the Q0 region while ions

are being mass-selectively ejected from the linear ion trap. Use fixed fill time with this parameter. Either select or clear the feature as required by the experiment. The recommended fixed fill time to use with Q0 trapping is 20 ms or greater.

1.18.7.9 Collision Energy Spread (CES)

The CES parameter, in conjunction with the CE parameter, determines which three discreet collision energies are applied to the precursor mass in an Enhanced Product Ion (EPI) or MS/MS/MS (MS3) scan when CES is used. When a collision energy spread value is entered, CES is automatically turned on. In EPI o MS3 experiments we can use a CES preset value or optimize this parameter for the compound.

1.18.7.10 Q3 Entry Barrier

The Q3 Entry Barrier parameter is used to transfer the ions from the Q2 collision cell into the linear ion trap.

1.18.7.11. MS/MS/MS Fragmentation Time

The MS/MS/MS Fragmentation Time parameter controls the amount of time that the excitation energy is applied. It is used in combination with the excitation energy to fragment the isolated second precursor ion.

1.18.7.12 Fixed LIT Fill Time

The Fixed LIT Fill Time parameter controls the amount of time that the LIT fills with ions. Use the preset value and adjust it to achieve the desired signal response based on sample concentration.

1.18.7.13 Dynamic Fill Time (DFT)

The DFT parameter dynamically calculates the amount of time that ions are collected in the linear ion trap based on the incoming ion signal. When DFT is turned on, the signal is optimized to either increase sensitivity or minimize space-charging. the DFT settings are optimized for the 10 000 Da/s scan speed. These settings are also suitable for other LIT scan speeds.

1.18.7.14. CEM- Detector

The CEM parameter controls the voltage applied to the detector, which influences the detector response.

1.18.8 Analyst® Software Overview and Data Handling

The Analyst® software 1.7.3. is used both for instrument control (HPLC and mass spectrometer) and for data processing. It runs in computers equipped with Windows 10 operating system. During system operation, the acquired data are sent to the Analyst® software, where it can be visualized as either full mass spectra, intensity of single or multiple ions over time, or total ion current over time. At the end of each acquisition, we can choose three different data views:

Total Extracted Ion Chromatogram (XIC): An ion chromatogram created by taking intensity values at a single, discrete mass value or a mass range, from a series of mass spectral scans. It indicates the behavior of a given mass or mass range as a function of time.

Spectra: The distribution characteristic of a physical system or phenomenon.

Ion Chromatogram (TIC): The plot of the total ion current as a function of time.

II. Research Project

For many years, vitamin D has been acknowledged for its role in the calcium and phosphorus homeostasis and bone metabolism. However, recently, scientific literature suggests a link not only between VDD and human skeletal physiopathology but also with extra-skeletal health disorders. Moreover, several studies have shown that 1,25-(OH)2D3, the bioactive metabolite of vitamin D, is also involved in skeletal and extra skeletal metabolism. In reference to this, several years ago it was proposed a role of vitamin D in the regulation of the immune system; and it is thought how also 1,25-(OH)2D3 can exert immunomodulatory and pleiotropic functions. Latest studies have also shown an inverse correlation between the VDD and the increased susceptibility to respiratory infections, such as acute respiratory distress syndrome (ARSD), one of the most severe complications of coronavirus disease 2019 (COVID-19). COVID-19 severity condition consists of a hyperinflammatory syndrome induced by an excessive production of pro-inflammatory cytokines which can cause a systemic inflammation leading to progressive tissue damage, organ dysfunction and death. The outbreak of the pandemic COVID-19 has aroused great interest in the discovery of new biomarkers related to the severity of this disease. The hypothesis of a possible correlation between VDD, 1,25-(OH)2D3 levels and the rates of positivity at SARS-CoV2 (severe acute respiratory syndrome), as well as the severity of the pathology COVID-19, has been formulated. Several methods have been routinely used to measure 25OHD3 levels, including competitive protein-binding (CPB) assays, radioimmunoassays (RIA), chemiluminescence immunoassays (CLIA), liquid chromatography (LC) with UV detection, and liquid chromatography-mass spectrometry (LC-MS) or tandem mass spectrometry (LC-MS/MS). In clinical practice, immunological tests are the most common assays due to their high-throughputness, even if the methods based on chromatography are generally more

accurate because less susceptible to matrix effects. However, vitamin D is characterized by complex metabolic and catabolic pathways, and simultaneous measurement of multiple vitamin D metabolites may provide a more accurate interpretation of vitamin D3 status in COVID-19. For this purpose, we developed the first LC-MS/MS method for the simultaneous detection of four vitamin D3 metabolites, e.i. 25-OHD3, 1,25-$(OH)_2$D3, 24,25-$(OH)_2$D3, and vitamin D3, in the plasma matrix. The quantification of the vitamin D3 metabolites/catabolites in plasma always represented a tough challenge due to their low concentrations, in the order of ng/mL for 25-OHD3 and 24,25-$(OH)_2$D3 and pg/mL for 1,25-$(OH)_2$D3 and vitamin D3. To date, LC-MS/MS is considered the gold standard method for the quantification of 25-OHD3 in biological samples because its sensitivity and analytical specificity guarantees the best accuracy among the available technologies. The optimized and validated method was used to measure the levels of the four metabolites in a population of healthy subjects and patients with COVID-19 in order to evaluate any differences in the vitamin D3 status and to obtain some information about vitamin D3 metabolism and catabolism during SARS-CoV2 infection. We analyzed 30 plasma samples from healthy subjects, used as controls, and 69 plasmas from COVID-19 patients hospitalized at the University Hospital in Pisa between March and May 2020. To evaluate the robustness of the analytical procedure, the new method was cross-validated by assaying the 69 COVID-19 positive samples for 25-OHD3 levels by using MSMS VitD Kit PerkinElmer commercial method, which is a reference method by the Joint Commitee for Traceability in Laboratory Medicine to determine the Vitamin D3 status [24][128]. Moreover, considering the role of vitamin D in the immune system regulation, we evaluated the relationship between 25-OHD3 levels, used as a reference for the vitamin D3 status, and a biochemical panel of inflammatory markers in a wider cohort of patients (n=93) with COVID-19 related pneumonia, in correlation with

complementary clinical parameters.

2.1. Analytical method development

The development of a LC-MS-MS method requires three separate methodologies to be developed:

- sample preparation
- chromatography
- Sample Reaction Monitoring (SRM)- or MS3-based mass spectrometry

An optimized LC-MS/MS method encompassing these three techniques may require an iterative approach, since changes in one of them can affect the others. Thus, the method development process includes several iterations, and is followed by method testing and further adjustments to obtain the final method. During LC-MS/MS method development, the chemical and physical characteristics of the analytes were taken into account and chromatographic techniques already present in the literature were reviewed and evaluated. Until recently HPLC with ultraviolet detection was considered the standard chromatographic technique for the quantification of vitamin D3[129], however the detection limits (LOD) and the amount of sample required is generally inadequate for the purposes of our study. LC-MS/MS/MS methods have lower limits of quantification (LOQ), especially when coupled with atmospheric pressure ionization, such as ESI and APCI [29]. With reference to these, it is known that 1,25-$(OH)_2$D3 and 24,25-$(OH)_2$D3 have low concentration levels and due to their non-polar structure have poor ionization efficiency; in addition, the quantification of 1,25-$(OH)_2$D3 is also hard for the presence of potential interference due to other di-hydroxylates metabolites of vitamin D3, including 24,25-$(OH)_2$D3, which have the same molecular masses and

similar fragmentation patterns. In order to improve ionization efficiency and specificity, a derivatization with Cookson-type reagents may be used. Derivatization is a chemical reaction that converts a compound into a product with a higher mass, detectable at higher values of the mass to charge ratio in the mass spectrum, where chemical noise is significantly lower and less interferences are present. Moreover, derivatization has the additional advantage of leading to the formation of fragment ions of the derivatized compounds that are unique. The most common Cookson-type reagent used for the derivatization of vitamin D3 and its metabolites is 4-phenyl-1,2,4-triazoline-3,5-dione (PTAD), a dienophile compound that reacts with the s-cis-diene structure of the vitamin D3 metabolites (Fig. 27). In some cases, additives such as formic acid (98-100%), ammonium hydroxyde (99.99% trace metal basis), lithium acetate (99.95% trace metal basis) or methylamine ($MeNH_2$ 2.0 M in MeOH), are added to improve the ionisation efficiency with adducts formation [130].

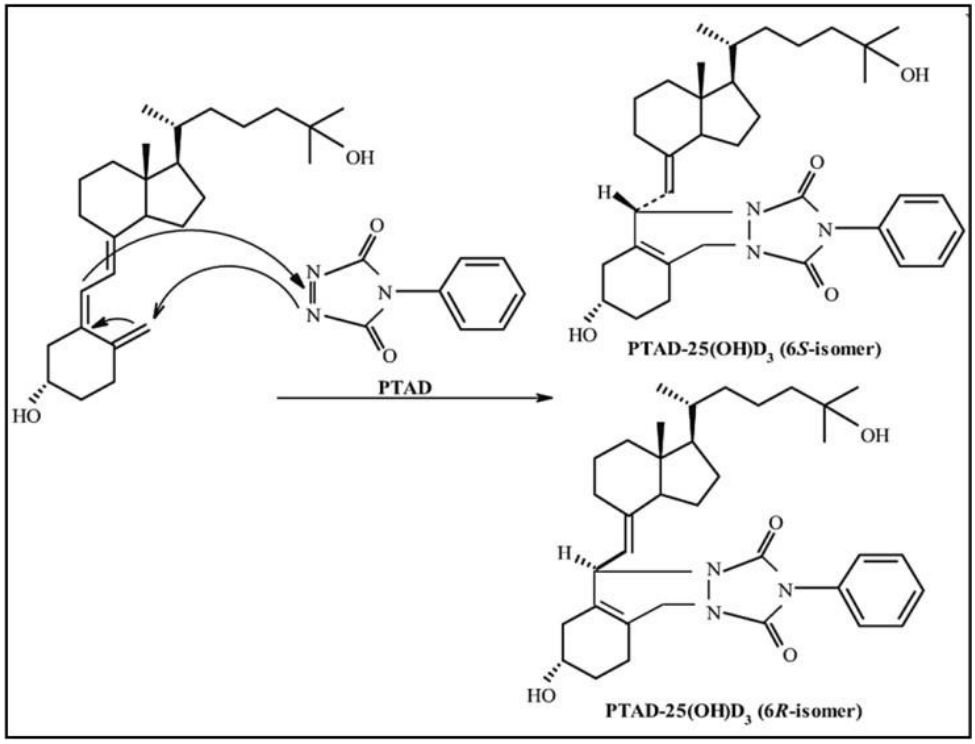

Fig. 27- Diels-Alder reaction using PTAD

At first, the LC-MS/MS method was optimized to detect the non-derivatized analytes. An appropriate amount of lithium acetate was added to the mobile phase, and lithium adducts $[M+Li]^+$ of the four vitamin D3 metabolites and their internal standards (ISs) were monitored. The development of the chromatographic method was conducted using a HPLC Perkin-Elmer Brownlee C18 column, 5 μm 50x2.1 mm, which was available in our laboratory and was previously used for dosing 25-OHD3. The selectivity, e.i the ability of the chromatographic system to 'chemically' distinguish between sample components, was evaluated according to the eluent mixture composition, flow, and temperature. However, the tested chromatographic conditions did not allow the detection of 1,25-$(OH)_2$D3 in our samples. Hence, derivatization with PTAD was chosen to modify the analytes' structure and thus increase the instrumental response. Briefly, derivatization process consists as follows: 50 μl PTAD is added to the dry residue of sample (100 μl), the obtained solution is vortexed 15 minutes; then 50 μl quench solution (solution that stops the reaction) is added, the mixture is vortexed for a further 5 minutes and the resulting solution is then dried under a nitrogen stream (N_2) and reconstituted for the injection into the HPLC-MS/MS system. This process was optimized by varying the incubation time, temperature, and amount of PTAD. Results from MRM and Q1 full scan experiments showed that the reaction yield is around 100%. However, the structural change with PTAD was not sufficient for an adequate detection of 1,25-$(OH)_2$D3 in our samples; in addition, due to matrix effect the signals of 24,25-$(OH)_2$D3 and vitamin D3 were very low. To enhance the analytes signals we added $MeNH_2$ to the mobile phase, and a mixture containing 50% MeOH, 50% H2O, with 0.5 mM $MeNH_2$ was used to reconstitute the dry samples. $MeNH_2$ improves the

ionization efficiency of vitamin D3 metabolites, forming the positive adducts $[M+MeNH_2]^+$, which provide an increased instrumental response. Optimization of chromatographic and mass spectrometry conditions was conducted for the adducts, too. During the HPLC optimization method, several chromatographic columns and mobile phase compositions were tested in order to improve both peak intensity and shape; the best results were obtained with an Acquity UPLC BEH Phenyl (1.7 μm, 50x2.1 mm) column, H2O + 0.5 mM $MeNH_2$ (eluent B, B) e MeOH + 0.5 mM $MeNH_2$ (eluent A, A), by using gradient conditions. The effects of the eluent flow and of the chromatographic column temperature on the chromatographic performances were studied, as well as the chromatograms quality, e.i. the retention time and the resolution of the analytes, with particular care to the separation between 1,25-$(OH)_2$D3 and 24,25-$(OH)_2$D3, which possess very similar retention times. The most suitable chromatographic separation was achieved by using an eluent flow of 650 μl/min and a column temperature of 60 ºC.

2.2. MS/MS Method optimization

The first step in the method development process is the evaluation of the MS response. The obtained information can be used to develop a MRM-based method that provides the best possible sensitivity as regards to the compounds of interest. A preliminary evaluation requires investigating:

- whether each compound can be detected by mass spectrometry without the need for chemical modification,
- the most suitable ionization method between ESI and APCI,
- the ionization polarity that provides the best response.

The following development of the MRM method can be laborious and, once again, involves a series of iterations to achieve the optimal settings. Once derivatization was found advantageous, standard solutions of the analytes and their internal standard (IS) at the final concentration of 1 μg/ml were submitted to reaction with

50 µl of PTAD and the obtained product mixture was reconstituted with 100 µl of 50% MeOH + 0.5 mM $MeNH_2$ and 50% H2O + 0.5 mM $MeNH_2$. The final solutions were then infused into the mass spectrometer using a syringe pump to identify precursor ions $[M+MeNH_2]^+$, select the fragment ions, and identify compound and source instrumental parameters that would allow the maximum sensitivity.

2.2.1 MS optimization of 25-OHD3, and d6- 25-OHD3 (26,26,26,27,27,27-d6)

The detection of the $[M+H+MeNH_2]^+$ precursor ions of 25-OHD3 and d6-25-OHD3 (26,26,26,27,27-d6), respectively at m/z 607.3 and m/z 613.4, was performed in full-scan positive ion mode, i.e. using the first quadrupole Q1 in scan mode (Q1 MS, Fig. 28).

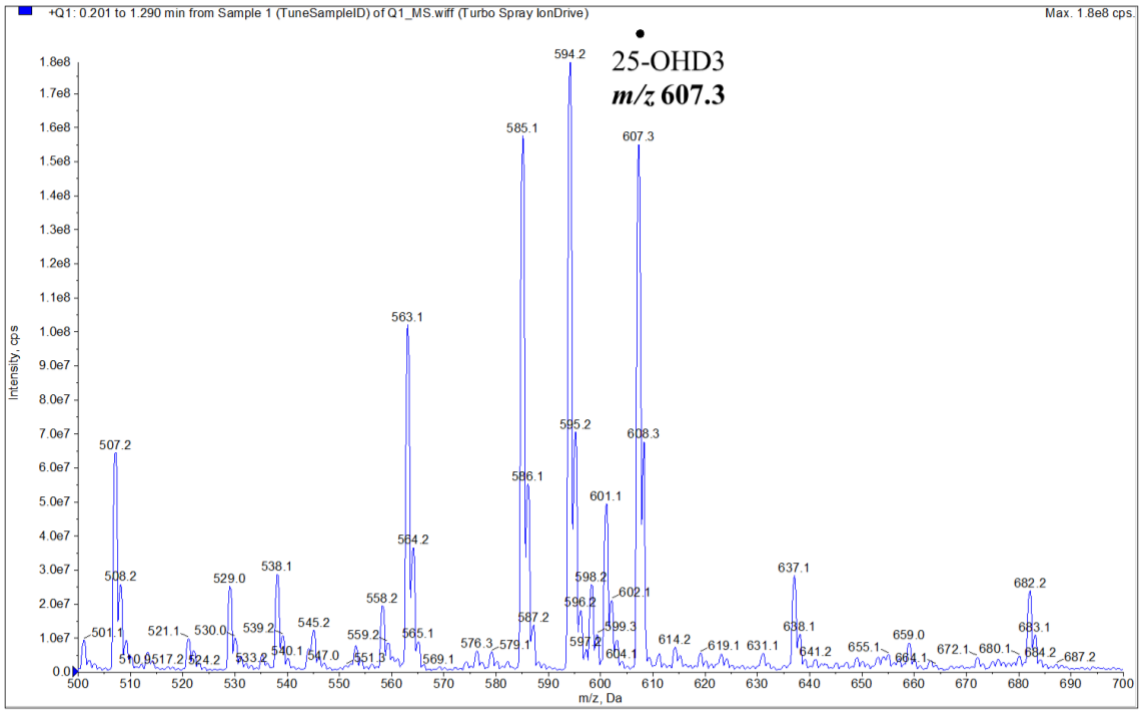

Fig. 28 - Full scan spectrum (Q1) of 25-OHD3.

Then, the main compound parameters were optimized by using the Q1 Multiple Ion analysis (Q1 MI). In this frame, voltage ramps (progressive variation of the voltage with constant increase over time) were carried out to identify the optimal values of Declustering Potential (DP) and Entrance Potential (EP). After that, a Product Ion Scan (MS2) experiment, using an CE ramp, were performed to identify the fragment ions for analyte and its IS. As far as Vitamin D3 is concerned, we have chosen the most abundant fragment ions among those representatives of the structure (Fig.29).

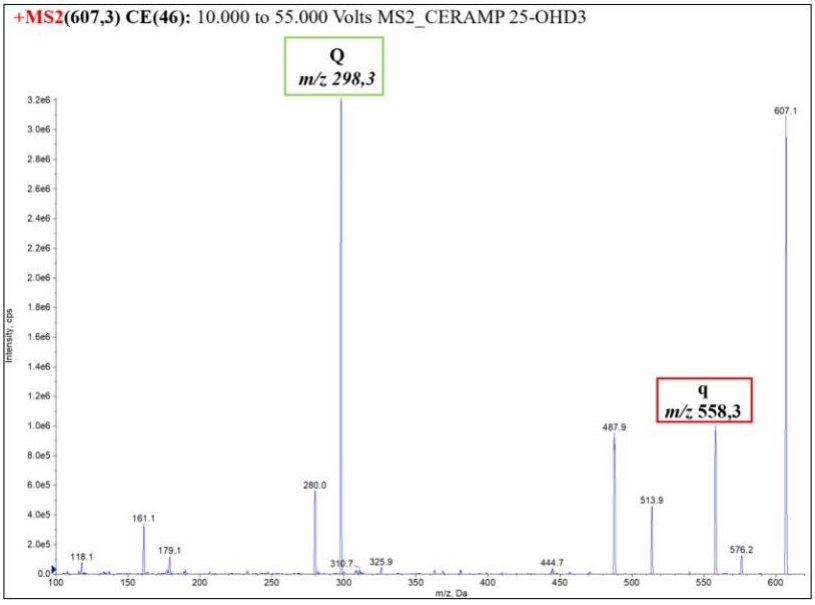

Fig. 29 - Mass spectrum of 25-OHD3 fragmentation.

Then MRM experiments were conducted to optimize Collision Energy (CE) and Collision Exit Potential (CXP).

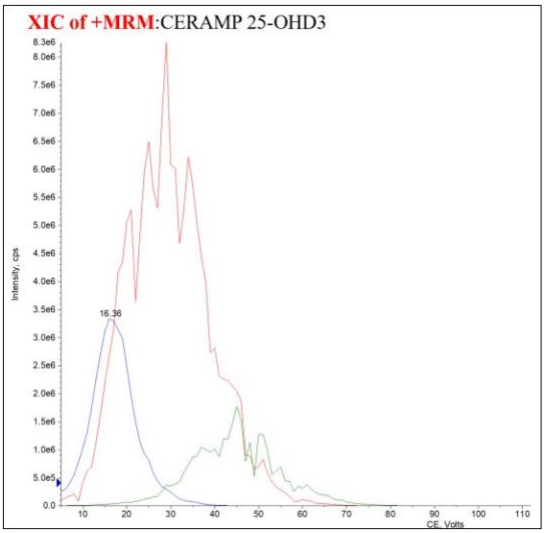

Fig. 30 - 25-OHD3 MRM experiment with CE ramping.

Collision energy was optimized in a single MRM experiment, by monitoring the transitions of the selected ions all together (Fig. 30), while CXP was optimized by a separate monitoring of the individual transitions, because the specific tool inside the management software does not allow a simultaneous optimization of all the transitions. Then the two most significant transitions were chosen for both compounds (25-OHD3 and IS): that with the highest signal/noise ratio (S/N) was then used for quantification (Quantifier), while the other was used for the compound confirmation (qualifier).

2.2.2. *MS optimization of vitamin D3 and d3-vitamin D3 (6,19,19-d3)*

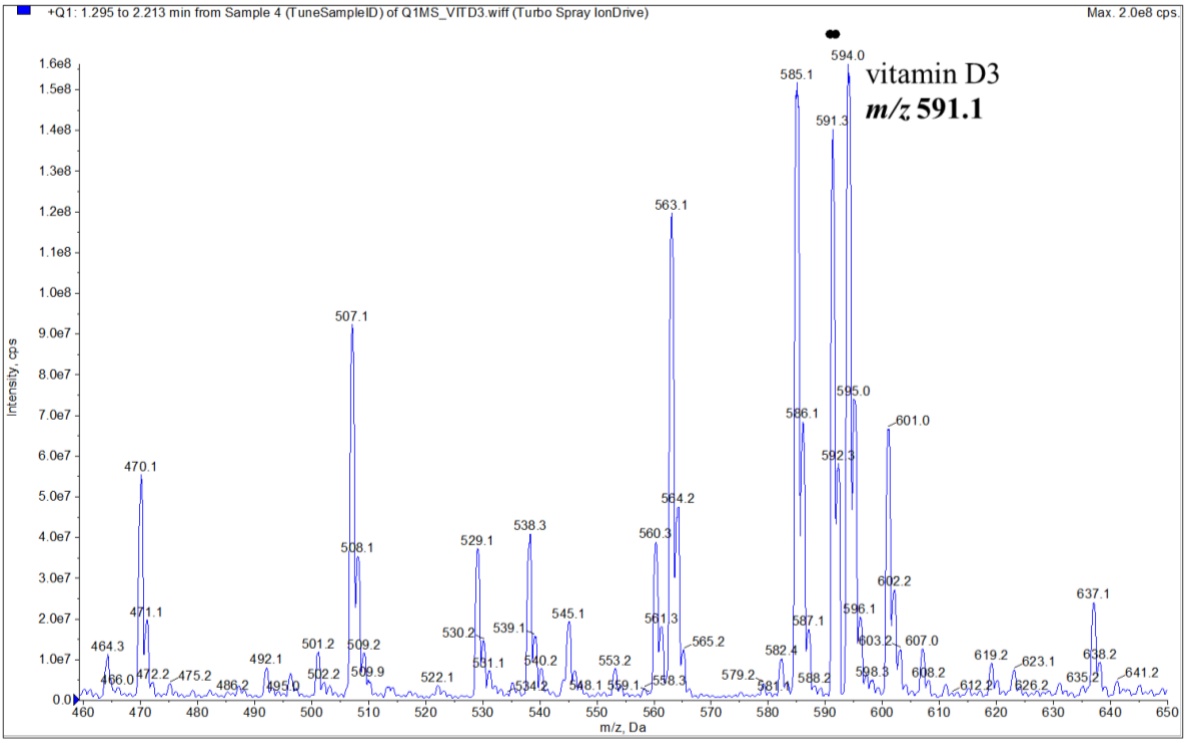

Fig. 31 - Vitamin D3 Q1 scan spectrum.

Similarly to the optimization of 25-OHD3, also for vitamin D3 and d3-vitamin D3 (6,19,19-d3) molecular ions $[M+H+MeNH_2]^+$ were identified by Q1 MS full scan in positive ions mode, at *m/z* 591.1 and *m/z* 594.4 (Fig. 31). Then DP and EP were optimized by Q1 Multiple Ion analysis (Q1 MI), performing suitable voltage ramps. Using a CE ramp in a Product Ion Scan (MS2) experiment, the fragment ions of Vitamin D3 and of its IS have been identified and, among these, the most specific and abundant fragments have been selected (Fig. 32).

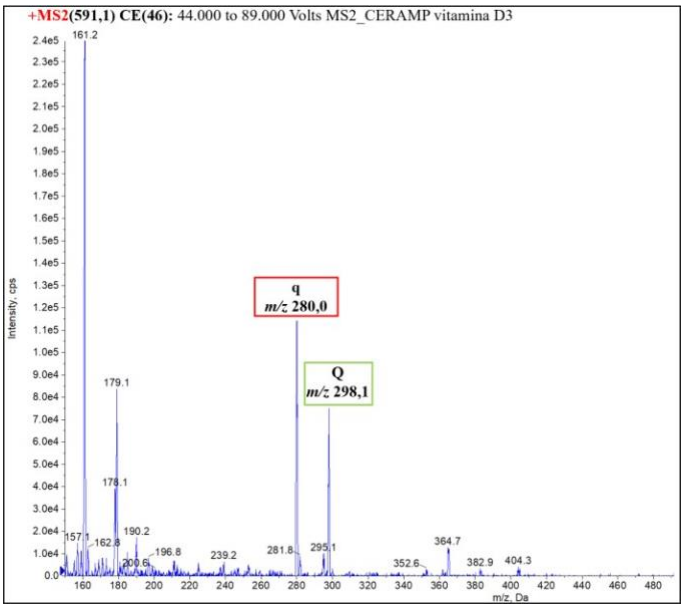

Fig. 32 - Mass spectrum of vitamin D3 fragmentation.

Then MRM experiments were carried out to optimize CE and CXP: The collision energy was optimized in a single experiment by monitoring all the transitions of the selected ions (Fig. 33), while the CXP was optimized by monitoring the individual transitions. Again, the two most significant transitions for both compounds were chosen, one of which for quantification (Quantifier) and the other one for the qualitative confirmation of the compound under investigation (qualifier).

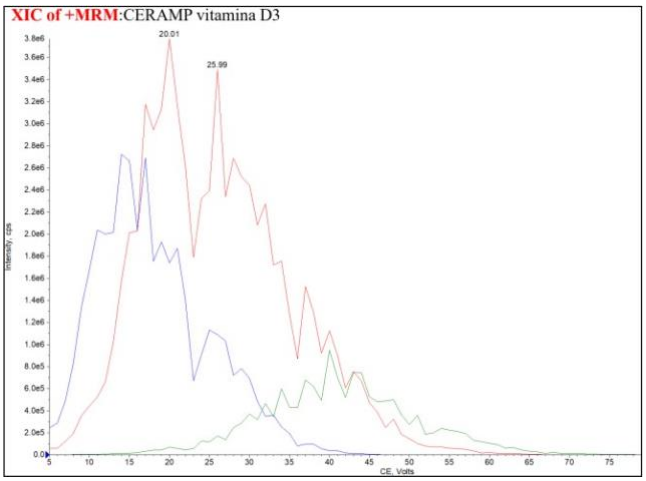

Fig. 33 - CE ramps of vitamin D3 in MRM mode.

2.2.3. MS optimization of 24,25-(OH)2D3 and d6-24,25-(OH)2D3 (26,26,26,27,27,27-d6)

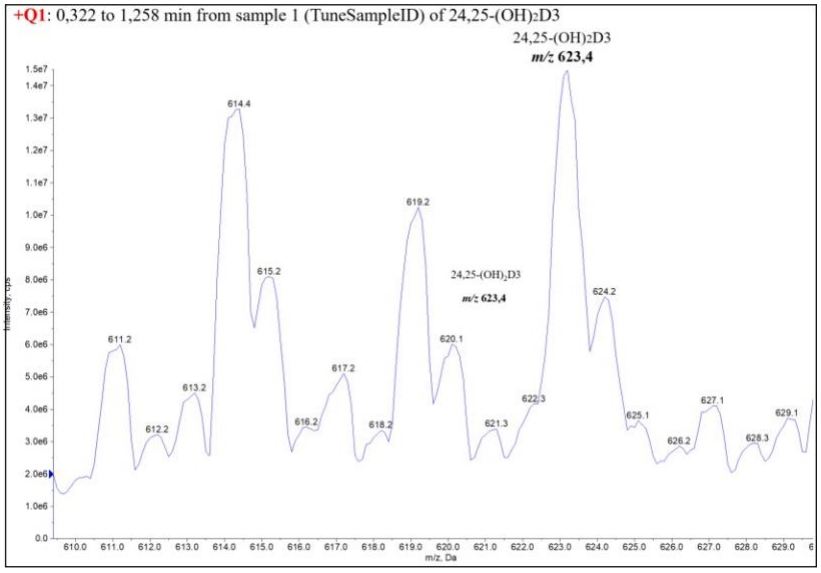

Fig. 34 - 24,25-$(OH)_2$D3 full scan (Q1) spectrum.

The previously mentioned procedure was used also for the optimization of 24,25-$(OH)_2$D3 and d6-24,25-$(OH)_2$D3 (26,26,26,27,27,27-d6), which had *m/z* 623.4 and *m/z* 629.5 as a $[M+H+MeNH_2]^+$ precursor ion, respectively. Figure 34 shows the result of a full scan experiment (Q1 MS) in positive ion mode, while Figure 35 shows the subsequent Product Ion Scan (MS2) spectrum, which was acquired by making use of a CE ramp for the identification of the most suitable fragment ions among those with structural significance.

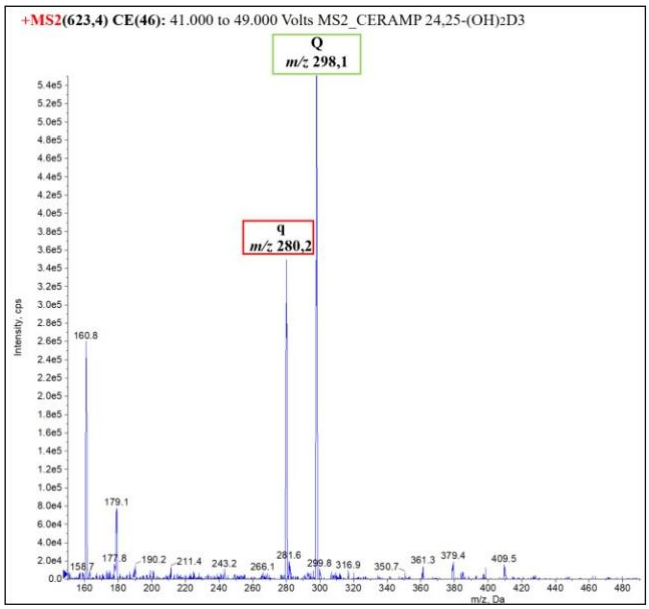

Fig. 35 - Mass spectrum of 24,25-$(OH)_2$D3 fragmentation.

Again, MRM experiments were carried out to optimize CE (Fig. 36) and CXP and the two most significant transitions for both compounds were chosen as a Quantifier and qualifier.

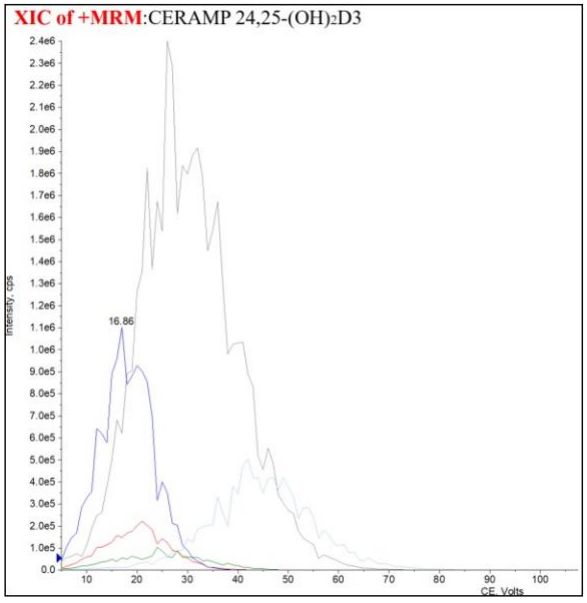

Fig. 36 - CE ramp of 24,25-$(OH)_2$D3 in MRM mode.

2.2.4. MS optimization of 1,25-(OH)2D3 and 13C3-1,25-(OH)2D3

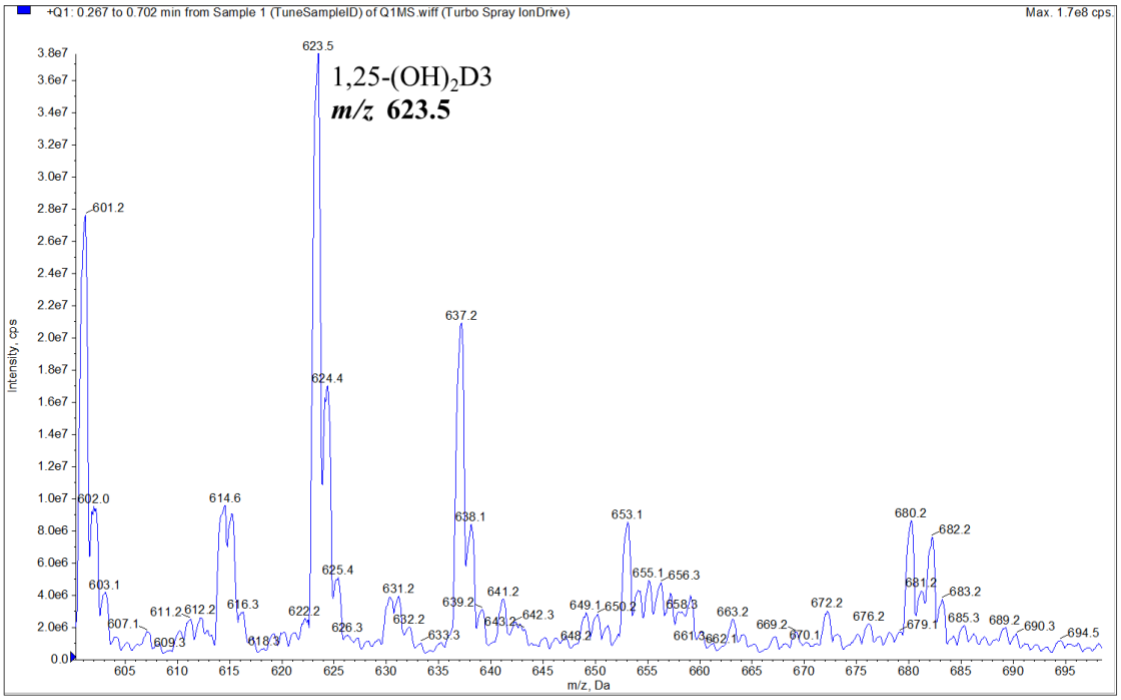

Fig. 37- 1,25-$(OH)_2$D3 full scan (Q1) spectrum.

$[M+H+MeNH_2]^+$ precursor ions of 1,25-$(OH)_2$D3 and ^{13}C3-1,25-$(OH)_2$D3, respectively at m/z 623.5 and m/z 626.4, were detected in full-scan positive ion mode (Fig. 37). As usual, the optimization of precursor ions was carried out in Q1 Multiple Ion mode, ramping DP and EP, while detection and selection of fragment ions was performed by ramping CE in Product Ion Scan (MS2) mode. Among the product ions, the most abundant fragments with structural significance were chosen (Fig. 38).

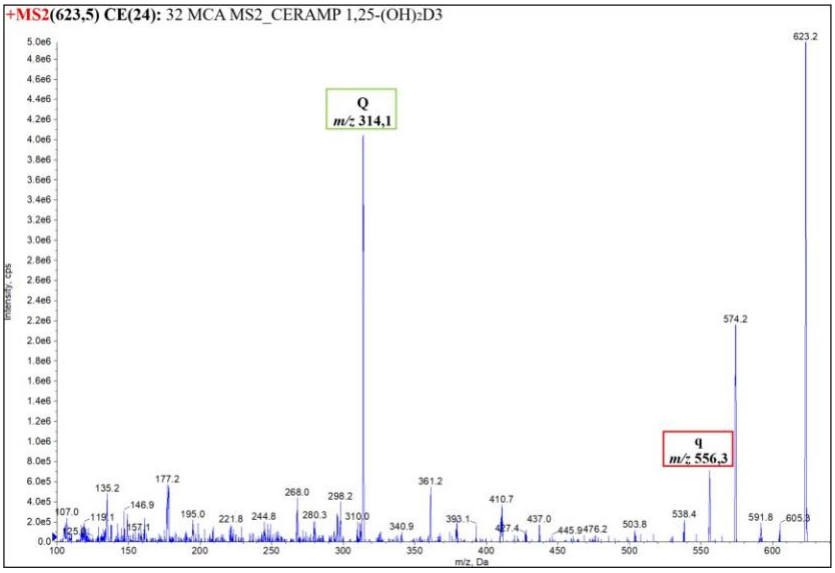

Fig. 38 - 1,25-(OH)$_2$D3 fragmentation spectrum.

CE and CXP were optimized by using MRM experiments. The collision energy has been optimized in different experiments, as well as the CXP parameters, each of the selected ion transitions was optimize separately (Fig. 39).

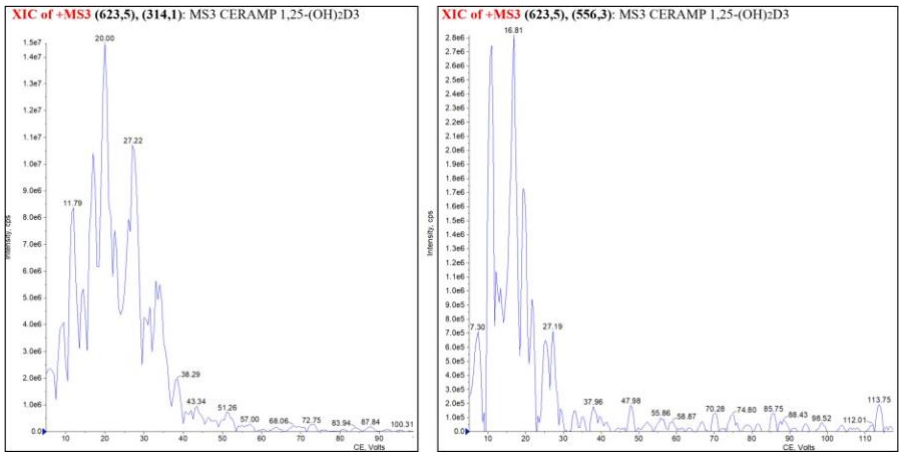

Fig. 39 -1,25-(OH)2D3 CE ramps in MS3 mode.

Two most significant transitions for the analyte 1,25-(OH)$_2$D3 have been chosen, one of quantification (Quantifier) and one used for the qualitative confirmation of

the compound (qualifier), while for the ^{13}C3-1,25-(OH)$_2$D3 was chosen only one transition and used as the quantification transition (Quantifier). The ion trap parameters were then optimized to obtain the best sensitivity. The MS3 detection, which is a scanning mode of Q-Q-Trap tandem mass spectrometry, was used to increase the low signal of 1,25-(OH)$_2$D3 in real samples. For MS3 detection, the precursor ion of target compounds was firstly selected in Q1 and then it was fragmented into product ions in the collision cell (Q2), the product ions generated in Q2 were then captured and accumulate in linear ion trap. Finally, the selected product ions were further fragmented in linear ion trap and the second-generation fragment ions are scanned out to the detector. MS3 is a more sensitive and specific detection mode, since noise is usually low, and it provided better quantitative results and a lower limit of detection value for 1,25-(OH)$_2$D3.

2.3. Optimization of Source Conditions

Several parameters affect the performance of the source. The optimization of these parameters maximizes the signal-to-noise ratio and signal stability. After the development of the MRM method for 25-OHD3, 24,25-$(OH)_2$D3, vitamin D3 and their ISs and MS3 method for 1,25-$(OH)_2$D3 and its ISby FIA (Flow injection analysis) experiments, the following source parameters were optimized:

- Ion Spray Voltage (IS)
- Gas Source 1 (GS1)
- Gas Source 2 (GS2)
- Source Temperature (TEM)
- Collision gas (CAD)

In the LC-MS method these values must be the same for all compounds, because their variation is not instantaneous as in the case of the potentials of the various lenses, but requires relatively long times, a compromise value between the optimal values has been used, chosen according to the sensitivity needs of the individual analytes.

2.4. Development of LC method.

Developing a robust chromatography is fundamental to get a successfully analytical method. The goal of a good chromatography is to separate the analyte(s) of interest from the endogenous interferences, since the coelution of endogenous metabolites with other endogenous or exogenous species may cause ion signal suppression or enhancement, which could be both detrimental to the accuracy of the assay. So that, the chromatographic separation provides a significant contribution to selectivity, sensitivity, and accuracy of a LC-MS/MS method. A satisfactory separation between analytes and interferences can be achieved by adequately exploiting the retentive characteristics of the compound(s) of interest. This can be achieved by testing different high retention columns, such as C18, with different reversed-phase gradients at both low and high pH. This allows the selection of the most promising conditions from which to continue the development of the LC methodology. For this purpose, during the development of the LC method, the features of the derivatized vitamin D3 metabolites have been evaluated again. As mentioned above, with respect to analytes as they are, the derivatized analytes have a higher molecular weight and a greater ability to establish hydrophobic interactions with the stationary phase, resulting in an increase in their retention time. Actually, the derivatization reaction and the formation of the $MeNH_2$ adduct change the structure of the analytes, making them more similar to the stationary phase of the Acquity UPLC BEH Phenyl (1.7 µm, 50x2.1 mm) column, with undoubtful advantage in terms of HPLC separation (selectivity). In addition, the structural changes introduced with derivatization improve instrumental sensitivity, because they increase nebulization and ionization efficiency in the MS source. An example of the signal obtained for the derivatized analytes is shown in Fig. 40.

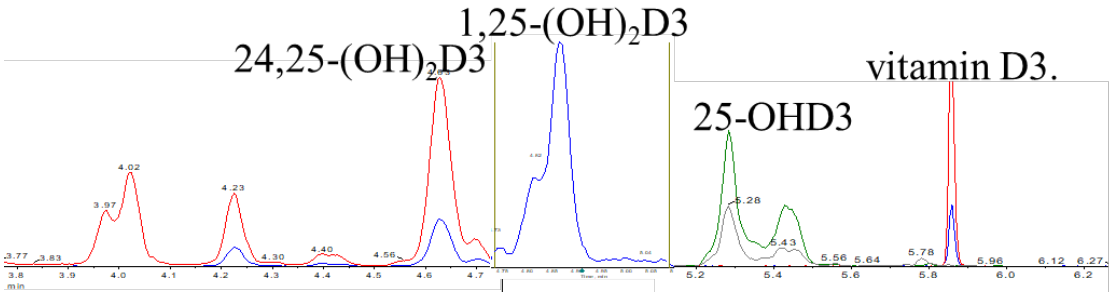

Fig. 40 - Chromatograms of vitamin D3 metabolites.

2.5. Sample Preparation

Selection of the most suitable sample preparation depends on the sample matrix complexity and the assay sensitivity and throughputness required. The two most common biological samples to be analyzed are plasma/serum and urine. The sample preparation process fulfills three major roles:

1. removal of protein and phospholipids that may contaminate the chromatography column,
2. elimination of endogenous compounds, such as phospholipids, that are the major cause of ion suppression/enhancement in LC/MS,
3. concentration to increase assay sensitivity.

Common sample preparation methods are based on protein precipitation with acid or organic solvent, solid-phase extraction (SPE), and liquid/liquid extraction. In our experiments we have also tested a simple, fast, and cheap protein precipitation procedure combined with columns or plates specific for phospholipid removals, such as Phenomenex Iphree and Waters Ostro. Actually, commercial SPE devices are avaible as a single SPE device and 96 well plates with many different stationary phases for sample clean-up, which can be appropriately selected according to the physical-chemical properties of the compounds of interest. Hence SPE can be extremely versatile and efficient in the removal of interfering components and in

the production of a very clean and concentrated sample for subsequent analysis. We developed several SPE protocols, by using different stationary phase such as Waters HLB, Phenomenex Strata X and Strata C18, to reduce matrix effect and enhance the sensibility of the method. Unfortunately, SPE did not provide good results in terms of matrix effect and recovery, respectively. Therefore, we investigated the possibility of using a clean-up step based on a liquid/liquid extraction, trying to remove most of the interfering compounds, and reducing as much as possible the analytes loss. Thus, different solvents and solvents mixture were tested, including hexane, dichloromethane, ethyl acetate, acetone, chloroform, tert-butylmetyl ether (MTBE), as well as different solvent volumes, short and long extraction times, and single and multiple extractions (up to 3). The best results were obtained with 600 µL of a hexane/dichlorometane (1:1; V:V) mixture, where hexane was able to extract the less polar analytes (25-OHD3 and vitamin D3), and dichloromethane gave a significant contribution in the extraction of the most polar analytes (1,25-$(OH)_2$D3 e 24,25-$(OH)_2$D3), and repeating the extraction three times. However, when developing a sample preparation method consideration must be given to solvent cost and disposal, as well as to the possibility to use automation, which influences the method throughputness. Unfortunately, when automated preparers are not available, as in our case, LLE becomes labor-intensive. For this reason, we consider the developed sample preparation method as susceptible to improvement, in order to increase its throughputness.

2.6. Method Validation

The method was validated for selectivity, linearity, lower limit of detection (LLOD), lower limit of quantitation (LLOQ), recovery (RE), matrix effect (ME), accuracy, precision, and stability, in compliance with EMA (European medicines agency) guidelines [131]. Since the sample preparation included a derivatization process, the efficiency of the derivatization reaction was evaluated according to time (15, 40, and 60 min), temperature (40, 60, and 80 °C), and vitamin D3 metabolites concentration in water solution, in 2x charcoal stripped plasma and in native human plasma (QC1 QC2 QC3). Selectivity was assessed by the addition of an aqueous solution containing the four metabolites of vitamin D3, at known concentration, in a pool of plasma from healthy subjects. The retention time and peak shape were compared with standard solutions to exclude co-elution of structurally similar compounds. Linearity was evaluated by the correlation coefficient of 10 calibration curves, prepared and injected on different days. A parallelism experiment, showing the effects of dilution on the quantitation of vitamin D3 metabolites in three different matrices, namely acetonitrile, Monobind Inc. (Lake Forest, CA, USA) 2x charcoal stripped plasma (treated with activated charcoal to remove endogenous amounts of analytes of interest), and a pool of real human plasma from healthy volunteers, was carried out. Basically, it consisted in a comparison between the calibration curves built in the three matrices, prepared by spiking all of them with the same amount of vitamin D 3 metabolites and there IS, as reported in the "Preparation of stock solutions, calibrators and quality controls" section. This experiment was carried out to demonstrate that calibration standards in acetonitrile as well as in 2x charcoal stripped plasma well track the response of vitamin D3 in the biological samples. Stripped plasma resulted as the white matrix most similar to that of the real samples

and was chosen for the quantification of real samples. So that, on a routine basis calibration curves were prepared in stripped plasma, by using serial dilutions, in the following concentration ranges: 0.156-20.00 ng/mL, for 24,25-(OH)2D3; 0.015-1.92 ng/mL, for 1,25-(OH)2D3; 1.25-160.00 ng/mL, for vitamin D3 and 1.125-144.00 ng/mL for 25-OHD3. For each analyte, the curves were established by plotting analyte/IS area ratio (the y axis) versus the nominal concentration (the x axis) of each standard analyte. The analytical sensitivity was assessed by measuring instrumental LLOD and LLOQ, evaluated by injecting acetonitrile + 0.1% formic acid solutions containing 25-OHD3, 24,25-(OH)2D3, vitamin D3 e 1,25-(OH)2D3 at different known concentrations up to signal to noise ratios (S/N) of 3 and 10, respectively for LLOD e LLOQ, calculated by a specific software tool included in the Analyst software. Matrix effect (ME) is commonly caused by coelution of compounds with target analytes, resulting in either suppression or enhancement of analyte ionization. Thus, to achieve the desired accuracy, precision, and sensitivity, ME was evaluated and controlled during bioanalytical method development. We estimated the ME following the protocol by Matuszewski et al. [132]; because the IS showed a different behaviour (signal intensity) from the analytes, the ME was evaluated directly on the latter. For this purpose, solutions containing the 4 analytes, in methanol (A), were prepared, each with three different concentrations:

- $QC1_A$: 0.50 ng/mL, for 24,25-(OH)2D3, 0.03 ng/mL, for 1,25- (OH)2D3, 3,75 ng/mL, for vitamin D3 e 3.125 ng/mL, for 25-OHD3,
- $QC2_A$: 2.00 ng/mL, for 24,25-(OH)2D3, 0.12 ng/mL, for 1,25-(OH)2D3, 15.00 ng/mL, for vitamin D3 e 12.50 ng/mL, for 25-OHD3,
- $QC3_A$: 8.00 ng/mL, for 24,25-(OH)2D3, 0.48 ng/mL, for 1,25-(OH)2D3, 60.00 ng/mL, for vitamin D3 e 50.00 ng/mL, for 25-OHD3;

These solutions were dried under gentle stream of N_2 at 40 ºC and derivatized with

PTAD. Five different human plasma matrices, treated as the sample as regards LLE, were added with suitable amounts of $QC1_A$, $QC2_A$, and $QC3_A$ after the extraction process to obtain plasma QCs (B). For each analyte, the difference between the chromatographic peak areas of each QCs in methanol has been calculated. The peak area of pure methanol (Blank), which was equal to zero, has been subtracted from $QC1_A$ corresponding areas. The peak areas corresponding to $QC1_A$ were subtracted from $QC2_A$ and the areas corresponding to $QC2_A$ were subtracted from $QC3_A$.The same process was applied to the plasma QCs_B. In that case the peak areas corresponding to the endogenous metabolites in the plasma matrix (Blank Plasma) was subtracted from $QC1_B$. ME was then calculated, for each analyte in the 5 different plasma matrices, as the ratio between the difference of the peak areas in the matrix B and methanol A, with the formula

$$ME\ (\%) = B / A \times 100$$

The RE was evaluated by the data obtained to following experiment: comparison between the peak areas obtained by analyzing a pool of human plasma spiked with the 4 analytes of interest, before the liquid/liquid extraction (C) and after the liquid/liquid extraction (D). The analytes were added in three different concentrations:

- for 24,25-$(OH)_2$D3: 0.50 ng/mL (C1, D1); 2.00 ng/mL (C2, D2); 8.00 ng/mL(C3, D3);
- for 25-OHD3: 3,125 ng/mL (C1, D1); 12,50 ng/mL (C2, D2); 50.00 ng/mL(C3, D3);
- for vitamin D3: 3,75 ng/mL (C1, D1); 15.00 ng/mL (C2, D2); 60.00 ng/mL(C3, D3);

- for 1,25-$(OH)_2$D3: 0,025 ng/mL (C1, D1); 0,10 ng/mL (C2, D2); 0,40 ng/mL (C3, D3).

The RE has been calculated as the ratio of the peak areas of each of the analytes according to the following formula:

$$RE\ (\%) = C / D \times 10$$

Intra-day and inter-day Accuracy (expressed as accuracy%) and precision (expressed as relative standard deviation%, RDS%) were assayed also on the quality controls, containing 4 analytes, in stripped plasma and prepared as referred below:

- QC1: 0.50 ng/mL, for 24,25-$(OH)_2$D3; 3.75 ng/mL, for vitamin D3;0.025 ng/mL, for 1,25-$(OH)_2$D3 e 3.125 ng/mL, for 25-OHD3;
- QC2: 2.00 ng/mL, for 24,25-$(OH)_2$D3; 15.00 ng/mL, for vitamin D3; 0.10 ng/mL, for 1,25-$(OH)_2$D3 e 12.50 ng/mL, for 25-OHD3;
- QC3: 8.00 ng/mL, for 1,25-$(OH)_2$D3; 60.00 ng/mL, for vitamin D3; 0.40ng/mL, for 1,25-$(OH)_2$D3 e 50.00 ng/mL, for 25-OHD3

All concentrations were assayed by 3 replicate injections, and the statistical parameters were calculated by using mean concentration values. Inter-day accuracy and precision were measured on different aliquots of the solutions used for the assessment of intra-day accuracy and precision on 3 different days. Intraday accuracy and precision, as well as inter-day accuracy and precision were considered acceptable when within ± 15%. Stability, which is the capability of a sample material to retain the initial property of a measurand when the sample is stored under defined conditions, was evaluated for the four analytes,

both in acetonitrile e in 2x stripped plasma. Stability was assessed after 24 hours exposure to −20 °C (one freeze–thaw cycle), 5 °C, and 25 °C. The results obtained from an aliquot of freshly prepared QCs were compared to the results provided by aliquots previously stored for 24 hours at 5 °C, 25 °C and at −20 °C, the latter aliquots were thawed at room temperature before preparation.

2.7. Materials and methods

2.7.1. Reagents and materials

Methanol standard solution of 25-OHD3 (5 µg/mL), d6-25-OHD3 (50 µg/mL), 1,25-$(OH)_2$D3 (5 µg/mL), ^{13}C3-1,25-$(OH)_2$D3 (5 µg/mL), vitamin D3 (1 mg/mL), d3-vitamin D3 (100 mg/mL),24,25-$(OH)_2$D3 (100 µg/mL) and d6-24,25-$(OH)_2$D3 (100 µg/mL), as well as methanol (LC-MS grande), ultrapure water (LC-MS grande), formic acid (MS Grade 99%), acetonitrile (LC-MS grade), methylamine solution (2.0 M in methanol) and PTAD powder were purchased from Merck KGaA (Darmstadt, Germany). The quench solution was provided by PerkinElmer (Waltham, MA, USA).

2.7.2. HPLC conditions

An Agilent Infinity UHPLC system (Santa Clara, CA, USA), consisting of a 1290 thermostated autosampler, a 1290 binary pump, and a 1290 column oven, was used for the samples injection and the chromatographic analysis. Chromatographic separation was achieved by a Waters (Milford, MA, USA) Acquity BEH Phenyl (1.7 µm, 50x2.1 mm) UPLC column, protected by a Acquity BEH Phenyl (1.7 µm 2.1x5 mm) Vaguard pre-column, kept at 60 °C. The eluents were supplied by the binary pump and consisted of methanol containing 0.5 mM $MeNH_2$ as solvent A and water containing 0.5 mM $MeNH_2$ as solvent B, at a flow rate of 650 µL/min, under the gradient conditions shown in Table 3. The injection volume of samples, quality controls, and calibrators was 10 µL. To ensure a good robustness of the method and instrumental cleaning, only the eluate in the retention time range of the analytes was introduced into the source, while the rest was sent to the waste. An instrument integrated six-port switching valve diverted eluent from the analytical column to either waste or mass spectrometer. Eluent was directed to waste in

the time ranges 0–3.0 and 7.0–10.0 min, to discard both head and tail of the HPLC run and keep the instrument as clean as possible.

	Total Time (min)	Flow Rate (µg/mL)	A (%)	B (%)
0	0,00	650	40,0	60,0
1	0,50	650	40,0	60,0
2	4,50	650	70,0	30,0
3	5,00	650	70,0	30,0
4	5,50	650	100,0	0,0
5	7,00	650	100,0	0,0
6	7,50	650	40,0	60,0
7	10,00	650	40,0	60,0

Tab. 3 - Chromatographic conditions

2.7.3. MS Conditions

All analyses were performed with a Sciex QTrap 6500+ mass spectrometer (Concord, ON, Canada), equipped with an IonDrive Turbo-V electrospray (ESI) ion source. The MS method to assay 25-OHD3, 24,25-(OH)2D3, vitamin D3, and their ISs was based on positive ion mode multiple reaction monitoring (MRM) and made use of two transitions, both for each analyte and the relative internal standard. In addition, the MS method contains a period optimized for the assessment of 1,25-$(OH)_2$D3 and its IS that was based on positive ion mode MS3 (MS/MS/MS) and that made use of two transitions for the analyte and one transition for $^{13}C_3$-1,25-$(OH)_2$D3. Only one transition was selected for $^{13}C_3$-1,25-$(OH)_2$D3 identification to avoid a possible trap saturation and the space charge effects that are known to limit the functional ion storage capacity of ion trap mass analyzers and this, in turn, can affect the quality of the mass spectral data generated[133]. Except for the latter, the transitions with the highest signal to noise ratio were used as quantifiers (Q), while the others as qualifiers (q). Declustering potentials (DP), entrance potentials (EP), collision energies (CE), and collision exit potentials (CXP) were optimized, and their values are reported in Table 4.

Scan type	*Analyte*	*SRM Transition*	*Operative Parameters*			
			DP	**EP**	**CE**	**CXP**
MRM	**24,25-(OH)2D3**	623,4 → 280,2 **(q)**	87.0	7.0	41.980	7.630
		623,4 → 298,1 **(Q)**			28.900	8.530
	d6-24,25-(OH)2D3 (IS)	629,5 → 385,6 **(Q)**	87.0	7.0	41.980	7.630
		629,5 → 298,1 **(q)**			28.900	8.530
MS3	**1,25-(OH)2D3**	623,5 → 314,1 **(Q)**	90.0	7.0	30.000	
	13C3-1,25-(OH)2D3 (IS)	626,5 → 314,4 **(Q)**	90.0	7.0	30.000	
MRM	**vitamin D3**	559,1 → 280,0 **(q)**	40.0	7.7	40.000	7.120
		559,1 → 298,1 **(Q)**			20.300	8.060
	d3-vitamin D3 (IS)	594,4 → 283,3 **(q)**	40.0	7.7	40.000	7.120
		594,4 → 301,4 **(Q)**			20.300	8.060
	25-OHD3	607,3 → 298,3 **(Q)**	80.0	10.0	28.880	8.290
		607,3 → 558,3 **(q)**			16.360	10.940
	d6-25-OHD3 (IS)	613,4 → 298,3 **(Q)**	80.0	10.0	28.880	8.290
		613,4 → 564,3 **(q)**			16.360	10.940

Tab. 4 -Mass spectrometry operative parameters.

In MS3 mode, the ion trap was used just to accumulate ions, and not to carry out a real fragmentation. In practice, specific primary fragments (or secondary precursors) from 1,25-$(OH)_2$D3 and the relative IS, produced inside the collision cell during the MS/MS process, were selected and trapped by using a zero collision energy (Excitation energy, AF2, at 0 V). An important parameter that was optimized to increase the signal intensity is the Fixed LIT fill time, that is the amount of time used to fill the LIT with ions before scanning. LIT Fill-time has been set to 45 ms, Q3 entry barrier was 8 V, and excitation time for MS/MS/MS fragmentation was 0.01 ms. The source parameters were optimized to get the maximum sensitivity: CUR 25; IS 5,5 kV; GS1 and GS2 zero air, 55 and 45 respectively; source temperature TEM, 450 °C; high collision gas CAD nitrogen was used during MS3 mode, while in MRM the operative pressure with CAD gas on, was 11.0 mPa. The Sciex Analyst 1.7.3 software was used for instrument control and data acquisition, while the Sciex Multiquant 3.0.3 software for data processing.

2.7.4. Sample preparation and storage.

After collection, plasma samples were stored at -20°C. When needed, samples were thawed at room temperature, vortexed (15 min) and a 100 µL aliquot was added with 300 µL of a freshly prepared daily precipitation solution (DPS) containing acetonitrile, formic acid 0.1% (V%), and ISs at the concentration of 5 ng/mL for d3-vitamin D3, 0.50 ng/mL for d6-24,25-$(OH)_2$D3, 0.25 ng/mL for $^{13}C_3$-1,25-$(OH)_2$D3, and 50.00 ng/mL, for d6-25-OHD3. The resulting suspensions were vortexed (15 min), centrifuged (18.620 × g 15 min), and 400 µL of the supernatants dried at 40 °C under a gentle stream of nitrogen. The dry residues were added with 300 µL di H_2O, sonicated (1 min), and then added with 600 µL of hexane/dichloromethane (1:1; V:V) mixture. The immiscible aqueous and organic phase were sonicated (1 min) and centrifuged (14.800 x g, 2 min); thus, the mixture of hexane/dichloromethane was collected and transferred in a clean tube. The extraction process was repeated three times, and the resulting organic mixture was dried under N_2, at 40 ºC. The dried samples were submitted to Diels-Alder reaction, consisting of their reconstitution with 50 µl of PTAD in acetonitrile (1.5 mg/ml) and vortexing (15 min) at room temperature in dark conditions; then, 50 µl of quench solution, which consists of H2O+ 0.1% FA, was added and the solution was vortexed for 5 min and dried again under N2 at 40 ºC. The dry residues were reconstituted with 100 µL of H_2O + 0.5 mM $MeNH_2$/MeOH + 0.5 mM $MeNH_2$ (50/50; V/V), vortexed (15 min), centrifuged (2 min), and put into a 96 wells plate for the HPLC-MS/MS analysis. 10 µl of the solutions obtained were injected into the LC-MS/MS instrument for analysis.

2.7.5. Preparation of stock solutions, calibrators and quality control

The standard stock solutions of the analytes and ISs, were stored in the freezer at -20°C. Calibrators were prepared by serial dilution in 2x plasma stripped at the following concentrations:

- L1: 0.156 ng/mL (24,25-$(OH)_2$D3), 0.015 ng/mL (1,25-$(OH)_2$D3), 1.25 ng/mL (vitamin D3), 1,125 ng/mL (25-OHD3);
- L2: 0.312 ng/mL (24,25-$(OH)_2$D3), 0.03 ng/mL (1,25-$(OH)_2$D3), 2.50 ng/mL (vitamin D3), 2.25 ng/mL (25-OHD3);
- L3: 0.625 ng/mL (24,25-$(OH)_2$D3), 0.06 ng/mL (1,25-$(OH)_2$D3), 5.00 ng/mL (vitamin D3), 4.50 ng/mL (25-OHD3);
- L4: 1.25 ng/mL (24,25-$(OH)_2$D3), 0.12 ng/mL (1,25-$(OH)_2$D3), 10.00 ng/mL (vitamin D3), 9.00 ng/mL (25-OHD3);
- L5: 2.50 ng/mL (24,25-$(OH)_2$D3), 0.24 ng/mL (1,25-$(OH)_2$D3), 20.00 ng/mL (vitamin D3), 18.00 ng/mL (25-OHD3);
- L6: 5.00 ng/mL (24,25-$(OH)_2$D3), 0.48 ng/mL (1,25-$(OH)_2$D3), 40.00 ng/mL (vitamin D3), 36.00 ng/mL (25-OHD3);
- L7: 10.00 ng/mL (24,25-$(OH)_2$D3), 0.96 ng/mL (1,25-$(OH)_2$D3), 80.00 ng/mL (vitamin D3), 72.00 ng/mL (25-OHD3);
- L8: 20.00 ng/mL (24,25-$(OH)_2$D3), 1.92 ng/mL (1,25-$(OH)_2$D3), 160 .00ng/mL (vitamin D3), 144.00 ng/mL (25-OHD3).

Quality control solutions were also prepared in 2x plasma stripped, by adding appropriate amounts of the analytes operative stock solution to achieve the following concentrations:

- QC1: 0.50 ng/mL, for 24,25-$(OH)_2D3$, 0.03 ng/mL, for 1,25$(OH)_2D3$, 3.75 ng/mL, for vitamin D3 e 3.125 ng/mL for 25-OHD3;
- QC2: 2.00 ng/mL, for 24,25-$(OH)_2D3$, 0.12 ng/mL, for 1,25$(OH)_2D$, 3.15 ng/mL, for vitamin D3 e 12.50 ng/mL for 25OHD3;
- QC3: 8.00 ng/mL, for 24,25-$(OH)_2D3$, 0.48 ng/mL, for 1,25$(OH)_2D$, 3.60 ng/mL, for vitamin D3 e 50.00 ng/mL for 25-OHD3.

Both calibrators and quality controls (100 μL each) were treated as the samples and analyzed twice (before and after samples injections) in each batch.

2.8. Vitamin D3 Status and inflammatory response in patients with COVID-19

The aim of this study is primarily to analyze the relationship between vitamin D status and a biochemical panel of inflammatory markers in a cohort of patients with COVID-19. As a secondary endpoint, we evaluated the correlation between 25-OHD3 levels and the severity of the disease.

2.9. Materials and Methods

2.9.1. Study Design and Patients

This was a retrospective, observational study conducted on available serum samples from 93 consecutive patients with COVID-19-related pneumonia, admitted from March to May 2020 in two hospital units (n = 64 from a pulmonary unit and n = 29 from a geriatric unit) in Pisa. The two units were designated acute care units for patients with COVID-19-

related pneumonia not requiring endotracheal intubation. Demographic data, clinical history, therapies, clinical data during hospitalization, routine blood data, blood coagulation parameters, arterial blood gas analysis, and imaging were available from the records of patients. In-hospital mortality and serious adverse events were also recorded.

2.9.2. Biochemical panel of inflammatory marker measurament and other measuraments

Samples from routine blood collection at hospital admission of all consecutive patients (n = 93) were stored at −20°C (protected from light to preserve vitamin D3). Analysis for cytokines (interleukins IL-1b, IL-6, and IL-10; tumor necrosis factor-a, TNF-α; monocyte chemotactic protein- 1, MCPI-1/CCL2) was performed in the laboratory of the Clinical Pathology Unit of the University Hospital of Pisa by a fully automated ELISA processing system (DSX DINEX Technologies) using commercial ELISA assays according to the instructions of the manufacturer. Hemogasanalysis was performed by GEM Premier 4000 Blood Gas Analyzer (Werfen, Spain), and gas exchange impairment was evaluated using arterial partial pressure of oxygen (PaO2) to fraction of inspired oxygen (FiO2) (P/F) (12). Patients were classified into three groups based on the lowest value recorded during hospital stay (P/F nadir): patients with a P/F nadir ≥300 mmHg were categorized as "controls", patients with a P/F nadir between 201 and 300 mmHg were categorized as mild acute respiratory distress syndrome (ARDS), and patients with a P/F nadir <200 mmHg were categorized as severe ARDS.

2.9.3. 25-OHD3 Measurement

25-OHD3 levels were measured in the whole group (n = 93) of patients (blood samples were collected at baseline evaluation and the relative plasmas were stored at −20°C) with tandem mass spectrometry coupled to high-performance liquid chromatography (HPLC-MS/MS), using the MSMS VitD Kit from PerkinElmer (Waltham, MA, USA). The

instrumental layout has been described in section 2.6.3, Sciex QTRAP 6500+ was equipped with an atmospheric pressure chemical ionization (APCI) source. The HPLC column was a PerkinElmer Brownlee Supra C18 3 μm, 50 × 2.1 mm, protected by a PerkinElmer Brownlee Supra C18 Guard Column. The separation was carried out with gradient elution reversed- phase chromatography that made use of methanol + 0.1% formic acid as solvent A and water + 0.1% formic acid as solvent B. The MS method was based on positive ion multiple reaction monitoring (MRM) with the following quantifying transitions: 25-OHD3, m/z 401 > 159; 2H3-25-OHD3 (IS), m/z 404 > 162; and 2H6-25-OHD3 (used in calibrators and quality controls in place of 25-OHD3), m/z 407 > 159 (10) [134]. Sample preparation consisted of conventional protein precipitation after the addition of a suitable amount of IS.

2.9.4. Statistical Analysis

Continuous variables were expressed as mean values ± standard deviations or median values and interquartile range (IQR—25° and 75° quartiles) according to whether they were normally distributed or not. Categorical variables were expressed as the number of cases and percentages. Non-parametric or parametric tests were performed accordingly. Comparisons of qualitative data were performed using the chi-square test. For continuous variables, assessments of any possible differences between the different groups considered were performed using Mann–Whitney U tests. The association between PaO2/FiO2 subgroups and circulating levels of 25-OHD3 levels was evaluated using the Jonckheere–Terpstra test for trend. Associations between serum 25-OHD3 levels and inflammatory markers were analyzed using the Pearson correlation coefficient. p-values < 0.05 were considered as statistically significant. The statistical package SPSS (27.0) was used for analysis.

III. Results

3.1. Validation of LC-MS-MS method

With regards to the quality of chromatography, it was good enough to separate the four metabolites of vitamin D3 from some potential interferences (Fig. 41), provided a symmetrical peak shape for endogenous analytes, with no clear evidence of overlapping with peaks from possible coeluted compounds, and it ensure the necessary selectivity of the method. As shown in the chromatogram, it is possible to clearly distinguish the peaks relative to 24,25-$(OH)_2$D3, with a t_R of 4.47 min, 1,25-$(OH)_2$D3, with a t_R of 4.82 min, 25-OHD3, with a t_R of 5.36 min, and that one of vitamin D3, with a t_R of 5.71 min. In particular, the chromatographic peaks before 24,25-$(OH)_2$D3, at a retention time of 4.18 min, and after vitamin D3 at a retention time of 5.85 min were well spaced from the peaks of main interest and do not interfere with them. Such peaks are associated to compounds of unknown structure, which are isobaric with 24,25-$(OH)_2$D3 and vitamin D3, and moderately respond just to the quantitative MRM transitions, while the response to the qualitative MRM transitions were very poor if not negligible. This MS behavior that is different from that of 24,25-$(OH)_2$D3 and vitamin D3 agrees with the different product ion spectra from the two isobaric quasi-molecular ions, that are clearly associable to different chemical structures. Vitamin D3 peak was narrow and well resolved, while 25-OHD3, 24,25-$(OH)_2$D3, and 1,25-$(OH)_2$D3 showed chromatographic peak splitting due to the presence of epimers (25-OHD3), and diasteroisomers which have been synthetized during the derivatization step (24,25-$(OH)_2$D3, and 1,25-$(OH)_2$D3). We could not separate such close peaks corresponding to the enantiomers, so we integrated them together as if they were a single chromatographic peak, ensuring a good quantitative analysis.

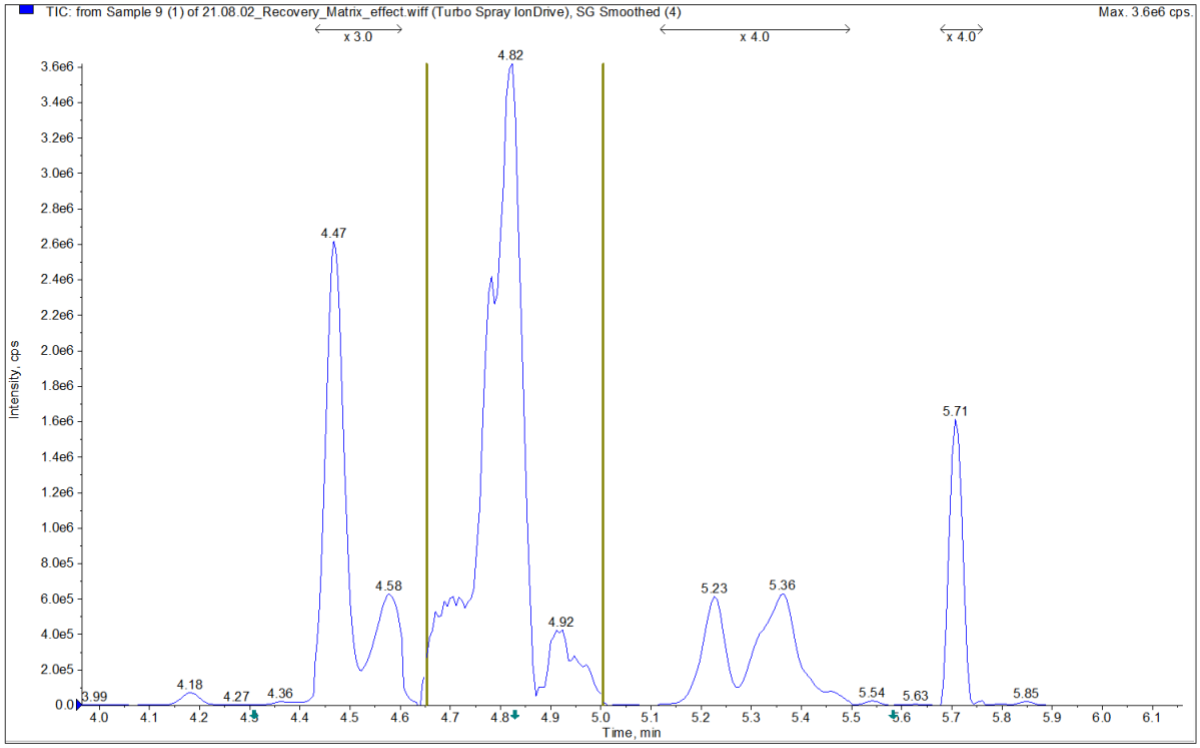

Fig. 41 – Chromatogram of a real sample.

The parallelism experiments demonstrated that the calibration curves built in water, 2x charcoal stripped plasma and native plasma by duplicate injections were all linear within the acquired concentration range (0.156-20.00 ng/mL, for 24,25-$(OH)_2$D3; 0.015-1.92 ng/mL, for 1,25-$(OH)_2$D3; 1.25-160.00 ng/mL, for vitamina D3 e 1.125-144.00 ng/mL for 25-OHD3), with a correlation coefficient always > 0.997, and showed superimposable slope values as reported in Fig. 42.

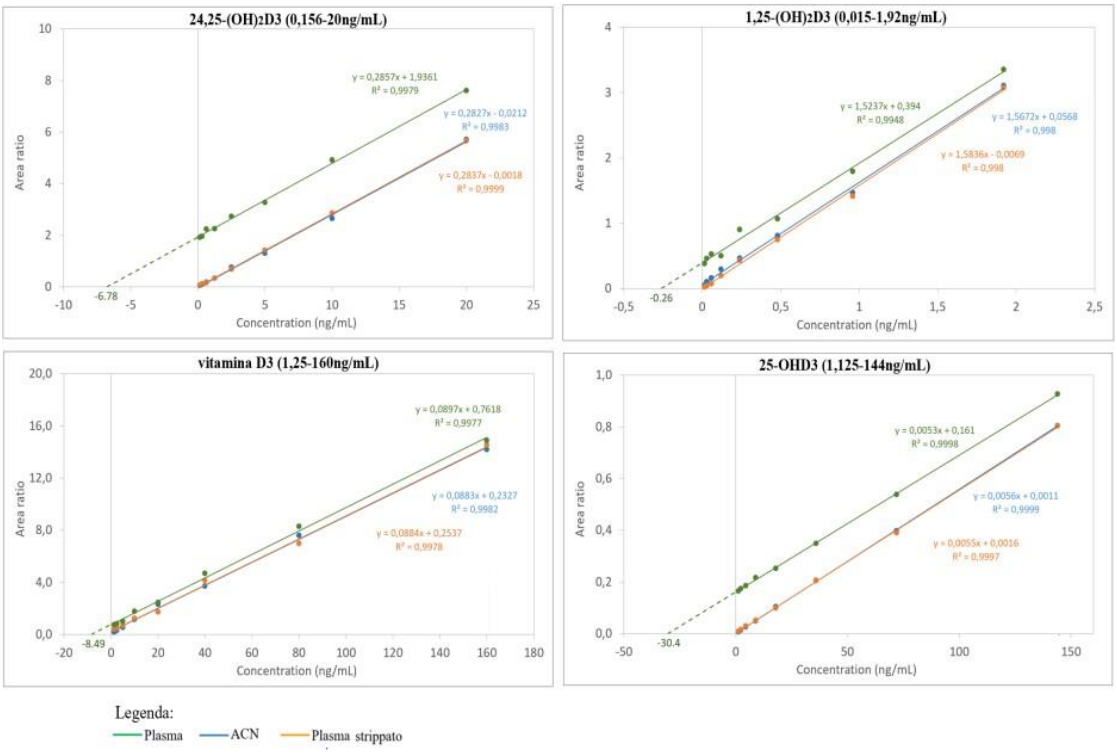

Fig. 42 – Graphical illustration of the parallelism experiment's results, achieved by plotting calibration curves built in acetonitrile (blue line), in a commercial 2x charcoal stripped plasma (yellow line), and in a human plasma sample from a healthy volunteer (green line). The negative x-intercepts of the extrapolated curves for the stripped and native plasma, provided the endogenous concentration of the vitamin D3 analytes in these two matrices.

The negative x-intercepts of the extrapolated curves for the stripped and native plasma, correspond to the absolute concentration value of the analyte to which the curve refers. The method is extremely sensitive with the following instrumental LLOD and LLOQ: 6.25 pg/mL and 12.5 pg/mL, respectively, for 24,25-$(OH)_2$D3; 12 pg/mL and 40 pg/mL, for 1,25-$(OH)_2$D3; 23.43 pg/mL and 46.87 pg/mL, for vitamin D3; 19.52 pg/mL and 40 pg/mL, for 25-OHD3. The matrix effect, expressed as % of residual signal compared to the theoretical value (the complement to 100 represents the signal actually suppressed by the matrix), tested on five different matrices of human plasma and expressed as mean (%) was equal to 38.7% for 24,25-$(OH)_2$D3, 45.8% for 1,25-$(OH)_2$D3, 12.0% for vitamin D3, and 13,4% for 25-OHD3 (Tab. 5).

		Nominal Conc. (µg/mL)	*Mean ME(%)*	
24,25-(OH)$_2$D3	C1	0,500	35,15	**38,7%**
	C2	2,000	42,86	
	C3	8,000	38,14	
1,25-(OH)$_2$D3	C1	0,030	36,33	**45,8%**
	C2	0,120	32,52	
	C3	0,480	68,66	
vitamina D3	C1	3,750	8,11	**12,0%**
	C2	15,000	11,53	
	C3	60,000	16,42	
25-(OH)D3	C1	3,125	21,38	**13,4%**
	C2	12,500	7,88	
	C3	50,000	11,28	

Tab. 5 – Matrix effect data.

Recovery, evaluated at three different concentration levels, for each of the four analytes, was almost independent from concentration itself and with values always around 100%. In particular, the mean value is equal to 100.56% for 24,25-(OH)$_2$D3, 100.75% for 1,25-(OH)$_2$D3, 103.23% vitamin D3, 99.19% for 25-OHD3 (Tab. 6).

		Nominal Conc. (µg/mL)	*RE(%)*	
24,25-(OH)$_2$D3	QC$_1$	0,500	102,24	**100,56%**
	QC$_2$	2,000	100,23	
	QC$_3$	8,000	99,21	
1,25-(OH)$_2$D3	QC$_1$	0,025	104,59	**100,75%**
	QC$_2$	0,100	98,15	
	QC$_3$	0,400	99,53	
vitamina D3	QC$_1$	3,750	101,18	**103,23%**
	QC$_2$	15,000	104,42	
	QC$_3$	60,000	104,09	
25-(OH)D3	QC$_1$	3,125	94,21	**99,19%**
	QC$_2$	12,500	99,91	
	QC$_3$	50,000	103,45	

Tab. 6 – Recovery data.

Good results were also obtained for intra- and inter-day accuracy and precision, as shown by the table below (Tab. 7).

		Nominal Conc. (µg/mL)	*Mean Conc. (µg/mL)*	*RSD(%)*	*Mean Accuracy (%)*
Intra-day	24,25-(OH)$_2$D3	QC_1	0,500	0,500	2,00	100,27
		QC_2	2,000	1,940	0,52	96,96
		QC_3	8,000	7,125	1,61	89,05
	1,25-(OH)$_2$D3	QC_1	0,025	0,030	0,00	106,94
		QC_2	0,100	0,115	4,35	113,22
		QC_3	0,400	0,470	0,00	117,42
	vitamina D3	QC_1	3,750	3,540	8,76	94,48
		QC_2	15,000	16,370	8,86	109,14
		QC_3	60,000	56,675	1,56	94,46
	25-(OH)D3	QC_1	3,125	3,200	3,75	102,43
		QC_2	12,500	13,185	2,01	105,50
		QC_3	50,000	51,065	0,62	102,13
Inter-day	24,25-(OH)$_2$D3	QC_1	0,500	0,510	3,06	101,94
		QC_2	2,000	2,017	2,22	100,85
		QC_3	8,000	7,980	2,58	99,74
	1,25-(OH)$_2$D3	QC_1	0,025	0,027	5,32	103,54
		QC_2	0,100	0,110	5,52	106,57
		QC_3	0,400	0,433	9,29	108,05
	vitamina D3	QC_1	3,750	3,536	9,44	95,05
		QC_2	15,000	15,487	6,34	103,24
		QC_3	60,000	59,260	5,33	98,77
	25-(OH)D3	QC_1	3,125	3,327	2,86	106,45
		QC_2	12,500	13,270	2,46	106,14
		QC_3	50,000	51,637	2,73	103,27

Tab. 7– Intra e inter-day accuracy and precision.

The stability, assessed at three different concentration levels in both acetonitrile and 2x stripped plasma after 24-hours of exposure to -20 °C, 5 °C e 25 °C for each of the four metabolites was found to be acceptable with the following values:

- 24,25-$(OH)_2$D3 (Tab. 8): at temperature of 5 °C, with a mean value of 109.06% in stripped plasma and 85.29% in acetonitrile; at temperature of -20 °C, with a mean value of 107.53% in stripped plasma and 90.46% in acetonitrile; at temperature of 25 °C, with a mean value of 105.58% in stripped plasma and 95.02% in acetonitrile.

		Nominal Conc. (ng/mL)	*Mean Conc. (ng/mL)*	*Stability(%)*
Fresh	QC_1 24,25-$(OH)_2$D3 plasma stripp.	0,50	0,48	
	QC_2 24,25-$(OH)_2$D3 plasma stripp.	2,00	1,97	
	QC_3 24,25-$(OH)_2$D3 plasma stripp.	8,00	8,44	
	QC_1 24,25-$(OH)_2$D3 ACN	0,50	0,50	
	QC_2 24,25-$(OH)_2$D3 ACN	2,00	2,01	
	QC_3 24,25-$(OH)_2$D3 ACN	8,00	8,00	
T: 5°C	QC_1 24,25-$(OH)_2$D3 plasma stripp.	0,50	0,53	110,94
	QC_2 24,25-$(OH)_2$D3 plasma stripp.	2,00	2,20	111,55
	QC_3 24,25-$(OH)_2$D3 plasma stripp.	8,00	8,84	104,69
	QC_1 24,25-$(OH)_2$D3 ACN	0,50	0,47	93,40
	QC_2 24,25-$(OH)_2$D3 ACN	2,00	1,62	80,62
	QC_3 24,25-$(OH)_2$D3 ACN	8,00	6,55	81,87
T: -20°C	QC_1 24,25-$(OH)_2$D3 plasma stripp.	0,50	0,50	104,82
	QC_2 24,25-$(OH)_2$D3 plasma stripp.	2,00	2,17	110,15
	QC_3 24,25-$(OH)_2$D3 plasma stripp.	8,00	9,08	107,62
	QC_1 24,25-$(OH)_2$D3 ACN	0,50	0,48	95,13
	QC_2 24,25-$(OH)_2$D3 ACN	2,00	1,77	87,86
	QC_3 24,25-$(OH)_2$D3 ACN	8,00	7,07	88,41
T: 25°C	QC_1 24,25-$(OH)_2$D3 plasma stripp.	0,50	0,52	108,84
	QC_2 24,25-$(OH)_2$D3 plasma stripp.	2,00	2,14	108,74
	QC_3 24,25-$(OH)_2$D3 plasma stripp.	8,00	8,37	99,17
	QC_1 24,25-$(OH)_2$D3 ACN	0,50	0,51	102,40
	QC_2 24,25-$(OH)_2$D3 ACN	2,00	1,66	82,63
	QC_3 24,25-$(OH)_2$D3 ACN	8,00	8,00	100,05

Tab. 8 – 24,25-$(OH)_2$D3 stability data.

- 1,25-$(OH)_2D3$ (Tab. 9): at temperature of 5 °C, with a mean value of 108% in stripped plasma and 110.2% in acetonitrile; at temperature of -20 °C, with a mean value of 108.4% in stripped plasma and 102.47% in acetonitrile; at temperature of 25 °C, with a mean value of 106.66% in stripped plasma and 96.24% in acetonitrile.

		Nominal Conc. (ng/mL)	*Mean Conc. (ng/mL)*	*Stability(%)*
Fresh	QC_1 1,25-$(OH)_2D3$ plasma stripp.	0,025	0,025	
	QC_2 1,25-$(OH)_2D3$ plasma stripp.	0,100	0,097	
	QC_3 1,25-$(OH)_2D3$ plasma stripp.	0,400	0,402	
	QC_1 1,25-$(OH)_2D3$ ACN	0,025	0,025	
	QC_2 1,25-$(OH)_2D3$ ACN	0,100	0,100	
	QC_3 1,25-$(OH)_2D3$ ACN	0,400	0,405	
T: 5°C	QC_1 1,25-$(OH)_2D3$ plasma stripp.	0,025	0,028	110,89
	QC_2 1,25-$(OH)_2D3$ plasma stripp.	0,100	0,105	108,09
	QC_3 1,25-$(OH)_2D3$ plasma stripp.	0,400	0,422	105,03
	QC_1 1,25-$(OH)_2D3$ ACN	0,025	0,027	107,11
	QC_2 1,25-$(OH)_2D3$ ACN	0,100	0,113	112,47
	QC_3 1,25-$(OH)_2D3$ ACN	0,400	0,450	111,02
T: -20°C	QC_1 1,25-$(OH)_2D3$ plasma stripp.	0,025	0,027	106,93
	QC_2 1,25-$(OH)_2D3$ plasma stripp.	0,100	0,107	110,28
	QC_3 1,25-$(OH)_2D3$ plasma stripp.	0,400	0,434	108,00
	QC_1 1,25-$(OH)_2D3$ ACN	0,025	0,025	100,00
	QC_2 1,25-$(OH)_2D3$ ACN	0,100	0,103	102,29
	QC_3 1,25-$(OH)_2D3$ ACN	0,400	0,426	105,14
T: 25°C	QC_1 1,25-$(OH)_2D3$ plasma stripp.	0,025	0,026	101,65
	QC_2 1,25-$(OH)_2D3$ plasma stripp.	0,100	0,109	112,58
	QC_3 1,25-$(OH)_2D3$ plasma stripp.	0,400	0,425	105,76
	QC_1 1,25-$(OH)_2D3$ ACN	0,025	0,023	92,97
	QC_2 1,25-$(OH)_2D3$ ACN	0,100	0,105	104,33
	QC_3 1,25-$(OH)_2D3$ ACN	0,400	0,370	91,42

Tab. 9 - 1,25-$(OH)_2D3$ stability data.

- vitamina D3 (Tab. 10): at temperature of 5 °C, with a mean value 104.98% in 2x plasma stripped and 98.64% in acetonitrile; at temperature of -20 °C, with a mean value 104,61% in stripped plasma and 98.34% in acetonitrile; at temperature of 25 °C, with mean value of 106.14% in stripped plasma and 98.51% in acetonitrile.

		Nominal Conc. (ng/mL)	*Mean Conc. (ng/mL)*	*Stability(%)*
Fresh	QC1 vitamina D3 plasma stripp.	3,75	3,31	
	QC2 vitamina D3 plasma stripp.	15,00	15,01	
	QC3 vitamina D3 plasma stripp.	60,00	60,01	
	QC1 vitamina D3 ACN	3,75	3,83	
	QC2 vitamina D3 ACN	15,00	15,48	
	QC3 vitamina D3 ACN	60,00	60,01	
T: 5°C	QC1 vitamina D3 plasma stripp.	3,75	3,78	114,17
	QC2 vitamina D3 plasma stripp.	15,00	15,09	100,57
	QC3 vitamina D3 plasma stripp.	60,00	60,14	100,22
	QC1 vitamina D3 ACN	3,75	3,79	98,97
	QC2 vitamina D3 ACN	15,00	15,01	96,96
	QC3 vitamina D3 ACN	60,00	60,01	100,00
T: -20°C	QC1 vitamina D3 plasma stripp.	3,75	3,77	113,83
	QC2 vitamina D3 plasma stripp.	15,00	15,01	100,03
	QC3 vitamina D3 plasma stripp.	60,00	60,01	99,99
	QC1 vitamina D3 ACN	3,75	3,76	98,12
	QC2 vitamina D3 ACN	15,00	15,00	96,90
	QC3 vitamina D3 ACN	60,00	60,01	100,00
T: 25°C	QC1 vitamina D3 plasma stripp.	3,75	3,84	116,16
	QC2 vitamina D3 plasma stripp.	15,00	15,08	100,47
	QC3 vitamina D3 plasma stripp.	60,00	61,09	101,80
	QC1 vitamina D3 ACN	3,75	3,77	98,36
	QC2 vitamina D3 ACN	15,00	15,01	96,93
	QC3 vitamina D3 ACN	60,00	60,15	100,24

Tab. 10 - Vitamin D3 stability data.

- 25-OHD3 (Tab. 11): at temperature of 5 °C, with a mean value of 89.47%in stripped plasma and 89.7% in acetonitrile; at temperature of -20 °C, with a mean value 91.4% in stripped plasma and 89.94% in acetonitrile; at temperature of 25 °C, with a mean value 87.96% in stripped plasma and 86.7% in acetonitrile.

		Nominal Conc. (ng/mL)	*Mean Conc. (ng/mL)*	*Stability(%)*
Fresh	QC1 25-OHD3 plasma stripp.	3,125	3,715	
	QC2 25-OHD3 plasma stripp.	12,500	14,066	
	QC3 25-OHD3 plasma stripp.	50,000	54,023	
	QC1 25-OHD3 ACN	3,125	3,294	
	QC2 25-OHD3 ACN	12,500	12,707	
	QC3 25-OHD3 ACN	50,000	49,366	
T: 5°C	QC1 25-OHD3 plasma stripp.	3,125	3,072	82,68
	QC2 25-OHD3 plasma stripp.	12,500	12,691	90,23
	QC3 25-OHD3 plasma stripp.	50,000	51,600	95,52
	QC1 25-OHD3 ACN	3,125	3,136	95,19
	QC2 25-OHD3 ACN	12,500	10,882	85,64
	QC3 25-OHD3 ACN	50,000	43,581	88,28
T: -20°C	QC1 25-OHD3 plasma stripp.	3,125	3,088	83,11
	QC2 25-OHD3 plasma stripp.	12,500	13,116	93,25
	QC3 25-OHD3 plasma stripp.	50,000	52,857	97,84
	QC1 25-OHD3 ACN	3,125	3,171	96,26
	QC2 25-OHD3 ACN	12,500	10,609	83,49
	QC3 25-OHD3 ACN	50,000	44,463	90,07
T: 25°C	QC1 25-OHD3 plasma stripp.	3,125	3,064	82,47
	QC2 25-OHD3 plasma stripp.	12,500	12,548	89,21
	QC3 25-OHD3 plasma stripp.	50,000	49,821	92,22
	QC1 25-OHD3 ACN	3,125	3,131	95,06
	QC2 25-OHD3 ACN	12,500	10,326	81,27
	QC3 25-OHD3 ACN	50,000	41,360	83,78

Tab. 11 -25-OHD3 stability data.

3.2. Vitamin D3 metabolites concentration in real samples

In this retrospective study, available plasma samples from 69 subjects with COVID-19, which were hospitalized at the University Hospital of Pisa and 30 healthy subjects (COVID-19 negative), used as controls, were analyzed. Concentration levels of 24,25-$(OH)_2$D3 were 0.41-6.13 ng/ml and 1.87-13.17 ng/ml, in positive COVID-19 patients and control subjects respectively, while the concentration of 1,25-$(OH)_2$D3 were in the range 0.03-0.76 ng/ml and 0.38-1.34 ng/ml, those of vitamin D3 were in the range 0.01-5.15 ng/ml and 1.01-8.7 ng/ml and finally those of 25-OHD3 were 1.92-53.99 ng/ml and 14.24-76.79 ng/ml. The median value for the concentration level of each of the 4 metabolites in COVID-19 positive patients is lower than in controls. The values increase respectively from 1.90 ng/mL to 6.98 ng/mL for 24,25-$(OH)_2$D3, from 0.20 ng/mL to 0.75 ng/mL for 1,25-$(OH)_2$D3, from 0.49 ng/mL to 3.97 ng/mL for vitamin D3, and from 19.92 ng/mL to 35.04 ng/mL for 25-OHD3 (Fig. 43). To compare the median values between patients with COVID-19 and controls a Mann-Whitney test was used. From this statistical analysis it emerged that the median concentration levels of 25-OHD3, 24,25-$(OH)_2$D3, 1,25-$(OH)_2$D3, vitamin D3 between the two groups are significantly different (P-value=0,0001, P-value<0,0001, P-value<0,0001, P-value<0,0001 rispectively).

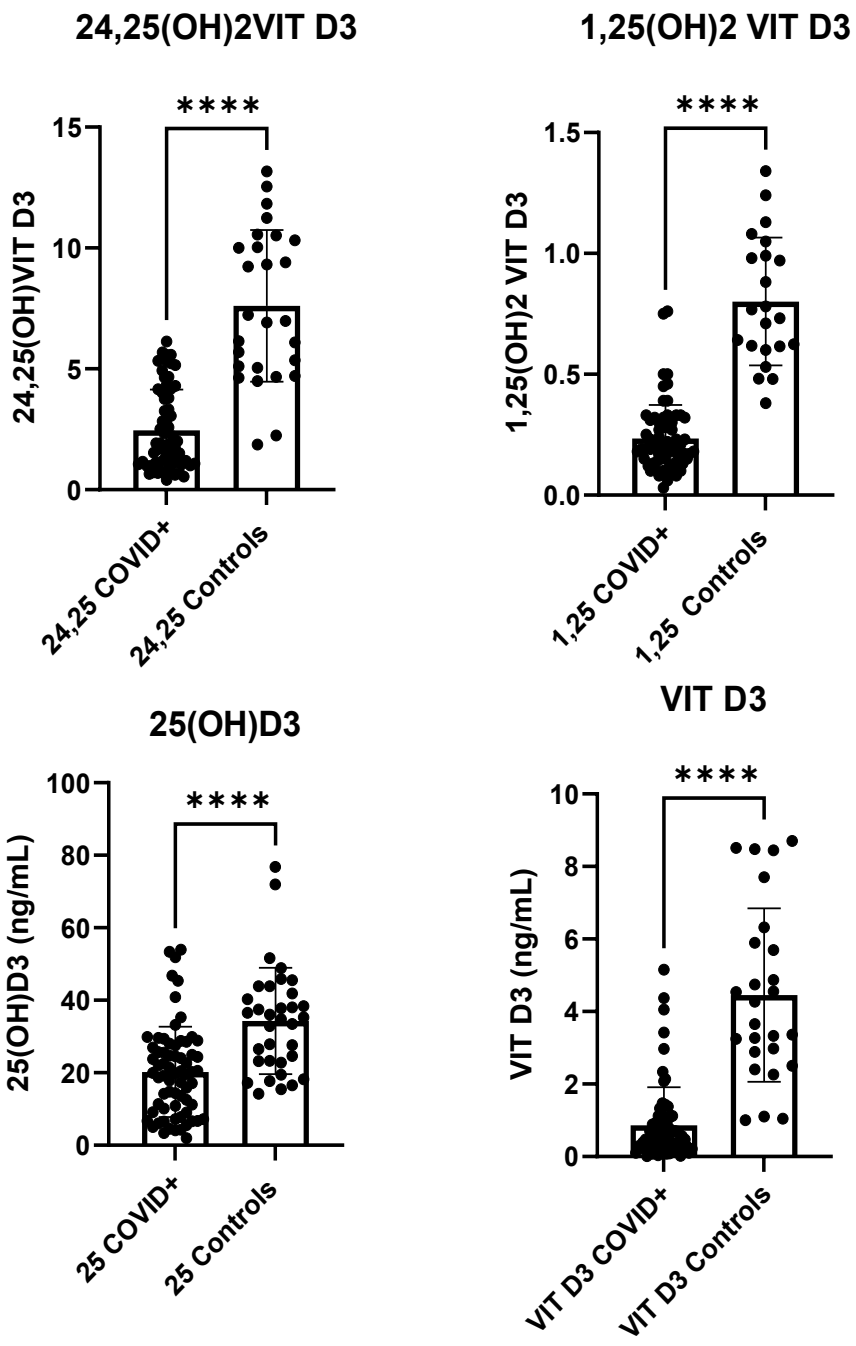

Fig. 43 – Bar plot of 4 metabolites of vitamin D3 in patients with COVID-19 and in controls.

3.3. Cross-Validation

As regards 25-OHD3, the home-built method was cross-validated with the PerkinElmer MSMS Vit D Kit, which was usually used in the mass spectrometry laboratory of the Santa Chiara hospital of Pisa on a routine basis [134]. The comparison was carried out by comparing the results relative to 69 serum samples from COVID-19 positive patients, with values in the range 3.39 ÷ 46.80 ng/mL, to the results obtained with the Kit. The normality of data distribution was assessed using Kolmogorov-Smirnov, Shapiro-Wilk, and D'Agostino-Pearson tests. Mean concentrations measured with our Lab LC-MS method and MSMS Vit D Kit were 19.54 ± 10.53 (median 19.88 range 3.39 - 46.80) ng/ml and 17.03 ± 8.86 (median 17.05, range 3.36 - 46.80) ng/ml, respectively. The difference was not statistically significant ($P = 0.1797$, Unpaired t test with Welch's correction). The intra-class correlation coefficient (ICC) for 25-OHD3 concentration was 0.9868 (95% confidence interval [CI] = 0.9774 ÷ 0.9923, $P < 0.0001$). The linear regression line, which is shown in Fig. 44 a, represents the relationship between LC-MS and MSMS Vitamin D Kit. It exhibited an equation slope of 1.173 ± 0.02645 (95% confidence interval [CI] = 1.120 ÷ 1.226, $P < 0.0001$), an Y-intercept of − 0.4347 (95% confidence interval [CI] = − 1.451 ÷ 0.5819), an X-intercept of 0.3706 (95% confidence interval [CI] = -0.5171 ÷ 1.190), and a correlation coefficient (r^2) of 0.9737. The Bland-Altman plot, reported in Fig. 44 b, confirmed the analogous concentration levels for MSMS Vitamin D Kit and Lab LC-MS since bias had a value of 2.507 (95% confidence interval [CI] = − 1.987 ÷ 7.001). Results are fully in compliance with EMA guidelines [131], which, for study samples, require a difference between the two values obtained by the different assays within 20% of the mean. The concentration levels of the 25-OHD3 were quite similar, although those obtained by MSMS Vitamin D Kit method are slightly lower.

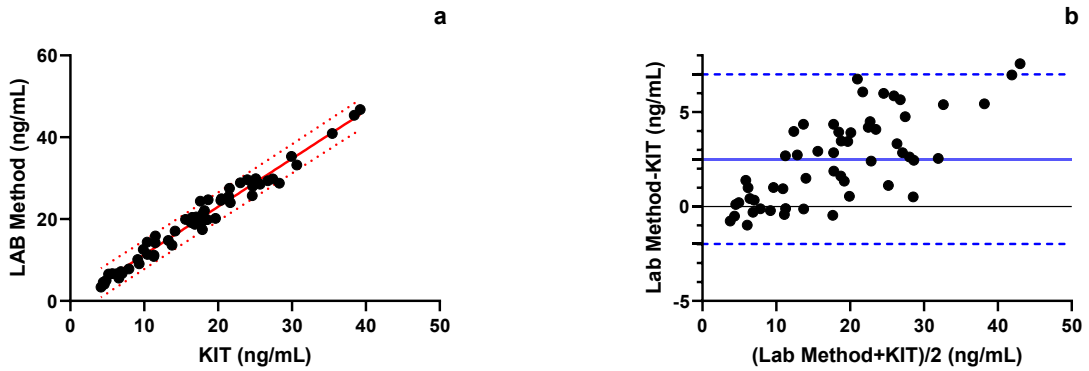

Fig. 44 - Comparison between MSMS Vitamin D KIT and LC-MS LAB Method in the assay of 25-OHD3: linear regression analysis provides a regression line with a slope of 1.173, an intercept of 0.3706 (-0.5171 ÷ 1.190), and a correlation coefficient (r^2) of 0.9720 (a), while Bland-Altman plot exhibits a bias of 2.507 units and 95% limits of agreement of − 1.987 and 7.001 (b).

3.4. Vitamin D3 Status and Association Between 25-OHD3 Levels and Inflammatory Markers

A total of 93 consecutive patients were included in the study, and they were mainly males (n = 64, 68.9%) with a mean age of 68 ± 16 years (median 69, i.r. 57–80). According to the P/F ratio, 20 patients (21.5%) were classified as severe ARDS (P/F nadir < 200 mmHg) and 39 patients (41.9%) as mild ARDS (P/F nadir between 201 and 300 mmHg), while 34 patients (36.5%) presented a P/F ratio higher than 300 mmHg. Median follow-up time was 26 (13–29) days; during the study period, 15 patients (16.1%) died. Clinical and biochemical data of the whole group of patients are reported in Table 12.

	Whole group (*n* = 93)	25OHD ≤ 20 ng/ml (*n* = 61)	25OHD > 20 ng/ml (*n* = 32)	*p*
Age (years)[a]	68 ± 16	68 ± 16	66 ± 15	0.43
Gender, *n* (%)[b]				
– Males	64 (68.8)	44 (72.1)	20 (62.5)	0.98
– Females	29 (31.2)	17 (27.9)	12 (37.5)	
BMI (kg/m²)[a]	25.9 ± 4.5	25.8 ± 4.4	26.1 ± 4.9	0.95
Smoking habits, *n* (%)[b]				
– Current smoker	4 (4.3)	4 (6.6)	0 (0)	0.199
– Never smoker	66 (71.0)	38 (62.3)	28 (87.5)	
– Ex-smoker	23 (24.7)	19 (31.1)	4 (12.5)	
Major comorbidities, *n* (%)[b]				
– Diabetes mellitus	23 (24.7)	18 (29.5)	5 (15.6)	0.041
– Cardiovascular disease	27 (29.0)	19 (31.1)	8 (25.0)	0.382
– Cerebrovascular disease	9 (9.7)	5 (8.2)	4 (12.5)	0.595
– COPD	8 (8.6)	3 (4.9)	5 (15.6)	0.107
– Dementia	10 (10.7)	7 (11.5)	3 (9.4)	0.657
– Malignant disease	15 (16.1)	11 (18.0)	4 (12.5)	0.391
PaO_2/FiO_2 ratio at nadir (mmHg)[a]	176 ± 159	161.5 ± 146.7	237.5 ± 99	0.250
PaO_2/FiO_2: <200, *n* (%)[b]	20 (21.5)	15 (24.6)	5 (15.6)	
PaO_2/FiO_2: 200–300, *n* (%)[b]	39 (41.9)	27 (44.3)	12 (37.5)	0.296
PaO_2/FiO_2: >300, *n* (%)[b]	34 (36.5)	19 (31.1)	15 (46.9)	
25OHD levels (ng/ml)[c]	16.5 (7.9–23.3)	11.3 (6.4–16.4)	27.2 (23.2–33.1)	**0.001**
IL-6 (pg/ml)[c]	15.2 (9.8–32.8)	20.8 (10.9–45.6)	12.9 (8.7–21.1)	**0.028**
IL-1β (pg/ml)[c]	1.5 (1–2)	1.5 (0.9–2.2)	1.6 (1–1.9)	0.74
IL-10 (pg/ml)[c]	3.1 (1.2–6.3)	3.7 (1.8–6.9)	2.3 (0.5–5.8)	**0.03**
TNF-α (pg/ml)[c]	8.3 (3.7–13.8)	8.9 (6.0–14.8)	4.4 (1.5–10.6)	**0.01**
GM-CSF (pg/ml)[c]	2.2 (1.4–3.1)	2.2 (1.7–3.1)	1.9 (1.1–2.6)	0.61
MCP-1 (pg/ml)[c]	571 (407–833)	590 (448–975)	550 (407–736)	0.25
CRP (mg/dl)[c]	8 (2.7–14.9)	10.7 (4.20–19.16)	5.89 (1.63–8.15)	**0.003**
Ferritin (ng/ml)[c]	562 (300–1,113)	784.0 (321.0–1,376.0)	441.5 (296.0–899.5)	0.22
D-dimer (mg/l)[c]	0.37 (0.2–0.61)	0.53 (0.27–0.72)	0.22 (0.17–0.35)	**0.002**

[a]Biochemical data are expressed as mean ± SD.
[b]Data are expressed as n and % of the column (group).
[c]Biochemical data are expressed as median and interquartile range.
In bold: statistically significant differences.

Table 12- Clinical and biochemical characteristics of patients in the whole group of patients and according to 25-OHD3 levels (cutoff 25-OHD3 = 20 mg/ml).

Mean 25-OHD3 was 17.3 ± 10.7 ng/ml, with a median of 16.5 ng/ ml (i.r. 7.9–23.3). 89% of patients had 25-OHD3 levels ≤30 ng/ml (n = 83), of those patients 65% (n = 54) had 25-OHD3 levels ≤20 ng/ml, and 35% (n = 29) had 25-OHD3 ≤10 ng/ml (severe vitamin D3 deficiency). In the overall group, an inverse correlation was found between 25(OH)D and IL-6 (r = −0.22, p = 0.03), between 25OHD3 and CRP (r = −0.21, p = 0.04), between 25-OHD3 and D-dimer (r = −0.43, p = 0.001), and between 25-OHD3 and IL-10 (r = −0.25, p = 0.02), but not with TNF-α (r = −0.12, p = 0.1) (Fig. 45 A–E). These correlations remained statistically significant in a multiple linear regression analysis, adjusted for age and sex (b = −0.64, p = 0.04, IL-6; b = −0.17, p = 0.03, CRP; b = −0.017, p = 0.001, D-dimer; b = −0.11, p = 0.02, IL-10).

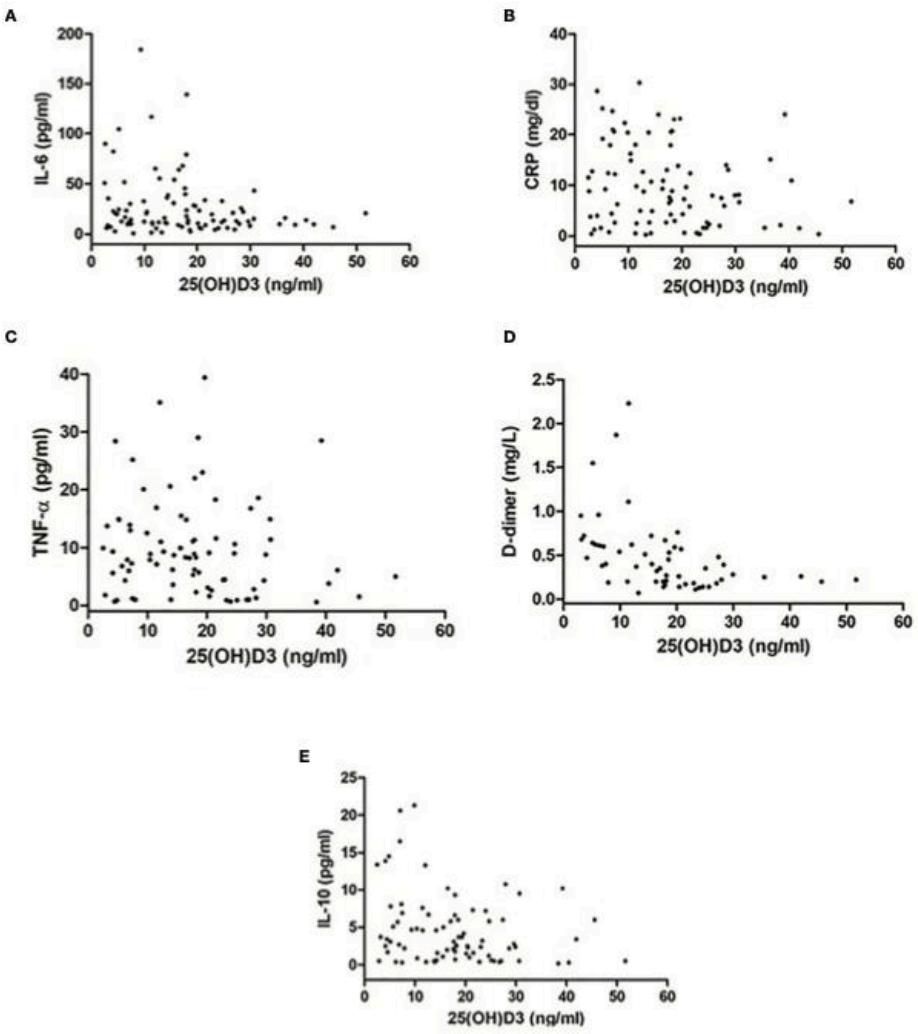

Fig. 45 - Difference in inflammatory markers [(A) IL-6, (B) CRP, (C) TNF-α, (D) D-dimer, (E) IL-10] between patients with 25-OHD3 levels >20 ng/ml and those with 25-OHD3 levels ≤20 ng/ml.

Inflammatory markers were measured in all patients and compared between patients with 25OHD levels >20 ng/ml and those with 25-OHD3 levels ≤20 ng/ml. The latter showed significantly higher IL-6 [20.8 (10.9–45.6) vs. 12.9 (8.7–21.1) pg/ml, p = 0.02], CRP [10.7 (4.2–19.2) vs. 5.9 (1.6–8.1) mg/dl, p = 0.003], TNF-α [8.9 (6.0–14.8) vs. 4.4 (1.5–10.6) pg/ml, p = 0.01], D-dimer [0.53 (0.25–0.72) vs. 0.22 (0.17–0.35) mg/l, p = 0.002], and IL-10 [3.7 (1.8–6.9) vs. 2.3 (0.5–5.8) pg/ml, p = 0.03] (Figures 46 A–E).

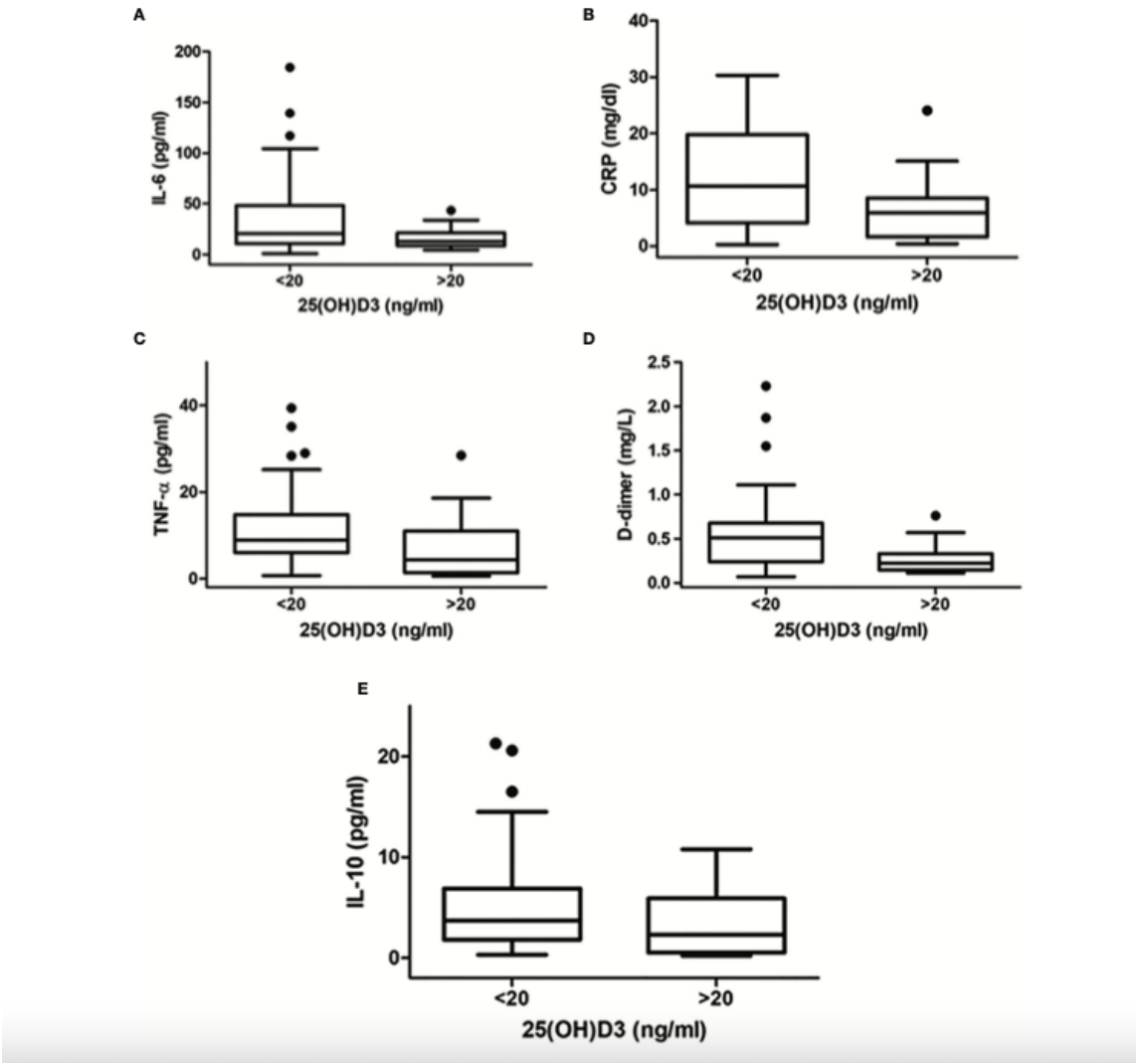

Fig. 46- Correlation between inflammatory markers [(A) IL-6, (B) CRP, (C) TNF-α, (D) D-dimer, (E) IL-10] and 25-OHD3 levels in patients with SARS-CoV-2.

3.5. Vitamin D3 Status and Severity of the Disease

The proportion of patients with vitamin D insufficiency (25-OHD3 levels ≤ 20 ng/ml) was significantly higher in patients with PaO2/FiO2 <200 mmHg, compared with those patients with PaO2/FiO2 201–300 mmHg and PaO2/FiO2 ≥300 mmHg (75% vs. 68% vs. 55%, $p < 0.001$) (Fig. 47). Finally, we evaluated the difference between 25-OHD3 levels in survivor patients and non-survivors, and we found that 25-OHD3 was significantly lower in the latter compared with the former [median 17.0 (8.6–24.3) vs. 12.7 (5.4–21.1), $p < 0.0001$] (Fig. 48)

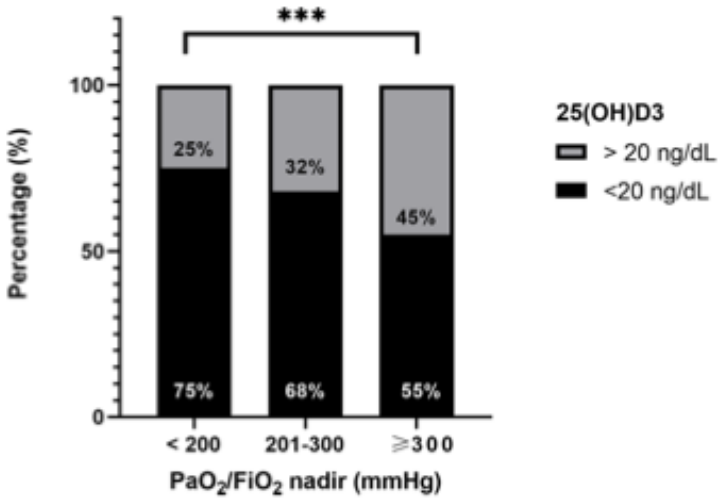

Fig.- 47 Difference in proportion of patients with vitamin D3 insufficiency (25-OHD3 levels ≤ 20 ng/ml) among patients with PaO2/FiO2 <200 mmHg, 201-300, and ≥300 mmHg. ***$p < 0.0001$.

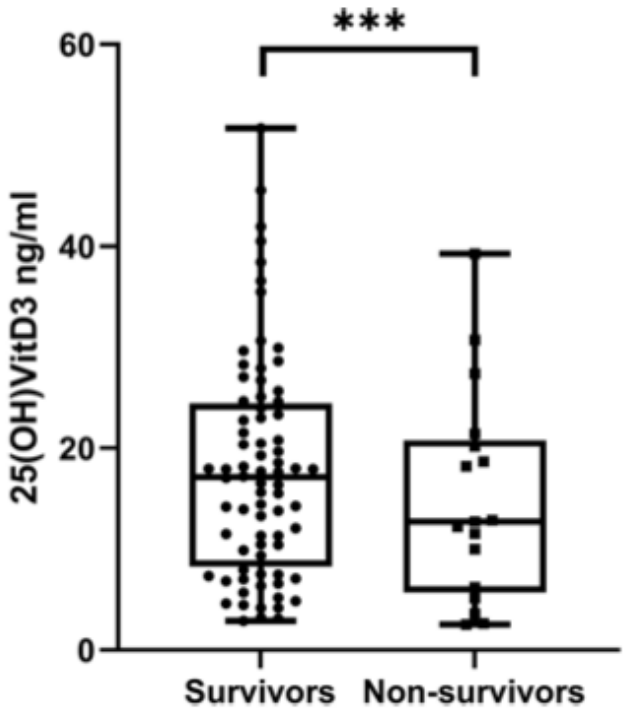

Fig. 48 - Difference in 25-OHD3 levels between survivors and non survivors patients. ***p < 0.0001.

IV. Discussion

Liquid chromatography-tandem mass spectrometry (LC-MS/MS) assays are considered the gold standard technique for determination of vitamin D3, because of their accuracy, their ability to simultaneously quantify multiple vitamin D3 metabolites, and to discriminate the metabolites of vitamin D3 from those of vitamin D2 [135]. On the contrary, immunoassays are often used to quantify single vitamin D metabolites. In particular, they still dominate clinical 25-OHD3 measurements on routine basis, although they often lack specificity and measure the total amount of 25-OHD3 and 25-OHD2 [136]. Noteworthy, constitutional isomers of vitamin D3 metabolites, e.g. 1,25$(OH)_2$D3 and 24,25$(OH)_2$D3, as well as stereoisomers and epimers, such as 3α-25-OHD3 and 3β-25-OHD3, often provide virtually identical collisionally activated dissociation (CAD) spectra in MS/MS analysis and therefore the separate quantification of these metabolites requires a LC separation prior to LC-MS/MS. So that, chromatographic separation of Vitamin D metabolites in biological samples takes on fundamental importance and its optimization requires the use of *ad hoc* strategies or specific materials. As a starting point of the chromatography development, we modify a chromatographic method described in the literature and tested several stationary phases (material, particle size and porosity), column types (length, diameter), mobile phases, flow rates and column temperatures to improve the separation efficiency. In a recently published HPLC-MS/MS methods, Ding S. *et al.* [29] and Aronov A. *et al.* [137] suggested the use of a Acquity BEH C18 column, which is an universal reverse phase C18 column suitable for different analytes in complex matrices, including also polar compounds, and works well with polar solvent such as water, acetonitrile or methanol. Other methods, such as those reported in a recent review article by Zelzer S. et al., used different reverse phase columns (C18), such as LiChrospher RP-18, Supelcosil LC-18, and Ascentis Express C18 (all from Merck, Germany), Zorbax Eclipse XDB C-18 and Zorbax SB-C18 (both from Agilent, USA), X Terra C18 (from

Waters, USA) Hypersil Gold (Thermo Scientific, USA) [31], [138], which gave a good retention and separation of one or at most three metabolites of vitamin D. We tested several analytical column equivalents to that of Ding S. et al., *i.e.* a Waters (Milford, MA, USA) Acquity UPLC BEH C18 column and a PerkinElmer (Waltham, MA, USA) Brownlee C18 column, but they both provided an unsatisfactory retention of four Vitamin D metabolites. To overcome these problems, it was used a Waters Acquity BEH Phenyl column, which showed the best chromatographic retention and separation of the analytes. The BEH Phenyl column has phenyl moieties linked to the C18 chains: this structural modification improves durability in an aggressive environment, with high temperatures and an extreme pH. Also, the phenyl moieties increase the hydrophobicity of the stationary phase, which is able to better separate 25-OHD3, 1,25-$(OH)_2$D3, vitamin D3, 24,25-$(OH)_2$D3. Vitamin D metabolites are very challenging to measure quantitatively, due to their low plasma concentration levels and low ionization efficiencies. Moreover, some of these species are regioisomers or epimers with virtually identical mass spectral dissociation behavior. To overcome the low ionization efficiency and unspecific fragmentation behavior, derivatization using Diels-Alder reactions with Cookson-type reagents, such as 4-phenyl-1,2,4-triazoline-3,5-dione (PTAD) are common. Sample derivatization enhances ionization and is particularly helpful when measuring analytes with a low concentration. Derivatization is a frequently used strategy in analytical chemistry where the analytes of interest are structurally modified to vary their physical and chemical characteristics. Because of its relative abundance 25-OHD3 does not necessarily require derivatization. However, metabolites that are present at low concentrations, such as 24,25$(OH)_2$D, 1,25$(OH)_2$D, and its precursor vitamin D3 need an amplification of the signal by derivatization. Various derivatization reagents have been described for the measurement of vitamin D metabolites [28]. The most frequently Cookson-type derivatizing agents are PTAD, 4-[4-(6-methoxy-2-benzoxazolyl)phenyl]-

1,2,4-triazoline-3,5-dione (MBOTAD), 4-ferrocenylmethyl-1,2,4-triazoline-3,5-dione (FMTAD), and 4-[2-(6,7-dimethoxy-4-methyl-3-oxo-3,4-dihydroquinoxalyl)-ethyl]-1,2,4-triazoline-3,5-dione (DMEQTAD). Cookson-type reagents are 4-substituted 1,2,4-triazoline-3,5-diones with a chromophore, fluorophore or electrophore at the 4-position that form a stable Diels-Alder adduct through which ionization efficiency improves 100 to 200 times [139]. The process with PTAD is quite easy to achieve, reliable and, under the optimized conditions described in the previous sections, the conversion of vitamin D metabolites in PTAD-vitamin D metabolites is complete. The latter is a key point, which could have a huge influence on the reproducibility of the results and sensitivity of the method. Derivatized Vitamin D metabolites were well retained by Phenyl HPLC columns, and the shape of their peak was pretty good. These derivatization reactions generally result in more complicated liquid chromatography separations, because both 6*R*- and 6*S*-diastereomers are formed during Diels-Alder reactions. Reagents attacking the cis-diene moiety of vitamin D compounds from the α- and β-sides of the molecule produce two stereoisomers (6R and 6S) [140](Fig.49).

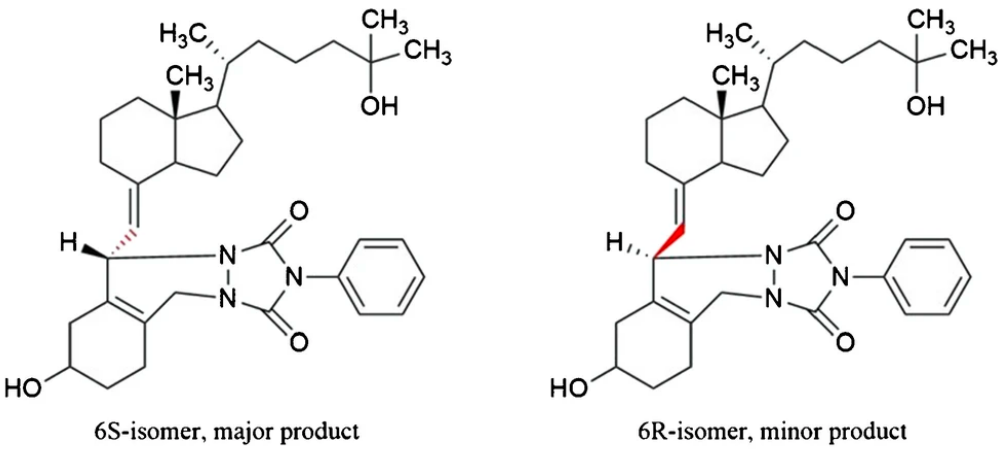

Fig. 49 - Diastereomers (6S and 6R) of the 25-OHD3-PTAD product.

Moreover the presence of C-3 epimers at high plasma concentration levels in plasma, such as the 3α-25-OHD3 and 3β-25-OHD3 epimers, increased the challenge of the chromatographic separation [30]. Differently from the reaction products of 24,25(OH)$_2$D3-PTAD, 25-OHD3-PTAD the 1,25(OH)$_2$D3–PTAD products almost coelute [30]. In our method the peak splitting, due to the formation of R and S isomer after derivatization was observed for 1,25(OH)$_2$D3–PTAD 24,25(OH)$_2$D3-PTAD, but not for vitamin D3-PTAD. The near peaks observed for the 25-OHD3 are probably due to the presence of epimers 3α-25-OHD3 and 3β-25-OHD3 in high concentrations and not to the formation of R and S isomers. The peaks corresponding to the R and S isomers of 25-OHD3 that are formed during the Diels-Alder reaction are probably hidden under the two peaks of the 3α-25-OHD3 and 3β-25-OHD3 epimers. The analysis of non-derivatized standard solutions mix of 3α-25-OHD3 and 3β-25-OHD3 support this hypothesis, as shown in the chromatogram Fig.50 two peaks are observed at the same time of retention time of the derivatized 25-OHD3. In contrast to its metabolites, vitamin D shows a unique and well-resolved peak. The peak splitting does not affect the results.

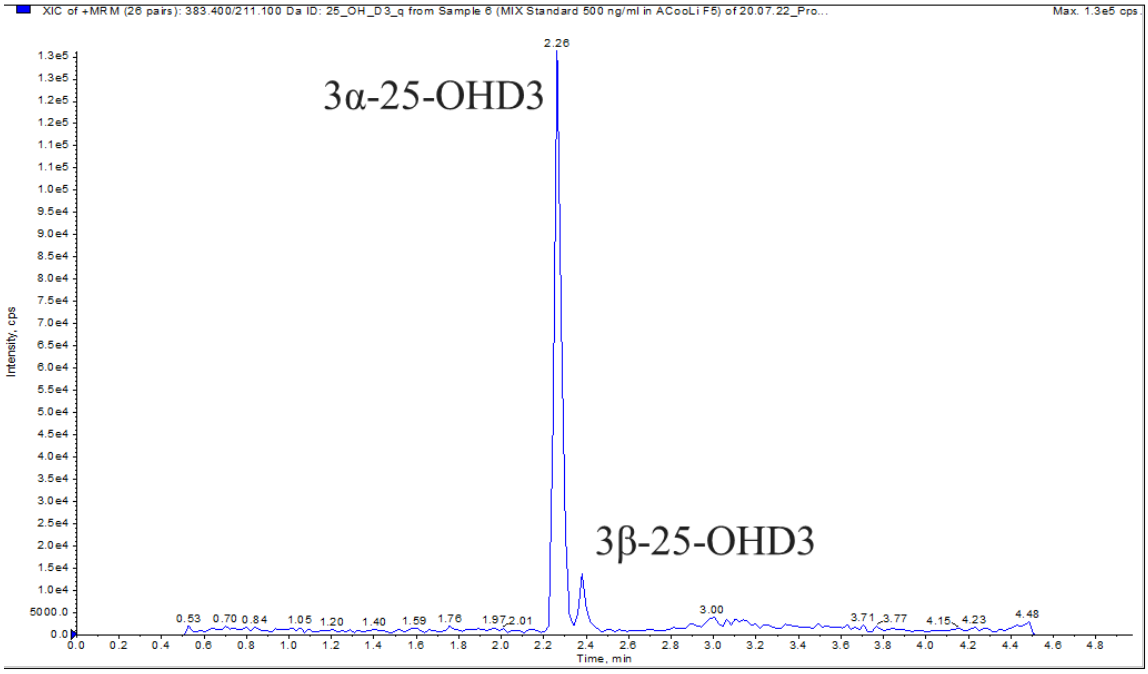

Fig. 50 – Chromatogram of 3α-25-OHD3 and 3β-25-OHD3 epimers.

The HPLC-MS/MS method developed in our laboratory was based on the isotope dilution technique, i.e. made use of stable isotope labeled analogues of Vitamin D3 metabolites as ISs, namely d6-25-OHD3, ^{13}C3-1,25-$(OH)_2$D3, d3-vitamin D3, and d6-24,25-$(OH)_2$D3. Unless the presence of primary and secondary isotope effects, the ISs have similar physical–chemical properties of 25-OHD3, 1,25-$(OH)_2$D3, vitamin D, 24,25-$(OH)_2$D3, and their use should avoid any variability induced by some potentially critical factors, such as MS ionization efficiency, sample degradation, extraction recovery or analyte loss during samples preparation, and sample degradation. Interferences from isobaric and isomeric represent a common problem and an important analytical challenge when measuring vitamin D metabolites by LC-MS/MS. Both analytes and ISs showed two close peaks each and the final concentration were obtained by adding the integration results of both peaks. Regarding to method sensitivity, the instrumental LLOD and LLOQ were extremely low for each analytes and they are in the order of pg/mL. The reference literature LOQs values were ~ 20 pg/mL for 1,25-$(OH)_2$D3, ~ 10.00 pg/mL 25-OHD3 [29],~ 0.5 ng/mL for vitamin D3 [114], and ~ 0.5 ng/mL for 24,25-$(OH)_2$D3 [141]. If compared to the reference LOQs our results were consistent with the literature data. As far as accuracy and precision, the results were well within the ± 15% suggested by the EMA guidelines [131]. As regard matrix effect if ME> 0%, a significant ion-suppression occurs; since ME is 61.30% for 24,25-$(OH)_2$D3, 54.20% for 1,25-$(OH)_2$D3, 87.98 % for vitamin D3, and 86.52 % for 25-OHD3 (see Tab. 5) the signal suppression was evaluated and reduced as far as possible. Matrix effect could be caused by matrix components, which prevent analyte from gaining access to the charge, interfere with analyte's ability to remain charged in the gas phase, increase surface tension of droplet or increase electric resistance. For this reason, we are trying to develop an online-SPE protocol to clean-up and to better purify the sample. The cross-validation study by using a certified and validated method suggests that the method developed and validated in our laboratory is able to accurately

quantify 25-OHD3. In addition, the mean concentrations of 25-OHD3 but also of 24,25-$(OH)_2$D3, 1,25-$(OH)_2$D3, and vitamin D3, which are determined with a home-built method, in the control group are well within the concentrations range reported in the literature [29], [140], [141]. The median concentration values of the four metabolites evaluated in COVID-19 positive patients and controls suggest possible role of vitamin D3 and its metabolites in SARS-COV2 infections. The median values in patients were lower than in controls. To compare the median values between patients with COVID-19 and controls an unpaired non parametric t test (Mann-Whitney test) was used. The Mann-Whitney U test is usually used to compare differences between two independent groups when the dependent variable is either ordinal or continuous, but not normally distributed, and it use also when the sample sizes are unequal (as in our study). Kolmogorov-Smirnov test and Shapiro-Wilk test are used to test the normality of the data. The COVID-19 positive samples didn't show a normal (gaussian) distribution. From this statistical analysis it emerged that the median concentration levels of 25-OHD3, 24,25-(OH)2D3, 1,25-(OH)2D3, and vitamin D3 between the two groups are significantly different with a P-value<0,0001 for all metabolites. These data were also confirmed by the comparison of the means, which were 2.44 ng/mL and 7.61 ng/mL for 24,25-$(OH)_2$D3, 0.24 ng/mL and 0.80 ng/mL for 1,25-$(OH)_2$D3, 0.80 ng/mL and 4.45 ng/mL for vitamin D3, 19.99 ng/mL and 34.29 ng/mL for 25-OHD3, for COVID-19 patients and controls, respectively. These data suggest an association between low plasma levels of vitamin D3 with a lower conversion of the latter in both liver and kidneys. The liver converts vitamin D3 into 25-OHD3, while the kidneys convert 25-OHD3 into 1,25$(OH)_2$D3 and 24,25$(OH)_2$D3. So, when the concentration of vitamin D3 is lower as in COVID-19 patients than in controls, the other metabolites should also have lower concentrations. The association between COVID-19 infection with a significant decrease of vitamin D3 and its metabolites has been demonstrated by analyzing the samples with our home-built method. So, the home-built

method is an important tool that allowed us to obtain preliminary data in this field. The different plasma concentrations of vitamin D3 and its metabolites in controls and COVID-19 patients suggest a possible protective role of vitamin D against the disease. Moreover, the method here described can be profitably used for important investigations about the vitamin D metabolism in COVID-19, since it provides significantly better performances with respect to the assays published so far. The second study of this thesis focuses on the link between vitamin D and inflammatory response, which is in turn correlated with the severity of COVID-19. To study that, we performed a systematic evaluation of multiple inflammatory markers all measured at the same moment at the beginning of hospitalization, we accurately measured 25-OHD3 levels by using the MS-MS Vitamin D kit, and we used P/F at nadir as the standardized index of the severity of the disease. Among several measured inflammatory markers, which best depict the inflammatory status of patients with COVID-19 infection, we found high levels of IL-6, CRP, TNF-α, IL-10, and D-dimer in patients with hypovitaminosis D. Further data revealed that there was an inverse correlation between these markers and 25-OHD3 levels, even when adjusted for age and sex. These findings allow a general overview on the cytokine response during viral infection from SARS-CoV-2 and suggest an interplay between inflammatory response and vitamin D metabolism. Other studies showed an association between inflammation and vitamin D status, even if they focused only on one or two markers individually. Our data regarding IL-6, TNF-α, CRP, D-dimer are also in agreement with those in the literature: these markers were significantly higher in patients with hypovitaminosis D, and an inverse correlation was observed [142]–[144]. The focus on the inflammatory status of patients with SARS-CoV-2 infection is built upon the knowledge that the inflammatory response of the host itself has a pivotal role in COVID-19 severity and mortality [89]. The contemporary evaluation of multiple inflammatory markers in our study, all converging to the same direction, suggests that the poorest is the

vitamin D condition and the highest is the inflammation response. A pathophysiological role for vitamin D deficiency in COVID-19 is sustained by the established involvement of the vitamin D active metabolite calcitriol $1,25(OH)_2D3$ in immune system regulation and modulation [128], [145]. Different from the classical endocrine role of $1,25(OH)_2D3$ in calcium homeostasis, the effect of active vitamin D either on innate and adaptive immune response seems to be mediated by a paracrine and intracrine mechanism, related to the local presence of the enzyme hydroxylase CYP27B1. About the innate immune response, $1,25(OH)_2D3$ can enhance antiviral defense by several mechanisms [39], and $1,25(OH)_2D3$ is also able to modulate acquired immune responses, decreasing the expression of MHC class II and co-signaling molecules on antigen-presenting cells, reducing TH1 and TH17 cell activity, and upregulating regulatory T cells [146]. Finally, $1,25(OH)_2D3$ has a role in reducing tissue factor activity, as well as prothrombotic factors and proinflammatory signals in blood vessel, which contribute to microvascular disease involvement of COVID-19 [147]. Consistently, hypovitaminosis D has been also correlated with cardiovascular impairment and prothrombotic and cerebrovascular events, in the context of well-known cardiovascular extraskeletal effects [3], [21], [147]. The secondary endpoint of this study was the evaluation of the relationship between vitamin D levels and COVID-19 severity and outcome, and we showed that vitamin D levels were lower in the group with more severe disease and in non-survivor patients. A strength of the present study is the use of the arterial partial pressure of oxygen (PaO2) to fraction of inspired oxygen (FiO2) (P/ F) measured as the lowest value recorded during hospital stay to stratify the severity of disease of the patients. A very recent systematic review of the literature included several studies with the specific aim of finding a relationship between COVID-19 infection and/or prognosis and vitamin D levels: some studies confirmed this link, and some others showed an association between hypovitaminosis D and COVID-19 poor outcome and mortality [148]. In summary, our study shows the following strengths:

i) simultaneous evaluation of several proinflammatory markers in patients with COVID-19, ii) direct correlation between these markers and 25-OHD3 levels, iii) 25-OHD3 levels measured by LC- MS-MS as the gold standard, and iv) evaluation of the severity of the disease by an objective outcome marker. Our study has also some limitations. Due to the possibility to collect data from patients hospitalized for COVID-19, this is a retrospective study, and we have no data regarding 25-OHD3 levels before hospitalization. Therefore, we cannot answer the question whether there is "causality or reverse causality". TNF-α when considered as a continuous variable had no statistically significant correlation with 25-OHD3 levels, even if it was significantly different between patients with and without hypovitaminosis. We do not have a clear explanation to these data, probably due to a non-linear correlation between TNF-α and vitamin D.

V. Conclusions

In conclusion, this thesis work firstly was focused on the development, optimization and validation of an LC-MS/MS method to measure the plasma levels of 25-OHD3, 1,25-$(OH)_2$D3, vitamin D3 and 24,25-$(OH)_2$D3, in a COVID-19 retrospective pilot study. Secondly, the study was focused on the relationship between vitamin D status and inflammatory response in a cohort of patients with COVID-19 regarding the severity of the disease. As regards the method, the result of this research has led to the definition of a new sensitive, accurate and low-cost analytical procedure, which up to date is the first analytical method that allows the simultaneous quantification of vitamin D and its three metabolites by using a small sample volume (100 µL). Our method demonstrated several advantages, including high sensitivity, selectivity, and versatility that make it a powerful tool to understand the role of vitamin D's metabolites and catabolites in COVID-19 physiopathology. Its general performances make it usable for routine analysis, as well as for research purposes, such as to investigate the complex interaction between vitamin D3, bone homeostasis and immune system, and to elucidate the biochemical mechanisms responsible for vitamin D3 metabolism and the monitoring of vitamin D3 status [22], [29], [31]. The validation process confirmed the method's robustness, meeting the criteria for selectivity, reproducibility, accuracy, recovery, repeatability, stability across different concentration levels, and proved a sensitivity that makes the method suitable for detecting the analytes of interest at trace levels in plasma samples. A strong signal suppression due to the matrix effect has emerged, which, however, does not affect the accuracy of the method. The method was successfully applied to analyze plasma samples from 69 positive COVID-19 patients and 30 negative COVID-19 subjects, used as controls. Our data indicated a general decrease in the concentration levels of the four

analytes of interest in the COVID-19 positive patients compared to the controls, with a significant concentration reduction for 25-OHD3 e 24,25-$(OH)_2$D3. Nevertheless, this work is a preliminary study, carried out on a small sample population; the extension of the study to a larger number of samples could allow the identification of a reliable biomarker, among the metabolites of vitamin D3, that may be related to the degree of severity of COVID-19 disease. Regarding, the link between vitamin D and inflammatory response, which is in turn correlated with the severity of COVID-19. In conclusion, the observed relationship suggests that vitamin D status needs to be taken into account in the clinical management of patients with SARS-CoV2 infection as a marker of poor prognosis and complications or as a possible modifiable risk factor for susceptibility. Further studies are needed, but the whole body of evidence in the literature urgently claims to continue to challenge the research in understanding the binomial vitamin D and COVID-19.

Acknowledgement

The completion of this study could not have been possible without the expertise of Prof. Alessandro Saba, my mentor and supervisor. I would also like to thank Prof. Ele Ferrannini who believed in me and my abilities.

I would like to extend my heartfelt gratitude to CISUP (The Center for Instrument Sharing of the University of Pisa) for their invaluable support in enabling the acquisition of the Sciex 6500+ Qtrap instrument, which significantly contributed to the results discussed in my PhD thesis.

Last but not the least, I would like to thank my family, my friends and my colleagues; without you none of this would indeed be possible.

VI. Literature

[1] M. Wacker and M. F. Holick, "Vitamin D - effects on skeletal and extraskeletal health and the need for supplementation.," *Nutrients*, vol. 5, no. 1, pp. 111–148, Jan. 2013, doi: 10.3390/nu5010111.

[2] D. D. Bikle, "Vitamin D metabolism, mechanism of action, and clinical applications.," *Chem. Biol.*, vol. 21, no. 3, pp. 319–329, Mar. 2014, doi: 10.1016/j.chembiol.2013.12.016.

[3] M. F. Holick, "Vitamin D: extraskeletal health.," *Endocrinol. Metab. Clin. North Am.*, vol. 39, no. 2, pp. 381–400, table of contents, Jun. 2010, doi: 10.1016/j.ecl.2010.02.016.

[4] W. Dankers, E. M. Colin, J. P. van Hamburg, and E. Lubberts, "Vitamin D in Autoimmunity: Molecular Mechanisms and Therapeutic Potential.," *Front. Immunol.*, vol. 7, p. 697, 2016, doi: 10.3389/fimmu.2016.00697.

[5] J. S. Danik and J. E. Manson, "Vitamin d and cardiovascular disease.," *Curr. Treat. Options Cardiovasc. Med.*, vol. 14, no. 4, pp. 414–424, Aug. 2012, doi: 10.1007/s11936-012-0183-8.

[6] C. F. Gunville, P. M. Mourani, and A. A. Ginde, "The role of vitamin D in prevention and treatment of infection.," *Inflamm. Allergy Drug Targets*, vol. 12, no. 4, pp. 239–245, Aug. 2013, doi: 10.2174/18715281113129990046.

[7] T. M. Abugoukh *et al.*, "Does Vitamin D Have a Role in Diabetes?," *Cureus*, vol. 14, no. 10, p. e30432, Oct. 2022, doi: 10.7759/cureus.30432.

[8] A. C. Ross, C. L. Taylor, A. L. Yaktine, and H. B. Del Valle, Eds., *No Title*. Washington (DC), 2011. doi: 10.17226/13050.

[9] C. Moore, M. M. Murphy, D. R. Keast, and M. F. Holick, "Vitamin D intake in the United States.," *J. Am. Diet. Assoc.*, vol. 104, no. 6, pp. 980–983, Jun. 2004, doi: 10.1016/j.jada.2004.03.028.

[10] M. A. Zmijewski, "Vitamin D and Human Health.," *International journal of molecular sciences*, vol. 20, no. 1. Switzerland, Jan. 2019. doi: 10.3390/ijms20010145.

[11] R. Vieth *et al.*, "The urgent need to recommend an intake of vitamin D that is effective.," *The American journal of clinical nutrition*, vol. 85, no. 3. United States, pp. 649–650, Mar. 2007. doi: 10.1093/ajcn/85.3.649.

[12] R. Bouillon *et al.*, "Vitamin D and human health: lessons from vitamin D receptor null mice.," *Endocr. Rev.*, vol. 29, no. 6, pp. 726–776, Oct. 2008, doi: 10.1210/er.2008-0004.

[13] M. Imawari, K. Kida, and D. S. Goodman, "The transport of vitamin D and its 25-hydroxy metabolite in human plasma. Isolation and partial characterization of vitamin D and 25-hydroxyvitamin D binding protein.," *J. Clin. Invest.*, vol. 58, no. 2, pp. 514–523, Aug. 1976, doi: 10.1172/JCI108495.

[14] P. White and N. Cooke, "The multifunctional properties and characteristics of vitamin D-binding protein.," *Trends Endocrinol. Metab.*, vol. 11, no. 8, pp. 320–327, Oct. 2000, doi: 10.1016/s1043-2760(00)00317-9.

[15] D. D. Bikle and J. Schwartz, "Vitamin D Binding Protein, Total and Free Vitamin D Levels in Different Physiological and Pathophysiological Conditions.," *Front. Endocrinol. (Lausanne).*, vol. 10, p. 317, 2019, doi: 10.3389/fendo.2019.00317.

[16] H. A. Morris and P. H. Anderson, “Autocrine and paracrine actions of vitamin d.,” *Clin. Biochem. Rev.*, vol. 31, no. 4, pp. 129–138, Nov. 2010.

[17] A. Shieh *et al.*, “Associations Between Change in Total and Free 25-Hydroxyvitamin D With 24,25-Dihydroxyvitamin D and Parathyroid Hormone.,” *J. Clin. Endocrinol. Metab.*, vol. 103, no. 9, pp. 3368–3375, Sep. 2018, doi: 10.1210/jc.2018-00515.

[18] B. Al-Zohily, A. Al-Menhali, S. Gariballa, A. Haq, and I. Shah, “Epimers of Vitamin D: A Review.,” *Int. J. Mol. Sci.*, vol. 21, no. 2, Jan. 2020, doi: 10.3390/ijms21020470.

[19] A. Goździalska *et al.*, “Association of Calcium and Phosphate Balance, Vitamin D, PTH, and Calcitonin in Patients With Adolescent Idiopathic Scoliosis.,” *Spine (Phila. Pa. 1976).*, vol. 41, no. 8, pp. 693–697, Apr. 2016, doi: 10.1097/BRS.0000000000001286.

[20] L. Condamine, C. Menaa, F. Vrtovsnik, G. Friedlander, and M. Garabédian, “Local action of phosphate depletion and insulin-like growth factor 1 on in vitro production of 1,25-dihydroxyvitamin D by cultured mammalian kidney cells.,” *J. Clin. Invest.*, vol. 94, no. 4, pp. 1673–1679, Oct. 1994, doi: 10.1172/JCI117512.

[21] F. Saponaro, C. Marcocci, and R. Zucchi, “Vitamin D status and cardiovascular outcome.,” *J. Endocrinol. Invest.*, vol. 42, no. 11, pp. 1285–1290, Nov. 2019, doi: 10.1007/s40618-019-01057-y.

[22] S. J. Bruce *et al.*, “Analysis and quantification of vitamin D metabolites in serum by ultra-performance liquid chromatography coupled to tandem mass spectrometry and high-resolution mass spectrometry--a method comparison and validation.,” *Rapid Commun. Mass Spectrom.*, vol. 27, no. 1, pp. 200–206, Jan. 2013, doi: 10.1002/rcm.6439.

[23] M. C. Us *et al.*, “The role of free vitamin D and vitamin D binding protein in SARS-Cov-2 infection in children.,” *Pediatr. Int.*, vol. 65, no. 1, p. e15680, 2023, doi: 10.1111/ped.15680.

[24] M. Herrmann, C. J. L. Farrell, I. Pusceddu, N. Fabregat-Cabello, and E. Cavalier, “Assessment of Vitamin D status - A changing landscape,” *Clin. Chem. Lab. Med.*, vol. 55, no. 1, pp. 3–26, 2017, doi: 10.1515/cclm-2016-0264.

[25] G. Jones, D. E. Prosser, and M. Kaufmann, “25-Hydroxyvitamin D-24-hydroxylase (CYP24A1): its important role in the degradation of vitamin D.,” *Arch. Biochem. Biophys.*, vol. 523, no. 1, pp. 9–18, Jul. 2012, doi: 10.1016/j.abb.2011.11.003.

[26] A. Dugar *et al.*, “The Vitamin D Metabolite Ratio (VMR) is a Biomarker of Vitamin D Status That is Not Affected by Acute Changes in Vitamin D Binding Protein.,” *Clin. Chem.*, vol. 69, no. 7, pp. 718–723, Jul. 2023, doi: 10.1093/clinchem/hvad050.

[27] D. D. Bikle, “Vitamin D and bone.,” *Curr. Osteoporos. Rep.*, vol. 10, no. 2, pp. 151–159, Jun. 2012, doi: 10.1007/s11914-012-0098-z.

[28] J. M. W. van den Ouweland, M. Vogeser, and S. Bächer, “Vitamin D and metabolites measurement by tandem mass spectrometry.,” *Rev. Endocr. Metab. Disord.*, vol. 14, no. 2, pp. 159–184, Jun. 2013, doi: 10.1007/s11154-013-9241-0.

[29] S. Ding, I. Schoenmakers, K. Jones, A. Koulman, A. Prentice, and D. A. Volmer, “Quantitative determination of vitamin D metabolites in plasma using UHPLC-MS/MS.,” *Anal. Bioanal. Chem.*, vol. 398, no. 2, pp. 779–789, Sep. 2010, doi: 10.1007/s00216-010-3993-0.

[30] M. D. Teegarden, K. M. Riedl, and S. J. Schwartz, “Chromatographic separation of PTAD-derivatized 25-hydroxyvitamin D3 and its C-3 epimer from human serum and murine skin,” *J. Chromatogr. B*, vol. 991, pp. 118–121, 2015, doi: https://doi.org/10.1016/j.jchromb.2015.04.011.

[31] P. Schorr, C. S. Stokes, and D. A. Volmer, “Improved quantitative LC-MS/MS analysis of vitamin D metabolites in serum after one-pot double derivatization.,” *J. Pharm. Biomed. Anal.*, vol. 234, p. 115522, Sep. 2023, doi: 10.1016/j.jpba.2023.115522.

[32] Y. Song *et al.*, “Calcium transporter 1 and epithelial calcium channel messenger ribonucleic acid are differentially regulated by 1,25 dihydroxyvitamin D3 in the intestine and kidney of mice.,” *Endocrinology*, vol. 144, no. 9, pp. 3885–3894, Sep. 2003, doi: 10.1210/en.2003-0314.

[33] S. J. Khundmiri, R. D. Murray, and E. Lederer, “PTH and Vitamin D.,” *Compr. Physiol.*, vol. 6, no. 2, pp. 561–601, Mar. 2016, doi: 10.1002/cphy.c140071.

[34] F. S. van Dijk *et al.*, “Osteogenesis Imperfecta: A Review with Clinical Examples.,” *Mol. Syndromol.*, vol. 2, no. 1, pp. 1–20, Dec. 2011, doi: 10.1159/000332228.

[35] M. Salzmann, C. Krohn, and N. Berger, “[Erratum to: Osteogenesis imperfecta].,” *Der Orthopade*, vol. 44, no. 9. Germany, p. 702, Sep. 2015. doi: 10.1007/s00132-015-3151-7.

[36] F. S. Van Dijk and D. O. Sillence, “Osteogenesis imperfecta: clinical diagnosis, nomenclature and severity assessment.,” *Am. J. Med. Genet. A*, vol. 164A, no. 6, pp. 1470–1481, Jun. 2014, doi: 10.1002/ajmg.a.36545.

[37] D. O. Sillence, A. Senn, and D. M. Danks, “Genetic heterogeneity in osteogenesis imperfecta.,” *J. Med. Genet.*, vol. 16, no. 2, pp. 101–116, Apr. 1979, doi: 10.1136/jmg.16.2.101.

[38] D. J. Berry, K. Hesketh, C. Power, and E. Hyppönen, “Vitamin D status has a linear association with seasonal infections and lung function in British adults.,” *Br. J. Nutr.*, vol. 106, no. 9, pp. 1433–1440, Nov. 2011, doi: 10.1017/S0007114511001991.

[39] E. L Bishop, A. Ismailova, S. Dimeloe, M. Hewison, and J. H. White, “Vitamin D and Immune Regulation: Antibacterial, Antiviral, Anti-Inflammatory.,” *JBMR plus*, vol. 5, no. 1, p. e10405, Jan. 2021, doi: 10.1002/jbm4.10405.

[40] C. Aranow, “Vitamin D and the immune system.,” *J. Investig. Med. Off. Publ. Am. Fed. Clin. Res.*, vol. 59, no. 6, pp. 881–886, Aug. 2011, doi: 10.2310/JIM.0b013e31821b8755.

[41] M. Hewison, “Vitamin D and the intracrinology of innate immunity.,” *Mol. Cell. Endocrinol.*, vol. 321, no. 2, pp. 103–111, Jun. 2010, doi: 10.1016/j.mce.2010.02.013.

[42] T. S. Lisse *et al.*, “Gene targeting by the vitamin D response element binding protein reveals a role for vitamin D in osteoblast mTOR signaling.,” *FASEB J. Off. Publ. Fed. Am. Soc. Exp. Biol.*, vol. 25, no. 3, pp. 937–947, Mar. 2011, doi: 10.1096/fj.10-172577.

[43] Y.-G. Zhang, S. Wu, and J. Sun, “Vitamin D, Vitamin D Receptor, and Tissue Barriers.,” *Tissue barriers*, vol. 1, no. 1, Jan. 2013, doi: 10.4161/tisb.23118.

[44] A. Clairmont, D. Tessman, A. Stock, S. Nicolai, W. Stahl, and H. Sies, “Induction of gap junctional intercellular communication by vitamin D in human skin fibroblasts is dependent on the nuclear Induction of gap junctional intercellular communication by vitamin D in human skin fibroblasts is dependent on the nuclear vitamin ,”

Carcinogenesis, vol. 17, no. 6, pp. 1389–1391, Jun. 1996, doi: 10.1093/carcin/17.6.1389.

[45] I. Laaksi, J.-P. Ruohola, V. Mattila, A. Auvinen, T. Ylikomi, and H. Pihlajamäki, "Vitamin D supplementation for the prevention of acute respiratory tract infection: a randomized, double-blinded trial among young Finnish men.," *J. Infect. Dis.*, vol. 202, no. 5, pp. 809–814, Sep. 2010, doi: 10.1086/654881.

[46] J. R. Sabetta, P. DePetrillo, R. J. Cipriani, J. Smardin, L. A. Burns, and M. L. Landry, "Serum 25-hydroxyvitamin d and the incidence of acute viral respiratory tract infections in healthy adults.," *PLoS One*, vol. 5, no. 6, p. e11088, Jun. 2010, doi: 10.1371/journal.pone.0011088.

[47] T. Kawasaki and T. Kawai, "Toll-like receptor signaling pathways.," *Front. Immunol.*, vol. 5, p. 461, 2014, doi: 10.3389/fimmu.2014.00461.

[48] R. McGregor *et al.*, "An autocrine Vitamin D-driven Th1 shutdown program can be exploited for COVID-19.," *bioRxiv : the preprint server for biology*. United States, Jul. 2020. doi: 10.1101/2020.07.18.210161.

[49] M. Høyer-Hansen, S. P. S. Nordbrandt, and M. Jäättelä, "Autophagy as a basis for the health-promoting effects of vitamin D.," *Trends Mol. Med.*, vol. 16, no. 7, pp. 295–302, Jul. 2010, doi: 10.1016/j.molmed.2010.04.005.

[50] G. Balogh, A. R. de Boland, R. Boland, and P. Barja, "Effect of 1,25(OH)(2)-vitamin D(3) on the activation of natural killer cells: role of protein kinase C and extracellular calcium.," *Exp. Mol. Pathol.*, vol. 67, no. 2, pp. 63–74, Oct. 1999, doi: 10.1006/exmp.1999.2264.

[51] M. Abdrabbo *et al.*, "Vitamin D and COVID-19: A review on the role of vitamin D in preventing and reducing the severity of COVID-19 infection.," *Protein Sci.*, vol. 30, no. 11, pp. 2206–2220, Nov. 2021, doi: 10.1002/pro.4190.

[52] S. Liang, J. Cai, Y. Li, and R. Yang, "1,25-Dihydroxy-Vitamin D3 induces macrophage polarization to M2 by upregulating T-cell Ig-mucin-3 expression.," *Mol. Med. Rep.*, vol. 19, no. 5, pp. 3707–3713, May 2019, doi: 10.3892/mmr.2019.10047.

[53] J.-H. Chang, H.-R. Cha, D.-S. Lee, K. Y. Seo, and M.-N. Kweon, "1,25-Dihydroxyvitamin D3 inhibits the differentiation and migration of T(H)17 cells to protect against experimental autoimmune encephalomyelitis.," *PLoS One*, vol. 5, no. 9, p. e12925, Sep. 2010, doi: 10.1371/journal.pone.0012925.

[54] L. E. Jeffery *et al.*, "1,25-Dihydroxyvitamin D3 and IL-2 combine to inhibit T cell production of inflammatory cytokines and promote development of regulatory T cells expressing CTLA-4 and FoxP3.," *J. Immunol.*, vol. 183, no. 9, pp. 5458–5467, Nov. 2009, doi: 10.4049/jimmunol.0803217.

[55] M. D. Griffin, W. H. Lutz, V. A. Phan, L. A. Bachman, D. J. McKean, and R. Kumar, "Potent inhibition of dendritic cell differentiation and maturation by vitamin D analogs.," *Biochem. Biophys. Res. Commun.*, vol. 270, no. 3, pp. 701–708, Apr. 2000, doi: 10.1006/bbrc.2000.2490.

[56] C. Almerighi, A. Sinistro, A. Cavazza, C. Ciaprini, G. Rocchi, and A. Bergamini, "1Alpha,25-dihydroxyvitamin D3 inhibits CD40L-induced pro-inflammatory and immunomodulatory activity in human monocytes.," *Cytokine*, vol. 45, no. 3, pp. 190–197, Mar. 2009, doi: 10.1016/j.cyto.2008.12.009.

[57] S. Chen, G. P. Sims, X. X. Chen, Y. Y. Gu, S. Chen, and P. E. Lipsky, "Modulatory effects of 1,25-dihydroxyvitamin D3 on human B cell differentiation.," *J. Immunol.*, vol. 179, no. 3, pp. 1634–1647, Aug. 2007, doi: 10.4049/jimmunol.179.3.1634.

[58] Y.-F. Zhou, B.-A. Luo, and L.-L. Qin, "The association between vitamin D deficiency and community-acquired pneumonia: A meta-analysis of observational studies.," *Medicine (Baltimore).*, vol. 98, no. 38, p. e17252, Sep. 2019, doi: 10.1097/MD.0000000000017252.

[59] M. E. Belderbos *et al.*, "Cord blood vitamin D deficiency is associated with respiratory syncytial virus bronchiolitis.," *Pediatrics*, vol. 127, no. 6, pp. e1513-20, Jun. 2011, doi: 10.1542/peds.2010-3054.

[60] A. C. Walls, Y.-J. Park, M. A. Tortorici, A. Wall, A. T. McGuire, and D. Veesler, "Structure, Function, and Antigenicity of the SARS-CoV-2 Spike Glycoprotein.," *Cell*, vol. 181, no. 2, pp. 281-292.e6, Apr. 2020, doi: 10.1016/j.cell.2020.02.058.

[61] F. Perrotta, M. G. Matera, M. Cazzola, and A. Bianco, "Severe respiratory SARS-CoV2 infection: Does ACE2 receptor matter?," *Respir. Med.*, vol. 168, p. 105996, Jul. 2020, doi: 10.1016/j.rmed.2020.105996.

[62] E. Ortiz-Prado *et al.*, "Clinical, molecular, and epidemiological characterization of the SARS-CoV-2 virus and the Coronavirus Disease 2019 (COVID-19), a comprehensive literature review.," *Diagn. Microbiol. Infect. Dis.*, vol. 98, no. 1, p. 115094, Sep. 2020, doi: 10.1016/j.diagmicrobio.2020.115094.

[63] C. J. Michel, C. Mayer, O. Poch, and J. D. Thompson, "Characterization of accessory genes in coronavirus genomes.," *Virol. J.*, vol. 17, no. 1, p. 131, Aug. 2020, doi: 10.1186/s12985-020-01402-1.

[64] P. Zhou *et al.*, "Addendum: A pneumonia outbreak associated with a new coronavirus of probable bat origin.," *Nature*, vol. 588, no. 7836, p. E6, Dec. 2020, doi: 10.1038/s41586-020-2951-z.

[65] D. Kim, J.-Y. Lee, J.-S. Yang, J. W. Kim, V. N. Kim, and H. Chang, "The Architecture of SARS-CoV-2 Transcriptome.," *Cell*, vol. 181, no. 4, pp. 914-921.e10, May 2020, doi: 10.1016/j.cell.2020.04.011.

[66] M. Rastogi, N. Pandey, A. Shukla, and S. K. Singh, "SARS coronavirus 2: from genome to infectome.," *Respir. Res.*, vol. 21, no. 1, p. 318, Dec. 2020, doi: 10.1186/s12931-020-01581-z.

[67] A. C. Brant, W. Tian, V. Majerciak, W. Yang, and Z.-M. Zheng, "SARS-CoV-2: from its discovery to genome structure, transcription, and replication.," *Cell Biosci.*, vol. 11, no. 1, p. 136, Jul. 2021, doi: 10.1186/s13578-021-00643-z.

[68] Y. Huang, C. Yang, X.-F. Xu, W. Xu, and S.-W. Liu, "Structural and functional properties of SARS-CoV-2 spike protein: potential antivirus drug development for COVID-19.," *Acta Pharmacol. Sin.*, vol. 41, no. 9, pp. 1141–1149, Sep. 2020, doi: 10.1038/s41401-020-0485-4.

[69] A. Ali and R. Vijayan, "Dynamics of the ACE2-SARS-CoV-2/SARS-CoV spike protein interface reveal unique mechanisms.," *Sci. Rep.*, vol. 10, no. 1, p. 14214, Aug. 2020, doi: 10.1038/s41598-020-71188-3.

[70] A. H. Khan, N. Nasir, N. Nasir, Q. Maha, and R. Rehman, "Vitamin D and COVID-19: is there a role?," *J. Diabetes Metab. Disord.*, vol. 20, no. 1, pp. 931–938, Jun. 2021, doi:

10.1007/s40200-021-00775-6.

[71] I. Krynytska, M. Marushchak, I. Birchenko, A. Dovgalyuk, and O. Tokarskyy, "COVID-19-associated acute respiratory distress syndrome versus classical acute respiratory distress syndrome (a narrative review).," *Iran. J. Microbiol.*, vol. 13, no. 6, pp. 737–747, Dec. 2021, doi: 10.18502/ijm.v13i6.8072.

[72] F. Yoshihara, "Association between blood pressure and COVID-19 severity.," *Hypertension research : official journal of the Japanese Society of Hypertension*, vol. 47, no. 3. England, pp. 683–684, Mar. 2024. doi: 10.1038/s41440-023-01557-8.

[73] Y. Odeyemi, A. G. De Moraes, and O. Gajic, "What factors predispose patients to acute respiratory distress syndrome?," *Evidence-Based Practice of Critical Care*. pp. 103-108.e1, 2020. doi: 10.1016/B978-0-323-64068-8.00024-9.

[74] J.-J. Zhang *et al.*, "Clinical characteristics of 140 patients infected with SARS-CoV-2 in Wuhan, China.," *Allergy*, vol. 75, no. 7, pp. 1730–1741, Jul. 2020, doi: 10.1111/all.14238.

[75] P. Zhang *et al.*, "Association of Inpatient Use of Angiotensin-Converting Enzyme Inhibitors and Angiotensin II Receptor Blockers With Mortality Among Patients With Hypertension Hospitalized With COVID-19.," *Circ. Res.*, vol. 126, no. 12, pp. 1671–1681, Jun. 2020, doi: 10.1161/CIRCRESAHA.120.317134.

[76] P. Habibzadeh, M. Mofatteh, M. Silawi, S. Ghavami, and M. A. Faghihi, "Molecular diagnostic assays for COVID-19: an overview.," *Crit. Rev. Clin. Lab. Sci.*, vol. 58, no. 6, pp. 385–398, Sep. 2021, doi: 10.1080/10408363.2021.1884640.

[77] A. La Marca, M. Capuzzo, T. Paglia, L. Roli, T. Trenti, and S. M. Nelson, "Testing for SARS-CoV-2 (COVID-19): a systematic review and clinical guide to molecular and serological in-vitro diagnostic assays.," *Reprod. Biomed. Online*, vol. 41, no. 3, pp. 483–499, Sep. 2020, doi: 10.1016/j.rbmo.2020.06.001.

[78] B. D. Kevadiya *et al.*, "Diagnostics for SARS-CoV-2 infections.," *Nat. Mater.*, vol. 20, no. 5, pp. 593–605, May 2021, doi: 10.1038/s41563-020-00906-z.

[79] M. Touma, "COVID-19: molecular diagnostics overview.," *J. Mol. Med. (Berl).*, vol. 98, no. 7, pp. 947–954, Jul. 2020, doi: 10.1007/s00109-020-01931-w.

[80] Z. Huang, J. Fang, M. Zhou, Z. Gong, and T. Xiang, "CRISPR-Cas13: A new technology for the rapid detection of pathogenic microorganisms.," *Front. Microbiol.*, vol. 13, p. 1011399, 2022, doi: 10.3389/fmicb.2022.1011399.

[81] C. M. Ackerman *et al.*, "Massively multiplexed nucleic acid detection with Cas13.," *Nature*, vol. 582, no. 7811, pp. 277–282, Jun. 2020, doi: 10.1038/s41586-020-2279-8.

[82] G. A. Storch, "CRISPR tool scales up to interrogate a huge line-up of viral suspects.," *Nature*, vol. 582, no. 7811. England, pp. 188–189, Jun. 2020. doi: 10.1038/d41586-020-01447-w.

[83] S. Ebrahimi *et al.*, "CRISPR-Cas System: A Promising Diagnostic Tool for Covid-19.," *Avicenna J. Med. Biotechnol.*, vol. 14, no. 1, pp. 3–9, 2022, doi: 10.18502/ajmb.v14i1.8165.

[84] G. Aquino-Jarquin, "Recent progress on rapid SARS-CoV-2/COVID-19 detection by CRISPR-Cas13-based platforms.," *Drug Discov. Today*, vol. 26, no. 8, pp. 2025–2035, Aug. 2021, doi: 10.1016/j.drudis.2021.06.005.

[85] A. Ghouneimy, A. Mahas, T. Marsic, R. Aman, and M. Mahfouz, “CRISPR-Based Diagnostics: Challenges and Potential Solutions toward Point-of-Care Applications.,” *ACS Synth. Biol.*, vol. 12, no. 1, pp. 1–16, Jan. 2023, doi: 10.1021/acssynbio.2c00496.

[86] H. Jayamohan *et al.*, “SARS-CoV-2 pandemic: a review of molecular diagnostic tools including sample collection and commercial response with associated advantages and limitations.,” *Anal. Bioanal. Chem.*, vol. 413, no. 1, pp. 49–71, Jan. 2021, doi: 10.1007/s00216-020-02958-1.

[87] D. Foley, R. Wardle, S. Ferries, R. Pattison, J. Warren, and L. J. Calton, “Advancing Research with the SARS-CoV-2 LC-MS Kit (RUO),” 2021, [Online]. Available: https://www.waters.com/nextgen/us/en/library/application-notes/2021/advancing-research-with-the-sars-cov-2-lc-ms-kit-ruo.html

[88] J. Kim, Y. L. Yang, S.-H. Jang, and Y.-S. Jang, “Human β-defensin 2 plays a regulatory role in innate antiviral immunity and is capable of potentiating the induction of antigen-specific immunity.,” *Virol. J.*, vol. 15, no. 1, p. 124, Aug. 2018, doi: 10.1186/s12985-018-1035-2.

[89] R. Channappanavar and S. Perlman, “Pathogenic human coronavirus infections: causes and consequences of cytokine storm and immunopathology.,” *Semin. Immunopathol.*, vol. 39, no. 5, pp. 529–539, Jul. 2017, doi: 10.1007/s00281-017-0629-x.

[90] R. Harne, B. Williams, H. F. M. Abdelal, S. L. Baldwin, and R. N. Coler, “SARS-CoV-2 infection and immune responses.,” *AIMS Microbiol.*, vol. 9, no. 2, pp. 245–276, 2023, doi: 10.3934/microbiol.2023015.

[91] J. R. Tisoncik, M. J. Korth, C. P. Simmons, J. Farrar, T. R. Martin, and M. G. Katze, “Into the eye of the cytokine storm.,” *Microbiol. Mol. Biol. Rev.*, vol. 76, no. 1, pp. 16–32, Mar. 2012, doi: 10.1128/MMBR.05015-11.

[92] A. G. Laing *et al.*, “Author Correction: A dynamic COVID-19 immune signature includes associations with poor prognosis.,” *Nature medicine*, vol. 26, no. 12. United States, p. 1951, Dec. 2020. doi: 10.1038/s41591-020-01186-5.

[93] P. Poletti *et al.*, “Association of Age With Likelihood of Developing Symptoms and Critical Disease Among Close Contacts Exposed to Patients With Confirmed SARS-CoV-2 Infection in Italy.,” *JAMA Netw. open*, vol. 4, no. 3, p. e211085, Mar. 2021, doi: 10.1001/jamanetworkopen.2021.1085.

[94] X. Xie, J. Chen, X. Wang, F. Zhang, and Y. Liu, “Age- and gender-related difference of ACE2 expression in rat lung.,” *Life Sci.*, vol. 78, no. 19, pp. 2166–2171, Apr. 2006, doi: 10.1016/j.lfs.2005.09.038.

[95] R. R. Gaddam, S. Chambers, and M. Bhatia, “ACE and ACE2 in inflammation: a tale of two enzymes.,” *Inflamm. Allergy Drug Targets*, vol. 13, no. 4, pp. 224–234, 2014, doi: 10.2174/1871528113666140713164506.

[96] F. Salamanna, M. Maglio, M. P. Landini, and M. Fini, “Body Localization of ACE-2: On the Trail of the Keyhole of SARS-CoV-2.,” *Front. Med.*, vol. 7, p. 594495, 2020, doi: 10.3389/fmed.2020.594495.

[97] Y. Imai *et al.*, “Angiotensin-converting enzyme 2 protects from severe acute lung failure.,” *Nature*, vol. 436, no. 7047, pp. 112–116, Jul. 2005, doi: 10.1038/nature03712.

[98] A. Martyniak and P. J. Tomasik, “A New Perspective on the Renin-Angiotensin System.,” *Diagnostics (Basel, Switzerland)*, vol. 13, no. 1, Dec. 2022, doi:

10.3390/diagnostics13010016.

[99] A. Hafiane, "SARS-CoV-2 and the cardiovascular system.," *Clin. Chim. Acta.*, vol. 510, pp. 311–316, Nov. 2020, doi: 10.1016/j.cca.2020.07.019.

[100] A. Radujkovic, T. Hippchen, S. Tiwari-Heckler, S. Dreher, M. Boxberger, and U. Merle, "Vitamin D Deficiency and Outcome of COVID-19 Patients.," *Nutrients*, vol. 12, no. 9, Sep. 2020, doi: 10.3390/nu12092757.

[101] L. Ball *et al.*, "Understanding the pathophysiology of typical acute respiratory distress syndrome and severe COVID-19.," *Expert Rev. Respir. Med.*, vol. 16, no. 4, pp. 437–446, Apr. 2022, doi: 10.1080/17476348.2022.2057300.

[102] C. M. Terzic and B. J. Medina-Inojosa, "Cardiovascular Complications of Coronavirus Disease-2019.," *Phys. Med. Rehabil. Clin. N. Am.*, vol. 34, no. 3, pp. 551–561, Aug. 2023, doi: 10.1016/j.pmr.2023.03.003.

[103] S. D. Alipoor, H. Jamaati, P. Tabarsi, and E. Mortaz, "Immunopathogenesis of Pneumonia in COVID-19.," *Tanaffos*, vol. 19, no. 2, pp. 79–82, Nov. 2020.

[104] M. A. Amini, J. Karimi, S. S. Talebi, and H. Piri, "The Association of COVID-19 and Reactive Oxygen Species Modulator 1 (ROMO1) with Oxidative Stress.," *Chonnam Med. J.*, vol. 58, no. 1, pp. 1–5, Jan. 2022, doi: 10.4068/cmj.2022.58.1.1.

[105] "COVID-19 Vaccines.," Bethesda (MD), 2006.

[106] J. Meng *et al.*, "The role of vitamin D in the prevention and treatment of SARS-CoV-2 infection: A meta-analysis of randomized controlled trials.," *Clin. Nutr.*, vol. 42, no. 11, pp. 2198–2206, Nov. 2023, doi: 10.1016/j.clnu.2023.09.008.

[107] N. Paiz, P. Alonso, and A. L. Portillo, "Vitamin D Status: Can It Affect the Risk of Infection and the Severity of COVID-19 Symptoms?," *Curr. Trop. Med. reports*, vol. 8, no. 3, pp. 204–211, 2021, doi: 10.1007/s40475-021-00236-3.

[108] C. Bonilla, A. R. Ness, A. K. Wills, D. A. Lawlor, S. J. Lewis, and G. Davey Smith, "Skin pigmentation, sun exposure and vitamin D levels in children of the Avon Longitudinal Study of Parents and Children.," *BMC Public Health*, vol. 14, p. 597, Jun. 2014, doi: 10.1186/1471-2458-14-597.

[109] Q. Shen *et al.*, "COVID-19 illness severity and 2-year prevalence of physical symptoms: an observational study in Iceland, Sweden, Norway and Denmark.," *Lancet Reg. Heal. Eur.*, vol. 35, p. 100756, Dec. 2023, doi: 10.1016/j.lanepe.2023.100756.

[110] H. Zhang *et al.*, "Mass Spectrometry Analysis for Clinical Applications: A Review.," *Crit. Rev. Anal. Chem.*, pp. 1–20, Nov. 2023, doi: 10.1080/10408347.2023.2274039.

[111] C. F. Poole, "Jürgen H. Gross: Mass Spectrometry. A Textbook, 3rd Edn," *Chromatographia*, vol. 81, no. 2, pp. 365–366, 2018, doi: 10.1007/s10337-017-3400-5.

[112] A. P. Bruins, "Mass spectrometry with ion sources operating at atmospheric pressure.," *Mass Spectrom. Rev.*, vol. 10, no. 1, pp. 53–77, 1991.

[113] Ioan Marginean; Peter Nemes; Lida Parvin; Akos Vertes, "How much charge is there on a pulsating Taylor cone?," *Appl. Phys. Lett.*, vol. 89, no. 6, 2006.

[114] J. F. Mora, V. B. GJ, C. G. Enke, R. B. Cole, M. Martinez-Sanchez, and J. B. Fenn, "Electrochemical processes in electrospray ionization mass spectrometry.," *J. Mass Spectrom.*, vol. 35, no. 8, pp. 939–952, Aug. 2000, doi: 10.1002/1096-

9888(200008)35:8<939::AID-JMS36>3.0.CO;2-V.

[115] T. G. I., "Disintegration of water drops in an electric field," *R. Soc.*, vol. 280, pp. 383–397, 1964.

[116] B. E. Winger, K. J. Light-Wahl, R. R. Ogorzalek Loo, H. R. Udseth, and R. D. Smith, "Observation and implications of high mass-to-charge ratio ions from electrospray ionization mass spectrometry.," *J. Am. Soc. Mass Spectrom.*, vol. 4, no. 7, pp. 536–545, Jul. 1993, doi: 10.1016/1044-0305(93)85015-P.

[117] B. A. T. J. V. Iribarne, "Field induced ion evaporation from liquid surfaces at atmospheric pressure," *J. Chem. Phys.*, vol. 71, no. 11, pp. 4451–4463, 1979.

[118] M. Gamero-Castaño, "Electric-field-induced ion evaporation from dielectric liquid.," *Phys. Rev. Lett.*, vol. 89, no. 14, p. 147602, Sep. 2002, doi: 10.1103/PhysRevLett.89.147602.

[119] M. Labowsky, J. B. Fenn, and J. Fernandez de la Mora, "A continuum model for ion evaporation from a drop: effect of curvature and charge on ion solvation energy," *Anal. Chim. Acta*, vol. 406, no. 1, pp. 105–118, 2000, doi: https://doi.org/10.1016/S0003-2670(99)00595-4.

[120] R. F. Straub and R. D. Voyksner, "Negative ion formation in electrospray mass spectrometry.," *J. Am. Soc. Mass Spectrom.*, vol. 4, no. 7, pp. 578–587, Jul. 1993, doi: 10.1016/1044-0305(93)85019-T.

[121] A. C. Susa, Z. Xia, H. Y. H. Tang, J. A. Tainer, and E. R. Williams, "Charging of Proteins in Native Mass Spectrometry.," *J. Am. Soc. Mass Spectrom.*, vol. 28, no. 2, pp. 332–340, Feb. 2017, doi: 10.1007/s13361-016-1517-7.

[122] L. Yang *et al.*, "Investigation of an enhanced resolution triple quadrupole mass spectrometer for high-throughput liquid chromatography/tandem mass spectrometry assays.," *Rapid Commun. Mass Spectrom.*, vol. 16, no. 21, pp. 2060–2066, 2002, doi: 10.1002/rcm.824.

[123] A. M. Haag, "Mass Analyzers and Mass Spectrometers.," *Adv. Exp. Med. Biol.*, vol. 919, pp. 157–169, 2016, doi: 10.1007/978-3-319-41448-5_7.

[124] A. K. Shukla and J. H. Futrell, "Tandem mass spectrometry: dissociation of ions by collisional activation.," *J. Mass Spectrom.*, vol. 35, no. 9, pp. 1069–1090, Sep. 2000, doi: 10.1002/1096-9888(200009)35:9<1069::AID-JMS54>3.0.CO;2-C.

[125] R. Jansen, G. Lachatre, and P. Marquet, "LC-MS/MS systematic toxicological analysis: comparison of MS/MS spectra obtained with different instruments and settings.," *Clin. Biochem.*, vol. 38, no. 4, pp. 362–372, Apr. 2005, doi: 10.1016/j.clinbiochem.2004.11.003.

[126] "6500 and 6500+ Series of Instruments System User Guide," no. August, 2015.

[127] AB SCIEX, "Turbo V Ion Source Operator Guide," *Ab Sciex*, no. January, pp. 26–32, 2022.

[128] J. Gervasoni, A. Cocci, C. Zuppi, and S. Persichilli, "Total 25-hydroxyvitamin D determination by an entry level triple quadrupole instrument: comparison between two commercial kits.," *Biomed Res. Int.*, vol. 2013, p. 270426, 2013, doi: 10.1155/2013/270426.

[129] L. Bilodeau *et al.*, "Determination of vitamin D3 and 25-hydroxyvitamin D3 in

foodstuffs by HPLC UV-DAD and LC–MS/MS," *J. Food Compos. Anal.*, vol. 24, no. 3, pp. 441–448, 2011, doi: https://doi.org/10.1016/j.jfca.2010.08.002.

[130] A. Kruve and K. Kaupmees, "Adduct Formation in ESI/MS by Mobile Phase Additives," *J. Am. Soc. Mass Spectrom.*, vol. 28, no. 5, pp. 887–894, 2017, doi: 10.1007/s13361-017-1626-y.

[131] European Medicines Agency, "Guideline on bioanalytical method validation," *Available at: https://www.ema.europa.eu/en/documents/scientific-guideline/ich-guideline-m10-bioanalytical-method-validation-step-5_en.pdf.*.

[132] B. K. Matuszewski, M. L. Constanzer, and C. M. Chavez-Eng, "Strategies for the assessment of matrix effect in quantitative bioanalytical methods based on HPLC-MS/MS.," *Anal. Chem.*, vol. 75, no. 13, pp. 3019–3030, Jul. 2003, doi: 10.1021/ac020361s.

[133] A. B. Hall, S. L. Coy, A. Kafle, J. Glick, E. Nazarov, and P. Vouros, "Extending the dynamic range of the ion trap by differential mobility filtration.," *J. Am. Soc. Mass Spectrom.*, vol. 24, no. 9, pp. 1428–1436, Sep. 2013, doi: 10.1007/s13361-013-0655-4.

[134] F. Saponaro *et al.*, "Vitamin D measurement and effect on outcome in a cohort of patients with heart failure.," *Endocr. Connect.*, vol. 7, no. 9, pp. 957–964, Sep. 2018, doi: 10.1530/EC-18-0207.

[135] C. Jenkinson, R. Desai, A. T. Slominski, R. C. Tuckey, M. Hewison, and D. J. Handelsman, "Simultaneous measurement of 13 circulating vitamin D3 and D2 mono and dihydroxy metabolites using liquid chromatography mass spectrometry.," *Clin. Chem. Lab. Med.*, vol. 59, no. 10, pp. 1642–1652, Sep. 2021, doi: 10.1515/cclm-2021-0441.

[136] A. M. Wallace, S. Gibson, A. de la Hunty, C. Lamberg-Allardt, and M. Ashwell, "Measurement of 25-hydroxyvitamin D in the clinical laboratory: current procedures, performance characteristics and limitations.," *Steroids*, vol. 75, no. 7, pp. 477–488, Jul. 2010, doi: 10.1016/j.steroids.2010.02.012.

[137] P. A. Aronov, L. M. Hall, K. Dettmer, C. B. Stephensen, and B. D. Hammock, "Metabolic profiling of major vitamin D metabolites using Diels–Alder derivatization and ultra-performance liquid chromatography–tandem mass spectrometry," *Anal. Bioanal. Chem.*, vol. 391, no. 5, pp. 1917–1930, 2008, doi: 10.1007/s00216-008-2095-8.

[138] A. Alexandridou and D. A. Volmer, "Stability of sample extracts of vitamin D(3) metabolites after chemical derivatization for LC-MS/MS analysis.," *Anal. Bioanal. Chem.*, vol. 415, no. 2, pp. 327–333, Jan. 2023, doi: 10.1007/s00216-022-04409-5.

[139] R. M. Gathungu, C. C. Flarakos, G. S. Reddy, and P. Vouros, "The role of mass spectrometry in the analysis of vitamin D compounds.," *Mass Spectrom. Rev.*, vol. 32, no. 1, pp. 72–86, 2013, doi: 10.1002/mas.21353.

[140] A. Alexandridou, P. Schorr, C. S. Stokes, and D. A. Volmer, "Analysis of vitamin D metabolic markers by mass spectrometry: Recent progress regarding the 'gold standard' method and integration into clinical practice," *Mass Spectrom. Rev.*, vol. 42, no. 5, pp. 1647–1687, 2023, doi: 10.1002/mas.21768.

[141] N. Fabregat-Cabello *et al.*, "A fast and simple method for simultaneous measurements of 25(OH)D, 24,25(OH)(2)D and the Vitamin D Metabolite Ratio (VMR) in serum samples by LC-MS/MS.," *Clin. Chim. Acta.*, vol. 473, pp. 116–123, Oct. 2017, doi:

10.1016/j.cca.2017.08.024.

[142] L. Wang, "C-reactive protein levels in the early stage of COVID-19.," *Med. Mal. Infect.*, vol. 50, no. 4, pp. 332–334, Jun. 2020, doi: 10.1016/j.medmal.2020.03.007.

[143] M. Demir, F. Demir, and H. Aygun, "Vitamin D deficiency is associated with COVID-19 positivity and severity of the disease.," *J. Med. Virol.*, vol. 93, no. 5, pp. 2992–2999, May 2021, doi: 10.1002/jmv.26832.

[144] S. Giannini *et al.*, "Effectiveness of In-Hospital Cholecalciferol Use on Clinical Outcomes in Comorbid COVID-19 Patients: A Hypothesis-Generating Study.," *Nutrients*, vol. 13, no. 1, Jan. 2021, doi: 10.3390/nu13010219.

[145] H. Yisak *et al.*, "Effects of Vitamin D on COVID-19 Infection and Prognosis: A Systematic Review.," *Risk Manag. Healthc. Policy*, vol. 14, pp. 31–38, 2021, doi: 10.2147/RMHP.S291584.

[146] P.-J. Martens, C. Gysemans, A. Verstuyf, and A. C. Mathieu, "Vitamin D's Effect on Immune Function.," *Nutrients*, vol. 12, no. 5, Apr. 2020, doi: 10.3390/nu12051248.

[147] F. Haider, H. Ghafoor, O. F. Hassan, K. Farooqui, A. O. M. Bel Khair, and F. Shoaib, "Vitamin D and Cardiovascular Diseases: An Update.," *Cureus*, vol. 15, no. 11, p. e49734, Nov. 2023, doi: 10.7759/cureus.49734.

[148] R. Taha *et al.*, "The Relationship Between Vitamin D and Infections Including COVID-19: Any Hopes?," *Int. J. Gen. Med.*, vol. 14, pp. 3849–3870, 2021, doi: 10.2147/IJGM.S317421.